



Infrared spectroscopy: Method development and
ligand binding studies

Licentiate thesis

Saroj Kumar

Department of Biochemistry and Biophysics
Stockholm University, Stockholm, Sweden 2010

Abstract

Infrared detect the molecular vibration, where one can assessed the properties of molecules and their environment. We were studied the phosphoenol pyruvate (PEP) in different ionization states by infrared spectroscopy combined with theoretical analysis. Theoretical calculations peaked the vibrational coupling between carboxyl group, phosphate group and carbon - carbon double bonds, which helped to assign the bands. The infrared spectrum of labeled PEP and infrared measurement in D₂O also helped in band assignment.

Infrared spectroscopy is a powerful technique to detect the ligand induced changes in biomolecules as it has distinct signals and provides different level of structural features. An addition of a dialysis accessory to attenuated total reflection infrared spectroscopy makes this technique more universal for ligand binding studies, where induce reaction or perturbation of macromolecules can observed. It becomes easier to study the ligand binding of substrates, activators, inhibitors and ions on macromolecules as well as effect of pH, ionic strength or denaturants on the structure of macromolecules, which has great role in drug development. This method was tested with two proteins *cyt c* and calcium ATPase. We use this method to understand the binding of PEP and Mg²⁺ to pyruvate kinase (PK), where conformational changes of PK was revealed upon binding of PEP and Mg²⁺. The effect of protein environment on the bound PEP, we also used the labeled PEP, which helped to assign and evaluate the infrared absorption bands. The difference of bound and free PEP indicates specific interactions between ligands and protein. The quantification of phosphate group revealed that the enzyme environment has little influenced on the P-O bond strengths, which is weakened by less than 3% in the catalytic reaction. The carboxylate absorption bands indicates the shortening of the C-O bond by 1.3 pm. The binding of PEP to PK in presence of monovalent cations K⁺ and Na⁺ showed that the binding interaction are very similar.

List of publications

- I S. Kumar, M. Krasteva and A. Barth. 2006. A dialysis accessory for attenuated total reflection IR spectroscopy. *Spectroscopy* 20, 89-94.
- II M. E. Rudbeck, S. Kumar, M. Blomberg, M-A. Mroginski, A. Barth. 2009. Infrared Spectrum of phosphoenol pyruvate: computational and experimental studies. *J. Phys. Chem. A*. 113, 2935-2942.
- III S. Kumar and A. Barth. 2010. Phosphoenolpyruvate and Mg^{2+} binding to pyruvate kinase monitored by infrared spectroscopy. *Biophys. J.* In press.

List of Abbreviations

IR:	Infrared
FTIR:	Fourier transform infrared
ATR:	Attenuated total reflection
MCT:	Mercury Cadmium Telluride
FFT:	Fast Fourier Transform
PK:	Pyruvate kinase
PEP:	Phosphoenol pyruvate
ADP:	Adenosine diphosphate
ATP:	Adenosine triphosphate
SR:	Sarcoplasmic reticulum
DFT:	Density functional theory
CPCM:	Conductor like polarizable continuum model

Table of contents

Abstract

List of publications

List of abbreviations

1. Introduction	1
1.1 General descriptions	1
1.2 Pyruvate kinase	3
1.3 Sarcoplasmic reticulum Ca^{2+} -ATPase	4
2. Biophysical methods	7
2.1 Infrared spectroscopy	7
2.2 Electromagnetic spectrum	7
2.3 Experimental techniques	9
2.3.1 Fourier transform infrared spectroscopy	10
2.3.2 ATR- FTIR spectroscopy	11
2.4 Difference spectra	13
2.4.1 Interpretation of difference spectra	13
2.5 Ligand binding	14
2.6 Evaluation of bond strength and bond lengths	16
2.7 Dialysis	17
3. Results and discussion	19
3.1 paper I	19
3.2 Paper II	20
3.2 Paper III	22
4. Future objectives	25
4.1 Project I	25
4.2 Project II	25
5. Acknowledgements	27
6. References	28

1. Introduction

1.1 General descriptions

Infrared spectroscopy is roughly 200 years old, when (1800) William Herschel discovered the infrared region of the electromagnetic spectrum. The development of the method gets momentum during World War II, where applications were more focused on petroleum products than biological applications. The application of infrared spectroscopy in biological field started after 1950 and gained pace mainly in last few decades. The Infrared spectrum exhibits distinct features for biomolecules like proteins, nucleic acids, lipids or fats, carbohydrates and sugars. Proteins are the building blocks of life. Infrared spectra of proteins provide different level of structural information like secondary structure, protein reaction mechanism, protein ligand binding and protein dynamics.

Elliot and Ambrose [1] did pioneer work in 1950 by studying the conformational structure of protein and polypeptides by use of infrared spectroscopy. In the field of biomolecules a new era started in the 1970s after the availability of Fourier transform infrared (FTIR) spectroscopy, which improved the accuracy, reproducibility and also the signal to noise ratio. By using FTIR spectroscopy it became possible to detect small absorbance changes on the order of 10^{-3} , which helps to perform difference spectroscopy, where one could detect the small absorption bands of functionally active residues from the large background absorption of the entire protein. The difference provides absorption bands only of groups undergoing reactions and cancels the background [2-8].

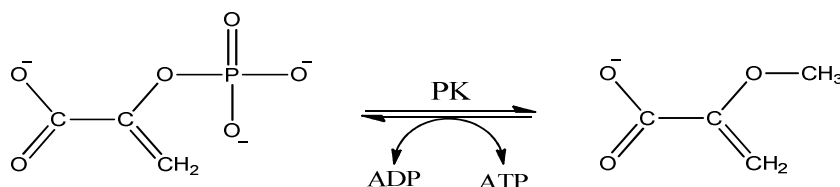
Understanding ligand binding to biomolecules plays a great role in drug development. The above development in the field of infrared spectroscopy gives possibility to study ligand binding to proteins on molecular level [3, 9- 11]. Infrared spectroscopy is able to detect the ligand induced conformational changes in proteins by analyses the secondary structure content like α - helix, β - sheets and turns. These structural changes have distinct infrared signals, which indicate the binding mode. The study of ligand binding is important to understand the mechanism of action of proteins (number of binding sites and their binding strength) and that help to understand the biological system where intracellular reactions in which binding is an integral part of chemical reactions.

Infrared spectroscopy has several advantages for elucidating the molecular mechanism of proteins, such as high time resolution, universal applicability from small soluble proteins to large membrane proteins, and high molecular information content combined with sensitivity high enough to detect a change in the environment around a single atom of a large protein. These properties make this method very useful to obtain information on enzyme-substrate recognition. Fourier transform infrared (FTIR) spectroscopy can provide potent dynamic and structural information, which sheds light on interactions occurring between enzyme and substrate during the catalytic process. Advantages of infrared spectroscopy are that it is applicable both to soluble proteins (pyruvate kinase) and membrane proteins (calcium ATPase), that it is cost effective and that it looks simultaneously at the whole protein as well as at specific sites. Also, infrared spectroscopy is a non-invasive technique. There is no need to label the protein and there is no perturbation of the original protein by an inserted label [12]. Infrared spectroscopy is very well suited for the study of different sizes and any types of protein. With NMR spectroscopy, it is not possible to study large proteins and by X-ray crystallography, it is difficult to study membrane proteins [13].

In paper I, we used two different proteins cytochrome *c*, a small soluble heme protein which plays a role in electron transport system to transfer electron between complex III and IV and the calcium ATPase, a P- type membrane protein which pump two calcium ions across the membrane to luminal side in the expanse of one ATP hydrolysis. In the paper III, we worked on pyruvate kinase, a key enzyme of the glycolytic pathway that catalyzes the transfer of phosphate from phosphoenolpyruvate to adenosine diphosphate. We observed the structural changes of PK upon ligand bindings. In both of the studies we used a dialysis accessory to ATR, in which a sample compartment in contact to the ATR crystal is separated by a dialysis membrane from a reservoir. The absorption of the solution in the sample compartment is probed by the infrared beam. The protein is confined to the sample compartment. The ligands on the other hand can exchange freely between the sample compartment and the reservoir via the dialysis membrane. Therefore the sample composition can be altered by adding a substance to the reservoir.

1.2 Pyruvate Kinase

Pyruvate kinase (PK) is a key enzyme of the glycolytic pathway that catalyzes the transfer of phosphate from phosphoenol pyruvate (PEP) to adenosine diphosphate (ADP).



The physiological reaction of pyruvate kinase proceeds in two chemical steps. The first step is phosphoryl transfer from PEP to ADP which produces ATP (adenosine triphosphate) and the enolate of pyruvate [14]. The second step is the addition of a proton to the enolate of pyruvate to produce pyruvate [15].

Rabbit muscle pyruvate kinase consists of four subunits of 530 residues each. Each subunit folds into four domains: A, B, C and N. Domain N (residues 1-42) is a short helix-turn-helix motif, domain A (residues 43-115 and residues 224-387) is a parallel $(\beta/\alpha)_8$ barrel, domain B (residues 116-223) is a nine stranded β -barrel and domain C (residues 388-530) is composed of five α -helices and a five stranded β -sheet. The active site lies in the pocket between domains A and B of the same subunit [16-19]. The structure of the active site with bound (PEP) indicates that the side chains of Arg⁷² and Lys²⁶⁹ bind the phosphate group of PEP or the γ -phosphate of ATP [18, 19].

Pyruvate kinase has four metal binding sites; it requires divalent cations [20-22] and monovalent cations [23-25] for activity. In the presence of divalent cations, pyruvate kinase is active in a medium containing the univalent cations K^+ , Rb^+ or NH_4^+ , but only weakly active in the presence of Na^+ [26, 27]. By use of NMR, Mildvan and Cohn [28] have observed that K^+ enhances the relaxation rate of water protons in the presence of the ternary complex pyruvate kinase-manganese-phosphoenolpyruvate. This indicates that K^+ affects the conformation of the enzyme in the presence of PEP and Mn^{2+} . The crystal structure of rabbit muscle pyruvate kinase [29, 30] provides insight into the roles of various groups in binding of divalent and monovalent cations. Mg^{2+} coordinates to the protein through the carboxylate side chains of Glu²⁷¹ and Asp²⁹⁵ and K^+ coordinate to four protein ligands: Thr¹¹³, Ser⁷⁶, Asn⁷⁴ and Asp¹¹².

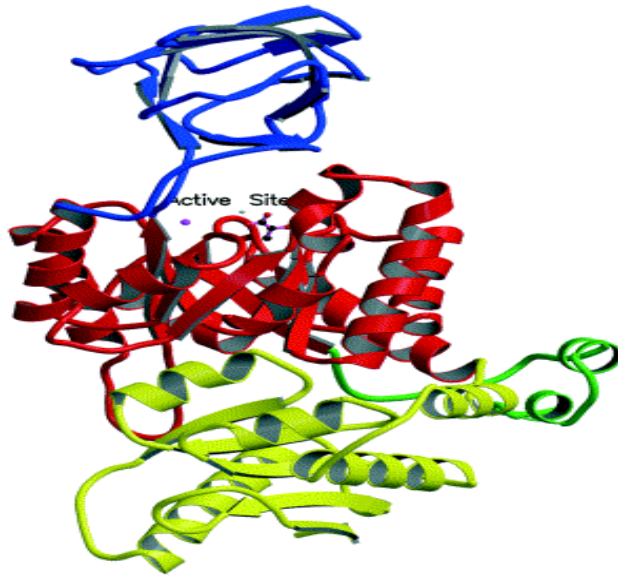


Figure1: Structure of rabbit muscle pyruvate kinase subunits. One of the four homologous subunits is shown. Each subunit consists of 4 domains: N (green), A (red), B (blue) and C (yellow). The active site is between domains A and B [16].

Pyruvate kinase deficiency is the most common enzyme defect affecting the glycolytic pathway of the erythrocyte. The erythrocyte pyruvate kinase deficiency causes hemolytic anemia [31]. This is inherited metabolic disorder occurs in the both forms autosomal dominant and recessive but autosomal recessive is more common [32, 33].

1.3 The Sarcoplasmic Reticulum Ca^{2+} -ATPase

The Ca^{2+} -ATPase (SERCA1a) from skeletal muscle sarcoplasmic reticulum (SR) is a P-type ATPase. The SR Ca^{2+} -ATPase consists of a single subunit with a molecular mass of 110 kD. The SR Ca^{2+} -ATPase has an important physiological function. Excitation of a muscle cell induces the release of Ca^{2+} from the SR into the cytosol, leading to an increase in the concentration of Ca^{2+} , triggering the muscle cell to contract. For the muscle cells to relax, the released Ca^{2+} has to be pumped back into the SR, which is done by the Ca^{2+} -ATPase [81-83].

1.3.1 P (phosphorylated)-type ATPases

The SR Ca^{2+} -ATPase is an important member of P- type ATPases, which are ATP powered ion pumps that transport ions across biological membranes against their concentration gradient in order to keep the internal milieu of the cell constant. A common

property for all P-type ATPase is that they bind the substrate ATP with very high affinity and then they phosphorylate a highly conserved aspartic acid residue during the transport process. The energy for active transport comes from the hydrolysis of the terminal phosphate bond of ATP [84]. The other prominent members of the family are Na^+ , K^+ -ATPase and gastric H^+ -ATPase.

1.3.2 Structure

The X-ray crystal structures show that the SR Ca^{2+} -ATPase has two main regions, a transmembrane region and a cytoplasmic region. The transmembrane region consists of ten transmembrane α -helices (M1-M10). In the crystal structure of the Ca^{2+} bound Ca^{2+} -ATPase, the two Ca^{2+} are bound by ligands from helices M4, M5, M6 and M8 [85]. The cytoplasmic region consists of three separate domains, the nucleotide binding (N) domain, the phosphorylation (P) domain and actuator (A) domain. The P domain contains the residue of phosphorylation (Asp 351) whereas the N domain contains the binding site for the adenosine moiety of ATP. Domain A may work as an actuator or anchor for the N domain and appears to be involved in bringing about major conformational changes [82].

1.3.3 Molecular mechanism

In the reaction cycle of Ca^{2+} transfer, the SR Ca^{2+} -ATPase undergoes conformational changes and forms at least four interconvertible phosphorylated and unphosphorylated intermediates. De Meis and Vianna proposed a model of the molecular mechanism of the Ca^{2+} -ATPase, which includes two main intermediate forms with distinct properties, E1 and E2 (see fig.1) [86].

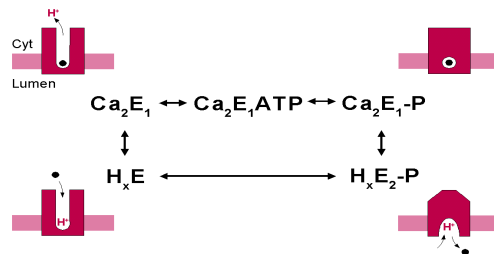


Figure 2. A scheme of the E1-E2 model of the SR Ca^{2+} -ATPase reaction cycle. When the protein is in the E1 conformation, two Ca^{2+} can bind to high affinity sites on the cytosolic surface. This activates the ATPase to use ATP as a substrate and then the

terminal phosphate bond of ATP is cleaved into ADP and inorganic phosphate (pi). The liberated phosphate group is then transferred to the Asp 351 residue [87], which results in the formation of the E1-P high energy phosphoenzyme intermediate. This state is ADP sensitive, meaning that it is able to synthesize ATP in the presence of ADP. In this state the Ca^{2+} is not accessible from either side of the membrane. The protein then changes its conformation from the ADP sensitive E1-P form to the ADP insensitive E2-P form, where it no longer can synthesize ATP, but instead could be dephosphorylated by water. This conversion is accompanied by the creation of low affinity binding sites from which the Ca^{2+} can dissociate into the SR. After the release of Ca^{2+} , the phosphate group is cleaved off and released to the cytoplasmic side and the cycle is completed by the reversion of the E2 form back to the E1 form. The conformational change also inactivates the Ca^{2+} binding sites on the luminal side and regenerates the high affinity Ca^{2+} binding sites facing the cytosol, making the cycle complete.

2. Biophysical methods

2.1 Infrared spectroscopy

Spectroscopy is the study of molecular or atomic structure of a substance by observation of its interaction with electromagnetic radiation (here infrared (IR) radiation). The transition energy of most molecular vibrations falls within the infrared region of the electromagnetic spectrum, which can therefore be detected in an infrared spectrum.

2.2 The electromagnetic spectrum

Electromagnetic radiation can be described in terms of a stream of photons, which are massless particles moving at the speed of light. Each photon contains a certain amount of energy. The only difference between the various types of electromagnetic radiation is the amount of energy found in the photons. The energy, E , associated with electromagnetic radiation follows the expression

$$E = h\nu$$

Where h is Planck's constant and ν is the frequency of radiation.

Electromagnetic radiation is characterized by its frequency, ν , or wavelength, λ . Wavelength and frequency are related to each other by the expression

$$\nu = c/\lambda \quad \text{where } c \text{ is speed of light.}$$

Instead of these quantities, infrared spectroscopists use wavenumber. Wavenumber is the reciprocal of the wavelength, which has the advantage of being proportional to the energy. The unit of wavenumber is cm^{-1} . The wavenumber of the absorbed or emitted photons is equal to the change in molecular energy expressed in wavenumbers.

2.1.1 Molecular vibrations

Photons in the infrared region can excite vibrations in molecules, and a vibration is said to be infrared active if IR energy absorption causes a vibrational excitation. Hence, nearly all polyatomic molecules absorb in the IR region, except diatomic homo-nuclear molecules such as O_2 and N_2 since their vibrations do not lead to a change in dipole moment. A non linear polyatomic molecule that consists of N atoms has $3N$ degrees of freedom of which six are translations and rotations of the entire molecules. The remaining $3N-6$ degrees of freedom correspond to the independent vibrational modes

called normal modes. If molecules are linear, one rotational degree of freedom is absent and the number of vibrations is $3N-5$. In each normal mode of vibration, the atoms vibrate with the same frequency and pass through their equilibrium positions simultaneously. Large molecules such as proteins have a vast amount of normal modes, many of which are degenerate, i.e. have the same energy as others [34].

Each normal mode behaves like an independent harmonic oscillator that is dependent on the force constant (of the mode) and the effective mass of the mode. Not all atoms are moved by the vibration, some are instead stationary. This is in particular true for heavier atoms, which can act as soft walls isolating vibrations of light atoms attached to them. This is similar to the situation of double and single bonds, where the vibrations of double bonds are more or less independent from the rest of the molecule because of their higher frequencies. Vibrations that are rather independent of the rest of molecule are called group vibrations. The main region of group vibrations is above 1500 cm^{-1} . The opposite situation also occurs, that is when vibrations are not independent but instead couple to each other. This can happen when the frequencies of vibrations are similar and the groups are adjacent in space. The vibrations then depend on the molecular geometry. When vibrations couple, their energy levels mix and they can no longer be assigned to only one bond. The bands associated with these vibrations tend to form an absorption pattern, a finger print of the molecule rather than representing a specific group.

Absorption bands may be regarded as arising from stretching or deformation vibrations. In some cases these can be considered as symmetric or anti-symmetric motions. Stretching vibrations involve a change in the bond-length and often have high energy since the bonding force directly opposes the change. Deformation vibrations involve a change in a bond angle of the group and can be classified as scissoring, wagging, rocking or twisting. Ring compounds can also undergo a symmetric stretching vibration, called breathing. The normal vibrations of a tri-atomic, non-linear molecule are shown in Fig. 3.

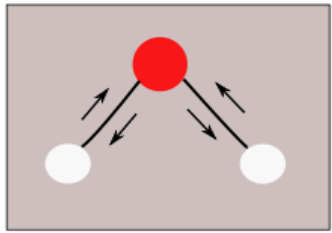
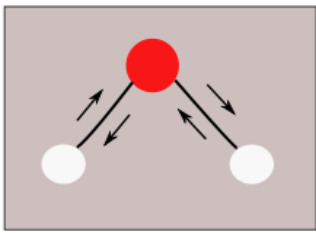
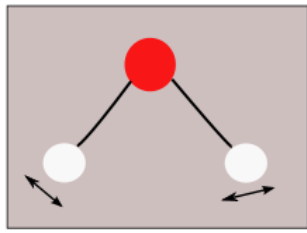
		
Symmetric stretching	Antisymmetric stretching	Bending mode

Figure 3. The normal vibrations of an AX₂ tri-atomic non-linear molecule.

2.1.2 Information from infrared spectra

An infrared spectrum yields information on several properties of the investigated molecules and their environment, such as bond lengths, bond strengths and conformational freedom. Everything that alters the electron distribution of the bonds or the environment will alter the vibrational frequency and will thus manifest itself in the infrared spectrum. The main contribution to the vibrational frequencies is the chemical structure of the molecule, since it defines the masses of the constitutive atoms and the strengths of the vibrating bonds. During a reaction, the chemical structure can be altered for example by phosphorylation, which changes the vibrational frequencies of the molecule.

Depending on the three-dimensional structure of the molecule, vibrations of similar frequency can couple. The frequencies of coupled vibrations are different from those of the uncoupled and can be detected in the spectrum, providing information on the conformation. Also, the band width in an infrared spectrum gives information on conformational freedom. This freedom can be related to entropy and in this way quantify entropic effects in catalysis [12].

2.3 Experimental technique

Two main types of infrared spectrometers exist, traditional dispersive spectrometers and Fourier-transform infrared (FTIR) spectrometers. Most instruments used for research today are FTIR-spectrometers. The fast data collection, strong signal, large signal to noise ratio, and less sample heat-up are the advantages of FTIR-spectrometers over dispersive ones.

2.3.1 Fourier Transform Infrared Spectroscopy

After the invention of the Michelson interferometer in 1880 by Albert Abraham Michelson, the development of FTIR started. The FTIR technique was widely accepted after the development of the fast Fourier-transform (FFT) algorithm by Cooley and Tukey [35]. This, together with the advances in the calculating capacities in minicomputers made it possible to develop modern FTIR systems.

At the heart of a Fourier transform spectrometers is an interferometer, a device for analyzing the radiation from the source.

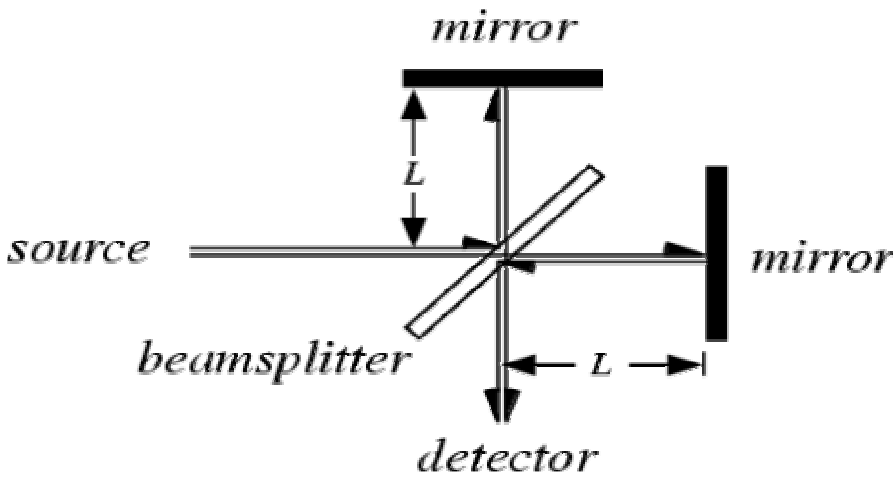


Figure 4. The principle of a Michelson interferometer

The interferometer consists of a beam splitter that ideally splits the beam from the light source into two equal parts that are reflected by two different mirrors, introducing a difference in optical pathlength. This difference in traversed path is varied by moving one of the mirrors, while the other is held at the fixed distance from the beam splitter. When the beams, after reflection, recombine in the beam splitter, there will be a phase difference between them, and they will interfere either constructively or destructively. 50% percent of the beam reflected from the fixed mirror is transmitted to the detector, while the remaining 50% is reflected back in the direction of the source. The same is applies for the movable mirror. A detector measures the light intensity in dependence of the position of the movable mirror. This results in an interferogram.

The intensity of the detected signal due to radiation in the frequency interval $[\nu, \nu + d\nu]$, denoted $I(p, \nu)d\nu$ varies with the difference in path length p as a cosine function

$$I(p, \nu) d\nu = I(\nu)(1 + \cos 2\pi \nu p) d\nu.$$

Taking into account that the signal is actually composed of contributions from signals in a wide range of wavenumbers, the total intensity $I(p)$ at the detector is the sum of all these contributions.

$$I(p) = \int I(\nu)(1 + \cos 2\pi \nu p) d\nu$$

Now, the desired function $I(\nu)$, the variation of the intensity with wavenumber, can be calculated from $I(p)$ by the standard mathematical procedure of Fourier transformation:

$$I(\nu) = 4 \int [I(p) - \frac{1}{2} I(0)] (\cos 2\pi \nu p) dp$$

This transformation is performed by the computer interfaced to the spectrometer. In total, two Fourier transformations are performed, one by the interferometer and one by the computer. Usually, to obtain a good signal to noise ratio, a large number of scans needs to be recorded and the resulting signals are averaged.

2.3.2 ATR-FTIR Spectroscopy

Infrared spectroscopy on biological systems is often performed in the **transmission mode**. This means that the IR beam of the spectrometer is passing through the sample and the transmitted IR intensity is measured. Owing to the high IR absorptivity of water, IR samples are very thin, the relative water content in transmission samples is therefore quite low, which may in some cases constitute a major problem. Moreover, it is quite difficult to change sample conditions during a measurement, e.g. by adding ligands, changing the pH or ion concentration.

An alternative to transmission mode experiments is offered by the **attenuated total reflection** (ATR) technique [36, 37]. In this technique, the IR beam is guided in an IR transparent crystal by total reflection. The electromagnetic field extends beyond the crystal surface (several microns) as so called **evanescent field**. By applying e.g. a protein sample directly on the surface of the crystal, it is sensed by this evanescent wave and contributes to the absorption of the IR beam. In the ATR technique, the applied protein may be in direct contact to a bulk water phase above, which is not sensed by the IR beam

due to small penetration length of the evanescent field. The sample may be therefore manipulated during the experiment e.g. by the addition of agents, which may change the properties of the protein [38].

Evanescent field

Newton discovered evanescent electromagnetic fields, fields that fade out exponentially within a few wavelengths. Due to advancement and desire to probe with nanometer resolution, optical evanescent fields are becoming more relevant in research.

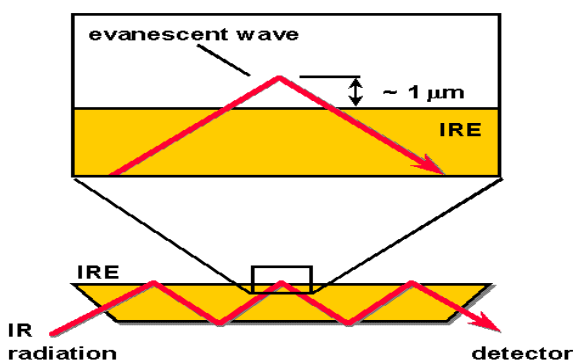


Figure 5. Attenuated total reflectance

The penetration depth (d) is given by:

$$d = \frac{\lambda}{2\pi [n_i^2 \sin^2 \phi_i - n_t^2]^{1/2}}$$

Where d is the positive, real, evanescent penetration depth, n is the refractive index, i and t are the incident and transmitted wave fronts respectively, λ and ϕ are the wavelength and angle of incident respectively.

To produce ATR, the medium must have an index of refraction such that the wave would not undergo total internal reflection. The evanescent field is then created between sample and crystal which is able to excite (penetrate) the sample medium, and perturb the internal reflection of the first medium.

The property of total internal reflection that allows a small evanescent field to leak through the back side of the reflecting medium (resulting phenomena) has a wide range of applications. New chemical and biological sensors are beginning to use evanescent fields to detect low concentrations of reagents.

2.4 Difference spectra

The infrared spectrum of proteins contains a lot of detailed information on the structure and interactions of different groups. An average protein has about 25,000 vibrational degrees of freedom. This gives a very complex spectrum with many overlapping bands and makes the extraction of information on specific groups difficult. Depending on the group of interest, one can either look in a spectral region where the group dominates the absorption or use difference techniques that allow selective observation of groups that actively participate in a reaction.

Infrared difference spectra are the result of subtracting a spectrum of the protein in state A from a spectrum of the protein in state B. In this way, only groups that actively participate in the reaction show, while the absorbance of groups that do not participate in the reaction is canceled in the subtraction, as illustrated in Fig. 5.

2.4.1 Interpretation of difference spectra

In difference spectra the absorption of the reaction products or product state shows as positive bands while negative bands are characteristic of the reactants or the reactant state. There are several causes for a change in absorbance, the reactants can for example be transformed into reaction products that absorb in different regions of the spectrum resulting in one negative peak and two positive peaks or the frequency might be shifted due to changes in the environment of the vibrating bond resulting in a negative and a positive band in close proximity.

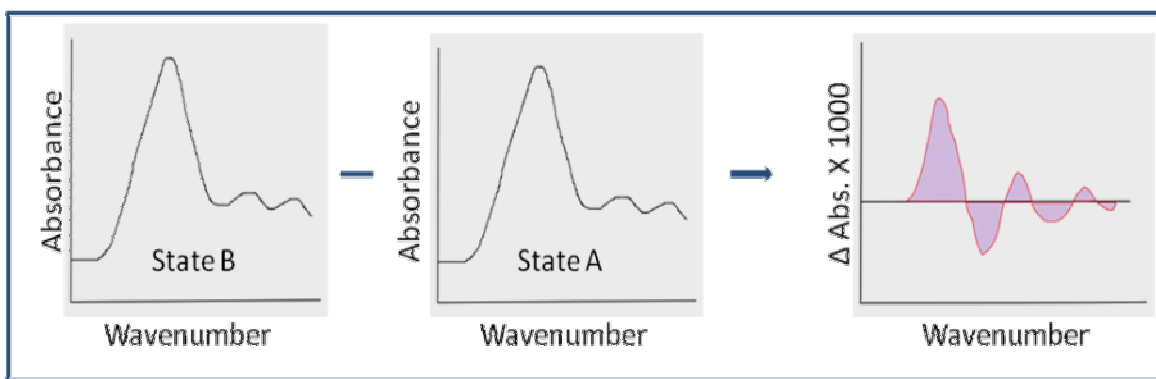


Figure 6. Calculation of a difference spectrum. A difference spectrum is the spectrum resulting from the subtraction of a spectrum in state A from a spectrum in state B.

As a first step in the interpretation of difference spectra it is very powerful to regard the spectrum as a characteristic fingerprint of the conformational change. The signals can be analysed according to their shape, time course and magnitude. The shape of the spectrum tells us how similar the conformational changes associated with different preparation or reactions of the protein are.

To assign the difference bands to vibrations is always a difficult task, which needs additional experiments such as isotopic labeling, site directed mutagenesis, ligands or computations. Computations are not easy for large macromolecules and site directed mutagenesis is not easily to achieve and its also affect the protein functions. Isotopic labeling is comparatively easy way, which does not alter the protein function. Since isotopes have different masses it sense different vibrational modes which could be detected by infrared difference spectrum by shift of bands. We achieved the simple isotopic exchange by replacing H_2O by D_2O , (where hydrogen is replace by deuterium) and more specific by labeled the ligands.

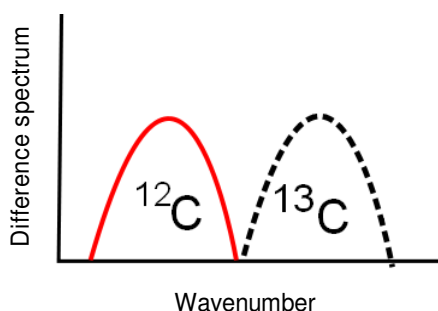


Figure 7. Band shift due to isotopic labeling.

2.5 Ligand Binding

A molecule that binds to a target molecule and forms a complex to serve a specific purpose is referred to as ligand. Incase of biomolecules, it serve a biological purpose. The binding of ligand to a target molecules mainly occurs by intermolecular forces such as hydrogen bonding, electrostatic interactions and vander Waals forces. In biochemistry, the ligand binds to specific target mainly proteins (enzymes and receptors). The binding of ligand molecules to the target molecules increases with increase the ligand

concentration until saturation is reached (all binding sites occupied). The binding of ligands to target molecules can be described by the dissociation constant (K_d).

$$K_d = \frac{[R][L]}{[RL]}$$

R; concentration of target molecules, L; concentration of ligand, RL; concentration of protein ligand complex.

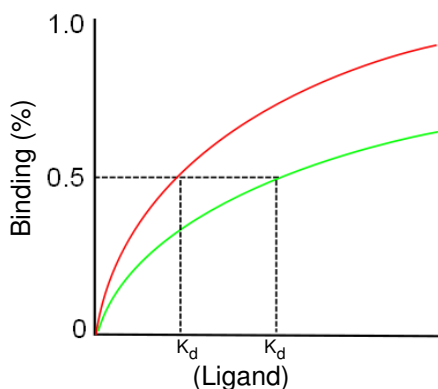


Figure 8. Illustrates the binding affinity.

K_d , tells about the strength of interaction, the lower the value stronger the interaction.

The effectiveness of binding depends on specificity (number of ligand binding to target molecule) and the strength of their bindings (affinity). Binding is often cooperative i.e; binding of the first ligand facilitates subsequent binding [39, 40]. Cooperativity may be positive if binding increases the binding of other ligand and negative if it decreases the binding of other ligands. Ligands can be substrates, inhibitors, activators and neurotransmitters. Binding of a ligand can be selective (binds to a specific protein) or non selective (binds to several proteins). It plays an important role in drug development where selective binding fulfill specific functions and non selective binding causes specific functions with side effects which play a major role on efficacy of a drug.

There different way is to experimentally measure binding like: mix the ligand with target molecules and free ligand separated by using equilibrium dialysis, membrane filtration and centrifugation or measure the binding by observing the spectral changes due to changes in physical properties of target molecules or ligand that is induced by binding.

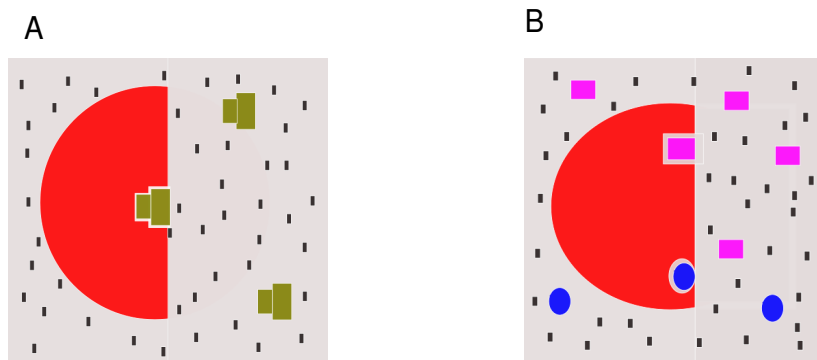


Figure 9. Schematic diagram of ligand binding to macromolecules. Fig. A shows a macromolecules (red) in solution, solvent molecules indicated as black lines and ligand is shown in green, whereas in B, the macromolecule (red) has two binding sites and the ligands are shown in pink and blue.

In the protein number of different ligands often binds on separate domains. Some ligands may not perturb the protein much and others ligand can perturb significantly. The structure of a protein domain generally does not change substantially upon ligand binding but small movements of atoms of the protein do occur in every binding event. Often structural changes involve the movements of flexible loops on protein surfaces. The changes in protein structure upon ligand binding help to maximize the interaction between the protein and ligand and to minimize the interaction with the other components of the solvent, while permitting the ligand to associate and to dissociate. The other role of domain or subunit movements upon ligand binding is to produce functional alterations at other sites of the protein (allosteric protein) [41-43]

2.6 Evaluation of bond strengths and bond lengths

Bond parameters for the phosphate group can be determined from the band positions of the symmetric and asymmetric stretching vibrations of the terminal P-O bonds. A fundamental frequency or wavenumber ν can be calculated according to $\nu = [(\nu_s^2 + 2\nu_{as}^2) / 3]^{1/2}$ [45]. The fundamental wavenumber can be used to calculate the bond valence of P-O bonds using the formula [45]

$$(1) \quad s = [0.175 \times \ln (224500 \text{ cm}^{-1} / \nu)]^{-4.29}$$

where s is bond valence in valence units (vu) of the terminal phosphate bonds and ν the fundamental wavenumber. Interactions between terminal phosphate oxygens and their environment were quantified according to the bond valence model [46], which states that the sum of all bond valences around oxygen atoms is two. This sum includes covalent bonds and external bonds, i.e. interactions with the environment. Thus, the bond valence due to the interactions to each of the terminal oxygens is 2 minus the bond valence of the terminal bond. Parameters for the bridging P-O bond can similarly be obtained by subtracting the summed bond valences of the terminal P-O bonds from the atomic valence of phosphorous, which is five.

Since bond valences are defined by experimentally determined bond lengths, bond lengths can be determined from bond valences. Equation 2 [46] with the parameters used to derive the frequency versus bond valence correlation (equation 1) [45]:

$$(2) \quad L_s^N = L_1^N/s$$

where L_s the bond length of a bond with bond valence s measured in vu, and L_1 the bond length of a bond with a bond valence of 1 vu. L_1 and N are constants for a given type of bond [47, 48]. For P-O bonds they are $N = 4.29$ and $L_1 = 1.622 \text{ \AA}$ [48].

To estimate the reduction of bond dissociation energy of the bridging P-O bond due to binding of ligand to protein two approaches can be use. (i) Bond dissociation energy can be regarded as linear to bond valence [49]. (ii) Bond length L and bond dissociation energy E are correlated: for several oxides, the inverse relationship $E \sim (L - L_0)^{-1}$ [50], where $L_0 = 1.171 \text{ \AA}$ for P-O bonds [51].

2.7 Dialysis

Membranes play a major role in biophysical chemistry. Generally use the dialysis for the purification of macromolecular substances and it also can be use to measure the binding of small molecules and ions to a large molecules. In the cell, the membrane has a similar role, serving to partition region of the cell and making a barrier that retains some substances and allows others to pass [39]. The main difference between these two is that those membranes use in the laboratory are always passive, that means they act only as a barrier and play no active role in the transport of materials [39].

In the dialysis process solutes diffuse across a membrane and move from higher concentration to lower concentration until equilibrium is reached (concentration on both sides becomes equal). The membrane is a thin layer of material that contains different size of pores. The movement of solutes across the membrane depends on the size of the membrane pores. Several factors affect the rate of dialysis like membrane pore size, concentration on both sides of the membrane. One can increase the rate of movement across the membrane by agitating the external solution with a stirrer. Initially the rate of diffusion becomes faster and later when concentrations from both sides approaches to equilibrium the rate of dialysis decreases. The speed of dialysis could also be increased by changing the external solution with fresh solution. The charge of the dialyzable molecules also affects the rate of dialysis. The diffusion of highly charged molecules is often slow because of Donnan potential, which can be improved by increasing the ionic strength of the solutions [39, 52].

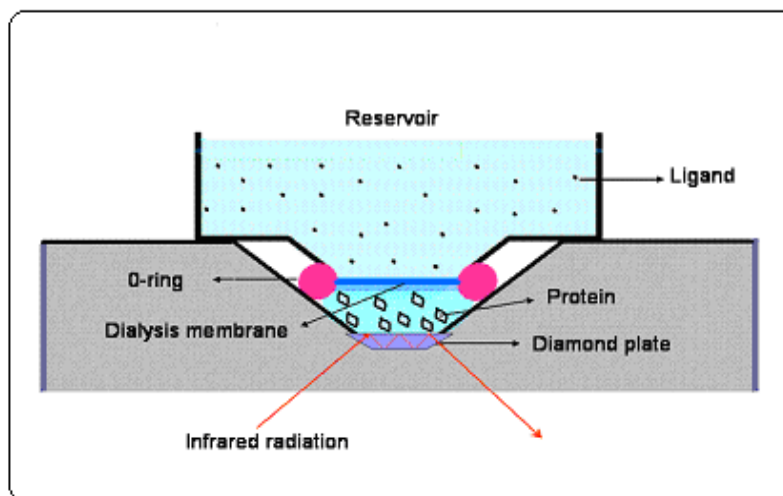


Figure 10. Dialysis accessory for ATR units

A dialysis accessory for ATR units is shown in Fig 10, it has a sample compartment in contact to the ATR crystal which is separated by a dialysis membrane from a reservoir [53-55]. The absorption of the solution in the sample compartment is probed by the infrared beam. The ligand on the reservoir can exchange freely between the sample compartment and the reservoir via the dialysis membrane.

3. Results and discussion

3.1 Paper I

In paper I, we developed a method to study ligand binding to macromolecules. A dialysis accessory coupled with ATR spectroscopy was constructed to investigate ligand binding. The main advantage of this method is the possibility to manipulate the sample of interest during experiment and performed multiple experiments with different ligands on the same sample which save times and material [53, 56-58].

In our dialysis accessory to our ATR unit, the membrane is fixed by an O- ring on the conical bottom of the reservoir, which is made of the nonreacting material delerin - a polyacetyl resin polyoxymethylene. We soaked the membrane in sample buffer before fixing it on the reservoir for two reasons; one is to fix it properly on the reservoir and the other to maintain the porosity of the membrane by not let them dry. Then, we assembled the dialysis accessory on the ATR unit by putting 3-5 μ l of sample on the ATR crystal and fixed the dialysis accessory by slide down the membrane attached reservoir through a thermostatic block. This process makes two compartments one down are sample, where macromolecules or target molecules reside and above the buffer compartment. As both compartments are separated by membrane, diffusion start across the membrane from higher concentration to lower concentration. It takes 30 minutes to several hours (4-5 hours) to get the equilibrium states (concentration of both side become equal) depending on the sample behavior (like charge of both sides which create Donnan potential) and concentration. We observed that the protein sample takes time to reach the equilibrium state due to process with in the sample and less samples takes shorter time. The approach to equilibrium was observed by continuous monitoring the absorption spectrum of the sample.

We have tested our dialysis accessory to the ATR unit with two different proteins. Cytochrome c, a small soluble heme protein present in mitochondria where it plays a major role in transfer electron between the complex III and IV. Calcium ATPase, a P-type ATPase which pumps two calcium ions across the membrane from cytosolic side to luminal side at the expense of the hydrolysis of one ATP molecule. First we introduced ATP into the buffer compartment and followed its arrival into the sample compartment

directly via observing the infrared absorption of the ATP. We noted that the high concentration ATP samples (10^{-2} M) were detected within 10s whereas less concentrated sample (10^{-4} M) taken more time around 100s. We have tested the protein cytochrome c which has been studied by infrared spectroscopy previously [55, 58-61]. The reaction induced difference spectra due to reduction and reoxidation of cytochrome c were studied. The reduction of cytochrome c was achieved by the reducing agent sodium dithionate and oxidation by the oxidizing agent potassium ferricyanide. Both redox induced difference spectra were mirror image of each other and fully reproducible in various cycles. The other protein we tested was calcium ATPase. The ligand induced conformational changes in calcium ATPase due to ATP binding was studied. We observed the absorption changes in calcium ATPase upon ATP binding within 120 s after the addition of ATP into the buffer compartment. The observed signal was agreement with previous spectra taken in the transmission mode by our group [62, 63].

We obtained high quality spectra of protein reactions which shows that our dialysis accessory to ATR can be used to study ligand binding to macromolecules. We also learned that this technique is simple to handle and that is easy to induce the reactions and observed ligand binding which makes it potential for drug development.

3.2 Paper II

In the paper II, we studied the infrared spectrum of PEP, the last substrate of the glycolytic pathway. Experimentally and supported by computationas. Band assignment of the experimental infrared spectra is based on knowledge of group frequencies, which makes a possible vibrational coupling between carboxyl group, the phosphate group and the carbon carbon double bond in PEP hard to predict. That can be achieved by the computational method. We studied PEP in three different ionization states and clarified some of the band assignments by recording the spectrum of $^{13}\text{C}_{2,3}$ labeled PEP. By computation we studied the several structures of PEP in three different ionization states. We used density functional theory (DFT) with the B3LYP functional and with the 6-31G (d, p), 6-31++G (d, p) and 6-311++G (d, p) basis sets for all ionization states and observed that the basis set 6-31G (d,p) generally overestimates with respect to experimental values while the other two basis sets are close to the experimental values,

therefore we used the basis set B3LYP/6-31++G (d,p) with the CPCM continuum in all of the computational results we presented in paper II.

FI-PEP (fully ionized PEP): The FI-PEP spectrum was measured experimentally at pH 9. The experimental infrared spectrum (1800 – 800 cm^{-1}) contains the 6 distinct bands. The bands at 1571 and 1410 cm^{-1} are from the antisymmetric and symmetric stretching vibrations of COO^- respectively, where the calculation reveals that the symmetric stretching vibration is coupled to the scissoring vibration of CH_2 . In the same way we also observed that the band at 1229 cm^{-1} has contributions from several internal coordinates, the C-O stretching of C-O(P) group and the rocking vibration of CH_2 . The bands at 1107 and 974 cm^{-1} are from the antisymmetric and symmetric PO_3^{2-} vibration respectively. The calculation we revealed that the 974 cm^{-1} also involves the C-O(P) stretching and CH_2 rocking vibrations. The 876 cm^{-1} band is due to the wagging vibration of the methylene group and the C1-C2 stretching vibration coupled with the scissoring of the carboxylate group, which is also established by the small shift in the experimental spectra of labeled PEP.

SP-PEP (singly protonated PEP): The PEP spectrum was measured at pH 4.6, and indicated that the hydrogen atom is positioned on the phosphate group in line with the pKa values of the carboxylate and the phosphate group. This fact is also established by the antisymmetric and symmetric stretching vibrations of carboxylate which were observed at 1575 and 1408 cm^{-1} respectively, as in FI-PEP. On the other hand the ionized phosphate bands at 1107 and 974 cm^{-1} no longer exist. SP-PEP adopts many conformations but we calculated two conformations which were energetically more favourable. The calculated spectra of both conformations were similar except for an extra vibration that was observed in case of conformation II. From P-O(H) in plane bending vibration, which is 317 cm^{-1} upshifted in compared to conformation I which does not contain the internal hydrogen bond between phosphate hydroxyl group and one of the oxygens of the carboxylate group. We also observed that the experimental band at 1217 cm^{-1} contains many vibrations such as C-O(P) stretching vibration, CH_2 rocking vibration, antisymmetric PO_2^- stretching as well as POH bending vibrations. The 1086 cm^{-1} band from the PO_2^- symmetric stretching vibration and the 996 cm^{-1} band arise from the coupling between C-O(P) stretching and CH_2 rocking vibrations. The small shoulder on

the low wavenumber side of the 996 cm^{-1} band is a residual band of FI-PEP, indicating that the small proportion of PEP remains unprotonated at pH 4.6. The bands in lower wavenumber region at 923 and 881cm^{-1} were difficult to assign by the calculation due to solvent effects. For that we also analysed SP-PEP with four explicit water molecules. The calculated spectra agreed with the model without explicit water molecules except for the P-O(H) stretching vibration which contributed along with the CH_2 wagging to the band 923 cm^{-1} .

DP-PEP (doubly protonated): The spectrum was measured at pH 2.1. The spectrum indicates protonation of the carboxylate group since the bands around 1575 and 1408 cm^{-1} no longer exist. We calculated the DP-PEP spectrum with four different conformations. The band at 1719 cm^{-1} is assign to the C=O stretching vibration and the 1627 cm^{-1} band to the C2=C3 stretching vibration. The experimental spectrum was almost featureless between 1600 and 1250 cm^{-1} ; whereas the calculated spectrum indicated strong absorption in this region which assigned to the delocalized mode involving the COH group. The band near 1200 cm^{-1} is an overlap of several normal modes such as C-O(H) stretching and bending, C1-C2 stretching, C-O(P) stretching, CH_2 rocking, PO_2^- antisymmetric stretching and POH bending vibrations. The contribution of POH and COH bending vibrations is also supported by the fact that the experimental absorption is reduced in heavy water. The remaining bands at 1088 , 1000 , 925 and 850 cm^{-1} are due to the same vibrations as described in SP-PEP.

3.3 Paper III

In paper III, we studied the conformational changes of PK upon ligand binding. We first measured unlabeled and labeled PEP at pH 7.5, which is ionized state and the spectra are described in detail in paper II. We also measured the pyruvate spectrum at pH 7.5. The band observed at 1708 cm^{-1} is from keto carbonyl stretching vibration and the antisymmetric COO^- stretching vibration observed at 1600 cm^{-1} while the symmetric stretching vibrations observed at 1421 and 1399 cm^{-1} [64]. The band observed at 1358 cm^{-1} from the CH_3 deformation vibration and the band at 1175 cm^{-1} is due to the C- CH_3 stretching vibration [65].

We observed the infrared difference spectra of PK upon PEP binding in presence of the monovalent cation K^+ and diavalent cation Mg^{2+} at pH 7.5. All the spectra were recorded

at room temperature within 4 minutes after PEP addition. We observed conformational changes of PK upon the first addition of PEP in the amide I region while the subsequent additions (2nd and 3rd) showed no such changes. This indicates that the binding sites saturate upon the first addition of PEP. The initial spectrum at 84 s after the first addition is mainly due to the formation of the PK.PEP complex, whereas the 240 s spectrum contain absorption of both the PK.PEP complex and of free PEP. This is supported by the shift of symmetric PO_3^{2-} stretching band from 966 to 970 cm^{-1} , as the PEP concentration increases. The PO_3^{2-} band position in the 240 s spectrum of the first addition is still 4 cm^{-1} lower than in the 2nd and 3rd additions, which indicates that almost 50% free PEP are present at the end of the first addition. To measure the PK.PEP complex concentration we evaluated the protein band at 1696 cm^{-1} , which is not disturbed by free PEP. This band is not observed in the 2nd and 3rd addition which also indicates that binding is complete in the first addition.

The amide I region is sensitive to protein backbone structure and has been used for secondary structure analysis. According to literature [66-73], we assigned the band at 1696 cm^{-1} to turns or β - sheets, the band at 1663 cm^{-1} to α - helical structures and bands in the spectral region 1647-1621 cm^{-1} to β - sheets. The above band assignments are supported by spectra recorded in D_2O where these bands are found at slightly lower wavenumber. Thus the spectra indicate a conformational change of PK upon PEP binding. The antisymmetric stretching vibrations of carboxylate group were observed at 1590 and 1551 cm^{-1} , which is supported by their upshift in D_2O . Experiments with labeled $^{13}\text{C}_{2,3}$ PEP indicate that the antisymmetric carboxylate stretching vibration of bound PEP absorbs near 1590 cm^{-1} . The band position is 21 cm^{-1} upshifted compared to the band position in aqueous solutions. The other carboxylate band at 1551 cm^{-1} is not perturbed by labeled PEP. We assign it to the carboxylate group of a Asp or Glu residue, tentatively to that of Asp²⁷¹ or Glu²⁹⁵ residue which coordinate with Mg^{2+} or to Asp¹¹² which bind to K^+ [19]. The symmetric stretching vibration of carboxylate group observed at 1415 cm^{-1} , which is supported by the 3 cm^{-1} shift upon isotopic labeling. The band at 1485 cm^{-1} which is shifted in D_2O to 1467 cm^{-1} may originate from the CH_3 bending vibration from Thr³²⁷ [74], since Thr³²⁷ is present in the active site and interacts with the carboxylate group of L-phospholactate [19]. The bands (at lower wavenumber)

at 1214 and 968 cm^{-1} are from the C-O stretching vibration and PO_3^{2-} symmetric stretching vibration respectively of bound PEP. These bands of PEP are observed at 1229 and 974 cm^{-1} in solution, which indicates that binding, changes the geometry and bond strength of phosphate groups.

We measured the effects of the activating monovalent cations K^+ and Na^+ on PEP binding. α -helical and turn structures are perturbed in a similar way in the presence of both of cations but in the β -sheet region, we observed bands at 1647 and 1641 cm^{-1} in the presence of K^+ and Na^+ respectively. Differences were also observed for the symmetric stretching vibration of the PEP carboxylate, the band of which was at 1417 and 1415 cm^{-1} in the presence of Na^+ and K^+ respectively. The rest of the spectrum is very similar with both cations. We also measured the absorbance changes of PK upon Mg^{2+} binding in H_2O and D_2O . According to literature [73, 75, 76] and shifts upon deuteration, we assigned the bands as follows: 1694 cm^{-1} (H_2O) \rightarrow 1675 (D_2O) assigned to the C=O stretching vibration of Asn or Gln. 1664 cm^{-1} (H_2O) \rightarrow 1647 cm^{-1} (D_2O , Asn, Gln), 1664 cm^{-1} \rightarrow 1606 cm^{-1} (Arg), 1645 \rightarrow 1647 cm^{-1} (β -sheet, band shift probably only apparent because of overlap by other bands), 1645/1630 cm^{-1} \rightarrow 1606/1587 cm^{-1} (Arg), 1616, 1596 cm^{-1} (H_2O , not observed in D_2O , Asn, Gln), 1569/1545 cm^{-1} \rightarrow 1587/1569 cm^{-1} (Asp, Glu, shift is larger than usual probably because of overlap by other bands), 1485 cm^{-1} (H_2O) \rightarrow 1467 cm^{-1} (D_2O , CH_3 bending mode of Thr³²⁷, also observed upon PEP binding), 1545 cm^{-1} (H_2O , not observed in D_2O , amide II), 1417 cm^{-1} (H_2O) \rightarrow 1421 cm^{-1} (D_2O , Symmetric stretching of COO^- group). By use of infrared spectroscopy one can monitor the enzymatic reaction by directly observed the consumption of reactants and formation of products. Here, we measured the catalytic reaction of PK. We observed the formation of pyruvate bands at 1600, 1358 and 1176 cm^{-1} and of ATP bands at 1248-1232, 989, 914 cm^{-1} . The negative band observed at 940 cm^{-1} is due to ADP consumption and those at 975 and 1103 cm^{-1} due to PEP consumption.

We used the change of backbone structure and interaction (COBSI) index [12, 62] to quantify the structural changes of polypeptide backbone of PK upon PEP binding and found a value of 0.0014 that indicates that around 1% of the peptide groups contribute to the net change in backbone structure. We calculated the bond parameters of the phosphate group of bound PEP according to previous procedures [78-80] and concluded

that the bond dissociation energy of bound PEP in compared to free PEP is 1.4% weaker, which means that the bond energy is reduced by 6 kJ/mol upon PEP binding. Regarding bond parameter of the carboxylate group of bound PEP, we observed that the bond lengths of the carboxylate group are only little perturbed upon PEP binding.

4. Future objectives

4.1 Project I

Energy coupling in the Ca^{2+} ATPase

Aim

The aim of the project is to understand how chemical energy from ATP is converted to directional Ca^{2+} transport by the Ca^{2+} -ATPase. We will study the molecular mechanism by which substitutions of amino acids interfere with the communication between phosphorylation site and Ca^{2+} transport site by monitor their effects on conformational changes, the phosphate group environment, kinetics of partial reactions and whether Ca^{2+} is released using infrared spectroscopy.

Strategy: We will express and purify the recombinant ATPase and studied with the time resolved infrared spectroscopy. This technique enables the sensitive detection of the minute absorbance changes associated with Ca^{2+} transport. By using selected substitutions, we will monitor their effects on conformational changes, the phosphate group environment, and kinetics of partial reactions and whether Ca^{2+} is released.

4.2 Project II

Ligand binding detected by change in water absorption

Absorption of water molecules in bulk is different from the absorption of water molecules that in the hydration shell around the ligand and the protein. When two molecules associate some of the waters around them are released to bulk water, which could be exploited to detect ligand binding. This method is universally applicable to detect ligand binding since the transfer of water molecules from hydration shell to bulk water takes place in all binding events. It has strong potential for drug design.

The aim of this work is to determine whether this change in water interactions can be detected by the infrared spectroscopy.

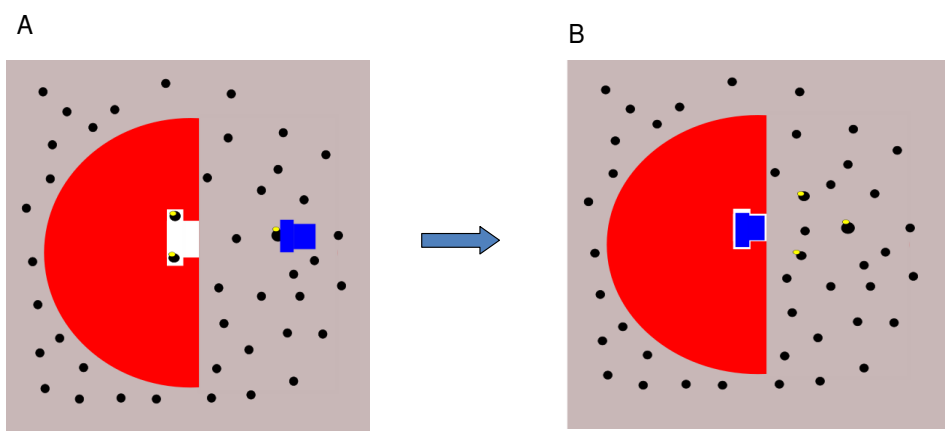


Figure 11. Illustrates the ligand binding upon water change. Fig A shows the protein (red), ligand (blue), bulk water (black) and bound water (black with yellow). Fig B shows release of bound water to bulk water upon ligand bound to protein.

Acknowledgements

This work is a step towards the fulfillment of my ambition to be a researcher.
My sincere gratitude to

Dr. Andreas Barth, I would like to thank for accepting me as a PhD student and his valuable guidance, advice unstinted support and encouragement. His innovative ideas, clear understanding of subject has left a deep impression on me.

Maria Krasteva, for the cooperation in paper I and her dedication to science, soft mannerism and encouraging words.

Maria E. Rudbeck, for the cooperation in Paper II where she did the computational part and her helpfulness.

Julia Anderson, Eeva-Liisa Karjalainen, Nadjeda Eremina for always be kind enough to give a solution to the problems and useful discussions.

Amelie Hardell, Harish, Henrik, Carolina, Gustav and all faculty and staff at the department, thank you for the support and congenial atmosphere.

Work support by **Lilly Lawskis, Vetenskapsrådet and Knut och Alice wallenbergs stiftelse** is gratefully acknowledged.

Endless love and encouragement given by my wife, parents and my family cannot be thanked in words. I owe them a lot.

6. References

1. Elliot A., Ambrose, E. J. Structure of synthetic polypeptides. *Nature*. 1950, 10;165 (4206):921–922.
2. Gerwert K (1999) Molecular Reaction Mechanisms of Proteins Monitored by Time-Resolved FTIR-Spectroscopy. *Biol Chem* 380: 931-935.
3. C. Zscherp and A. Barth, Reaction-Induced Infrared Difference Spectroscopy for the Study of Protein Reaction Mechanisms *Biochemistry* 40 (2001), 1875–1882.
4. W. Mäntele, Reaction-induced infrared difference spectroscopy for the study of protein function and reaction mechanisms. *Trends in Biochemical Sciences* 18 (1993), 197–202.
5. C. Jung. Insight into protein structure and protein-ligand recognition by Fourier transform infrared spectroscopy. *J. Molec. Recognit.* 13, 2000, 325–351.
6. C.W. Warton. Infrared spectroscopy of enzyme reaction intermediates *Nat. Prod. Rep.* 17 (2000), 447–453.
7. R. Vogel and F. Siebert. Vibrational spectroscopy as a tool for probing protein function *Curr. Opin. Chem. Biol.* 4 (2000), 518–523.
8. S. Kim and B. A. Barry. Reaction-induced FT-IR spectroscopic studies of biological energy conversion in photosynthesis and transport. 2001. *Journal of Physical Chemistry B*. 105, 4072-4083.
9. A. Barth, C. Zscherp (2000): Substrate binding and enzyme function investigated by infrared spectroscopy. *FEBS Lett.* 477, 151-156.
10. P.R. Carey and P.J. Tonge. Unlocking the Secrets of Enzyme Power Using Raman Spectroscopy. *Acc. Chem. Res.* 1995, 28, 8-13.
11. Deng, H., Callender, R. Raman spectroscopic studies of the structures, energetics and bond distortions of substrates bound to enzyme. *Meth. Enz.* 1999. 308, 176-201.
12. Barth, A., and Zscherp, C. 2002. What vibrations tell us about proteins, *Quart. Rev. Biophys.* 35, 369-430.
13. Surewicz, W. K., Mantsch, H. H., and Chapman, D. 1993. Determination of protein secondary structure by Fourier transform infrared spectroscopy: A critical assessment. *Biochemistry* 32, 389-394.
14. Seeholzer, S.H., Jaworowski, A., and Rose, I.A. 1991. Enolpyruvate: chemical

- determination as a pyruvate kinase intermediate. *Biochemistry* 30, 727-732.
15. Rose, I.A. 1970. Stereochemistry of pyruvate kinase, pyruvate carboxylase, and malate enzyme reactions. *J. Biol. Chem.* 245, 6052-6056.
 16. J. O. Wooll, R. H. E. Friesen, M. A. White. Structural and functional linkages between subunit interfaces in mammalian pyruvate kinase. *J. Mol. Biol.* 312, 525-540, 2001.
 17. Muirhead, H., Clayden, D. A., Barford, D., Lorimer, C. G., Fothergill-Gilmore, L. A., Schiltz, E. and Schmitt, W. 1986. The structure of cat muscle pyruvate kinase. *EMBO. J.* 5: 475-481.
 18. Larsen, T. M., M. M. Benning, I. Rayment, and G. H. Reed. 1998. Structure of the bis (Mg^{2+})-ATP-oxalate complex of the rabbit muscle pyruvate kinase at 2.1 Å resolution: ATP binding over a barrel. *Biochemistry* 37: 6247-6255.
 19. Larsen, T. M., M. M. Benning, G. E. Wesenberg, I. Rayment, and G. H. Reed. 1997. Ligand-induced domain movement in pyruvate kinase: structure of the enzyme from rabbit muscle with Mg^{2+} , K^+ and L-phospholactate at 2.7 Å resolution. *Arch. Biochem. Biophys.* 345: 199-206.
 20. Gupta, R. K., R. M. Osterling, and A. S. Mildvan. 1976. Dual divalent cation requirement for activation of pyruvate kinase: essential roles of both enzyme and nucleotide bound metal ions. *Biochemistry* 15:2881-2887.
 21. Gupta, R. K. and A. S. Mildvan. 1977. Structures of enzyme-bound metal nucleotide complexes in the phosphoryl transfer reaction of muscle pyruvate kinase. *J. Biol. Chem.* 252:5967-5976.
 22. Baek, Y. H., and T. Nowak. 1982. Kinetic evidence for a dual cation role for muscle pyruvate kinase. *Arch. Biochem. Biophys.* 217:491-497.
 23. Boyer, P. D., H. A. Lardy, and P. H. Phillips. (1942). The role of potassium in muscle phosphorylations. *J. Biol. Chem.* 146:673-682.
 24. Kayne, F. J. 1973. Pyruvate kinase. *Enzymes* (Boyer, P. D., ed.), pp 353-382, Academic, New York.
 25. Nowak, T., and C. H. Suelter. 1981. Pyruvate kinase: activation by and catalytic role of the monovalent and divalent cations. *Mol. Cell. Biochem.* 35:65-75.
 26. Suelter, C. H., R. Jr. Singleton, F. J. Kayne, S. Arrington, J. Glass, and A. S.

- Mildvan. 1966. Studies on the interaction of substrate and monovalent and divalent Cations with pyruvate kinase. *Biochemistry*, 5(1): 131-139.
27. Wilson, H. R., J. H. Evans, and R. R. Becker. 1967. The effect of univalent cation salts on the stability and on certain physical properties of pyruvate kinase. *J. Biol. Chem.* 242: 3825-3832.
 28. Mildvan, A. S., and M. Cohn. 1966. Kinetics and magnetic resonance studies of pyruvate kinase reaction. II. complexes of enzyme, metal and substrates. *J. Biol. Chem.* 241: 1178-1193.
 29. Larsen, T. M., T. Laughlin, H. M. Holden, I. Rayment, and G. H. Reed. 1994. Structure of rabbit muscle pyruvate kinase complexed with Mn^{2+} , K^{+} and pyruvate. *Biochemistry*, 33: 6301-6309.
 30. Nowak, T. 1978. Structural changes at the active site of pyruvate kinase during activation and catalysis. *J. Biol. Chem.* 253:1998-2004.
 31. Pissard, S., Max-Audit, I., Skopinski, L., Vasson, A., Vivien, P., Bimet, C., Goossens, M., Galacteros, F., and Wajcman, H. 2006. Pyruvate kinase deficiency in france: a 3 year study reveals 27 new mutations. *Birt. J. haem.* 133, 687-689.
 32. Etiemble, J., Picat, C., Dhermy, D., Buc, Ha., Morin, M., Boivin, P. (1984). Erythrocytic pyruvate kinase deficiency and hemolytic anemia inherited as a dominant trait. *American journal of hematology* 17 (3): 251–60
 33. Carey, P., Chandler, J., Hendrick, A., Reid, M., Saunders, P., Tinegate, H., Taylor, P. West, N. (2000). Prevalence of pyruvate kinase deficiency in northern European population in the north of England. Northern Region Haematologists Group. *Blood* 96 (12): 4005–6.
 34. Colthup, N., Daly, L. and Wiberley, S. 1990. Introduction to infrared and Raman spectroscopy, 3rd edition, Academic press, Inc., Boston.
 35. Cooley, James W., and John W. Tukey. 1965. An algorithm for the machine calculation of complex Fourier series. *Math. Comput.* 19, 297–301.
 36. Fringeli, U. P. 1992. in *Internal Reflection Spectroscopy. Theory and applications*, (Mirabella, F. M., ed.) p. 255, Marcel Dekker Inc. NY.
 37. Harrick, N. J. 1979. in *Internal Reflection Spectroscopy*. Harrick Scientific Corp., Ossining, NY.

38. Goormaghtigh E, Raussens V, Ruyschaert JM. Attenuated total reflection infrared spectroscopy of proteins and lipids in biological membranes. *Biochim Biophys Acta*. 1999 Jul 6;1422(2):105–185.
39. Van Holde, K. E. 1971. A good description of the theory of ligand binding. *Physical Biochemistry*. Prentice Hall.
40. David Freifelder. 1982. Application to biochemistry and molecular biology. *Physical Biochemistry*. 2nd Ed. W. H. Freeman & Company, San Francisco.
41. W. S. Bennett and R. Huber. 1984. Structural and functional aspects of domain motions in proteins. *Crit. Rev. Biochem.* 15, 291-384.
42. J. Janin and C. Chothia. 1990. The structure of protein- protein recognition sites. *J. Biol. Chem.* 265, 16027-16030.
43. S. J. Wodak. 1987. Computer studies of interactions between macromolecules. *Prog. Biophys. Mol. Biol.* 49, 29-63.
44. Brown, I. D. 2002. The chemical bond in inorganic chemistry. The bond valence model, Oxford University Press, Oxford.
45. Brown, I. D., and Shannon, R. D. 1973. Empirical bond-strength-bond-length curves for oxides. *Acta Cryst. A*. 29:266-282.
46. Brown, I. D., and Wu, K. K. 1976. Empirical parameters for calculating cation-oxygen bond valences. *Acta Cryst. B*. 32:1957-1959.
47. Ziolkowski, J. 1983. Advanced bond-strength model of active sites on oxide catalysis. *J. Catal.* 84:317-332.
48. Ziolkowski, J., and Dziembaj, L. 1985. Empirical relationship between individual cation-oxygen bond length and bond energy in crystals and in molecules. *J. Solid State Chem.* 57:291-299.
49. Ziolkowski, J. 1985. New relation between ionic radii, bond length, and bond strength. *J. Solid State Chem.* 57:269-290.
50. Barth, A., and W. Mäntele. 1998. ATP-induced phosphorylation of the sarcoplasmic reticulum Ca^{2+} ATPase: molecular interpretation of infrared difference spectra. *Biophys. J.* 75:538-544.
51. Takeuchi, H., H. Murata, and I. Harada. 1988. Interaction of adenosine 5' triphosphate with Mg^{2+} : vibrational study of coordination sites by use of O^{18} labeled

- triphosphates. J. Am. Chem. Soc. 110:392-397.
52. Voet, D., Voet, J. G., Pratt, C. W. Life at the molecular level. Fundamental of Biochemistry. 2nd Ed. John Willy and Sons Inc. 2006.
53. Fahmy, K. 1998. Binding of transducin and transducin-derived peptides to rhodopsin studied by attenuated total reflection Fourier transform infrared difference spectroscopy. Biophys. J. 75:1306-1318.
54. Krasteva, M., S. Kumar, and A. Barth. 2006. A dialysis accessory for attenuated total reflection infrared spectroscopy. Spectroscopy 20:89-94.
55. Gourion-Arsiquaud, S., S. Chevance, P. Bouyer, L. Garnier, J.-L. Montillet, A. Bondon, and C. Berthomieu. 2005. Identification of a Cd²⁺ and Zn²⁺ binding site in cytochrome *c* using FTIR coupled to an ATR microdialysis setup and NMR spectroscopy. Biochemistry, 44: 8652-8663.
56. Baenziger, J. E., Chew, J. P. (1997) Desensitization of the nicotinic acetylcholine receptor mainly involves a structural change in the solvent-accessible regions of the polypeptide backbone. Biochemistry 36:3617–3624.
57. F. Scheirlinckx, V. Raussens, J.-M. Ruyschaert and E. Goormaghtigh. Conformational changes in the gastric H⁺, K⁺- ATPase monitored by difference FTIR spectroscopy and hydrogen deuterium exchange. Biochem. J. 382 (2004), 121–129.
58. Nyquist RM, Heitbrink D, Bolwien C, Wells TA, Gennis RB, Heberle J. Perfusion-induced redox differences in cytochrome c oxidase: ATR/FT-IR spectroscopy. FEBS Lett. 2001 Sep 7;505(1):63–67.
59. D. Moss, E. Nabadryk, J. Breton and W. Mänte. Redox-linked conformational changes in proteins detected by a combination of infrared spectroscopy and protein electrochemistry. Eur. J. Biochem. 187 (1990), 565–572.
60. D. D. Schlereth and W. Mänte. Redox-induced conformational changes in myoglobin and hemoglobin: electrochemistry and ultraviolet-visible and Fourier transform infrared difference spectroscopy at surface-modified gold electrodes in an ultra-thin-layer spectroelectrochemical cell. Biochemistry 32 (1993), 1118–1126.
61. Ataka, K. and Heberle, J. (2003) Electrochemically induced surface-enhanced infrared difference absorption (SEIDA) spectroscopy of a protein monolayer. J. Am. Chem. Soc. 125, 4986–4987.

62. Barth, A., F. Von Germar, W. Kreutz, and W. Mänte. 1996. Time resolved infrared spectroscopy of the Ca^{2+} ATPase: the enzyme at work. *J. Biol. Chem.* 271: 30637-30646.
63. Von Germar, F., Barth, A., Mänte, W. Structural changes of the sarcoplasmic reticulum $\text{Ca}(2+)$ -ATPase upon nucleotide binding studied by fourier transform infrared spectroscopy. *Biophys J.* 2000, 78(3):1531–1540.
64. Wright, W. W., and J. Vanderkooi. 1997. Use of IR absorption of the carboxyl group of amino acids and their metabolites to determine pKs, to study proteins and to monitor enzymatic activity. *Biospectroscopy* 3:457-467.
65. Kakihana, M., and M. Okamoto. 1984. Vibrational analysis of pyruvate ion molecules and estimation of equilibrium constants for their hydrogen isotopic exchange reactions. *J. Phys. Chem.* 88: 1797-1804.
66. Susi, H., and D. M. Byler. 1987. Fourier transform infrared study of proteins with parallel beta chains. *Arch. Biochem. Biophys.* 258:465-469.
67. Arrondo, J. L. R., N. M. Young, and H. H. Mantsch. 1988. The solution structure of concanavalin a probed by FTIR spectroscopy. *Biochem. Biophys. Acta* 952:261-268.
69. Krimm, S., and J. Bandekar. 1986. Vibrational spectroscopy and conformation of peptides, polypeptides and proteins. *Adv. Prot. Chem.* 38:181-367.
70. Arrondo, J. L. R., A. Muga, J. Castresana, and F. M. Goni. 1993. Quantative studies of the structure of proteins in solution by Fourier transform infrared spectroscopy. *Prog. Biophys. Mol. Biol.* 59:23-56.
71. Jackson, M., and H. H. Mantsch. 1995. The use and misuse of FTIR spectroscopy in the determination of protein structure. *Crit. Rev. Biochem. Mol. Biol.* 30:95-120.
72. Barth, A. 2007. Infrared spectroscopy of proteins. *Biochim. Biophys. Acta–Bioenergetics* 1767:1073-1101.
73. Barth, A. 2000. The infrared absorption of amino acid side chains. *Prog. Biophys. Mol. Biol.* 74:141-173.
74. Pawluko, A., Leciejewicz, J., Tomkinson, J. and Parker, S. F. 2001. Neutron Scattering, infrared, Raman spectroscopy and ab initio study of L- threonine. *Spectrochimica. Acta A.* 57:2513-2523.
75. Chiragadze, Y. N., O. V. Fedorov, and N. P. Trushina. 1975. Estimation of amino

- acid residue side-chain absorption in the infrared spectra of protein solutions in heavy water. *Biopolymers* 14:679-94.
76. Venyaminov, S. Y., N. N. Kalnin. 1990. Quantitative IR spectrometry of peptide compounds in water (H₂O) solutions 1. Spectral parameters of amino-acid residue absorption bands. *Biopolymers* 30:1243-57.
 77. Thoenges, D., and A. Barth. 2002. Direct measurement of enzyme activity with infrared spectroscopy. *J. Biomol. Screen.* 7:353-357.
 78. Barth, A., and Bezlyepkina, N. 2004. P-O bond destabilization accelerates phosphoenzyme hydrolysis of sarcoplasmic reticulum Ca²⁺-ATPase. *J. Biol. Chem.* 279:51888-51896.
 79. Deng, H., Wang, J., Callender, R., and Ray, W. J. 1998. Relationship between bond stretching frequencies and internal bonding for [¹⁶O4] - and [¹⁸O4]phosphates in aqueous solution. *J. Phys. Chem. B.* 102:3617-3623.
 80. Brown, I. D. 2002. The chemical bond in inorganic chemistry. The bond valence model, Oxford University Press, Oxford.
 81. Carafoli, E. 2002. Calcium signaling: a tale for all seasons. *Proc. Natl. Acad. Sci. USA* 99, 1115-1122.
 82. Toyoshima, C., and G. Inesi. 2004. Structural basis of ion pumping by Ca²⁺-ATPase of the sarcoplasmic reticulum. *Annu. Rev. Biochem.* 73, 269–292.
 83. Lodish, H., Berk, A., Zipursky, S. L., Matsudaira, P., Baltimore, D., and Darnell, J. E. 1999. *Molecular Cell Biology*, 4th Edition, W.H. Freeman and Company, New York.
 84. Alberts, B., Bray, D., Lewis, J., Raff, M., Roberts, K., and Watson, J.D., *Molecular Biology of the cell*, 4th Edition, Garland Science, New York, 2001.
 85. Toyoshima, C., Nakasako, M., Nomura, H., and Ogawa, H. 2000. Crystal structure of the calcium pump of sarcoplasmic reticulum at 2.6 Å resolution, *Nature* 405, 647-655.
 86. Meis, L. D., and Vianna, A. 1979. Energy interconversion by the Ca²⁺ dependent ATPase of the sarcoplasmic reticulum, *Annu. Rev. Biochem.* 48, 275-292.
 87. Sørensen, T. L., Møller, J. V., and Nissen, P. 2004. Phosphoryl transfer and calcium ion occlusion in the calcium pump. *Science* 304, 1672-1675.

Paper I

A dialysis accessory for attenuated total reflection infrared spectroscopy

Maria Krasteva, Saroj Kumar and Andreas Barth *

Department of Biochemistry and Biophysics, Stockholm University, Stockholm, Sweden

Abstract. A dialysis accessory for attenuated total reflection (ATR) infrared spectroscopy is described together with an evaluation based on known systems with well-studied infrared spectra, such as chemical oxidation and reduction of cytochrome *c* and substrate binding to the Ca^{2+} -ATPase. Changes in the infrared spectra of the two proteins are successfully monitored with the dialysis accessory. The accessory was developed in our laboratory for the diamond 9-reflections SensIR ATR unit. It can be used to study absorbance changes of macromolecules which are induced by low molecular weight compounds, for example the binding of substrates, inhibitors or ions to macromolecules as well as effects of pH, ionic strength or denaturants on the structure of macromolecules. The dialysis accessory confines the macromolecule of interest to a sample compartment created between the ATR crystal and the dialysis membrane. On the other side of the dialysis membrane, a reservoir for the sample medium is created. In this way the low molecular weight compound of interest can exchange freely between the reservoir and the sample compartment via the dialysis membrane. This provides a flexible way to change sample conditions for the macromolecule of interest, allowing for example initiation of ligand binding.

Keywords: Dialysis, attenuated total reflection, ATR, vibrational spectroscopy, FTIR, ligand binding, protein

Abbreviations: FTIR-ATR = Fourier-transformed infrared attenuated total reflection; ATP = adenosine-5'-triphosphate.

1. Introduction

The use of reaction induced infrared (IR) difference spectroscopy yields valuable structural information at great detail [1–7]. A disadvantage of experiments using conventional transmission spectroscopy is the limited possibility to manipulate the sample once the IR cuvette has been closed. This has been overcome partly by applying attenuated total reflection (ATR) IR spectroscopy [8–10]. ATR spectroscopy for protein studies is mostly applied to protein films deposited on the internal reflection element. The ligands or in general any interacting compounds are exchanged on top [11–14]. Multiple experiments can be performed with different ligands on the same protein sample which saves material and time. In such experiments care must be taken so that the film is not disrupted during washing or repeated additions and withdrawals of the medium. Closing off a sample compartment by a dialysis membrane allows for precise variations of the sample conditions in a controlled way [15]. It also makes it possible to use ATR for proteins in solution. The protein is confined to a sample compartment between ATR crystal and dialysis membrane. Small molecules on the other hand can exchange freely between the reservoir and

*Corresponding author: A. Barth, Department of Biochemistry and Biophysics, The Arrhenius Laboratories for Natural Sciences, Stockholm University, S-106 91 Stockholm, Sweden. Tel.: +46 8 162452; Fax: +46 8 155597; E-mail: Andreas.Barth@dbb.su.se.

the sample compartment via the dialysis membrane. In this way one can initiate ligand binding or otherwise change sample conditions in the sample compartment. The first reported use of a dialysis setup in protein studies introduces guanosine-5'-triphosphate (GTP) *via* diffusion through the dialysis membrane and follows the effect of GTP on a complex of the membrane protein rhodopsin with transducin [15]. Another application of dialysis ATR is the preparation of an oriented monomolecular film of porin Omp32 on a Ge internal reflecting element. Dialysis is utilized here to wash away a detergent present initially in the protein sample in order to start film formation [16]. Application of a dialysis setup for the study of metal ion binding to a soluble protein, cytochrome *c*, was described recently [17]. There is a similar dialysis set up reported by Agic et al. [18]. Both dialysis devices are built for the same ATR accessory from SensIR Technology as ours. That described in [17] uses a flow-through cell commercially available from the same company and needs 2 μl of sample. That described in [18] is based on home-built cell for 4 μl of sample. There is a dialysis setup commercially available from Bruker Optics which needs 50 μl in the sample compartment (Anders Nilsson, Bruker Optics Scandinavia AB, private communication). Here we report our setup for the diamond 9 reflections SensIR FTIR-ATR accessory with a sample compartment of 3 μl .

2. Materials and methods

Circles of 8 mm in diameter, cut out of cellulose sheets CelluSep F3 of MWCO 12000–14000 dialysis membranes (Orange Scientific, Belgium), were used for the dialysis accessory.

Horse heart cytochrome *c* (cyt *c*) was purchased from Sigma and used without further purification. The cyt *c* samples were prepared in 100 mM phosphate buffer pH 6.8, containing 100 mM KCl. The final concentration of cyt *c* was 8 mM. Solutions of potassium ferricyanide and sodium dithionite for cyt *c* oxidation and reduction were both 200 mM.

The FTIR spectra of cyt *c* were recorded at 4 cm^{-1} resolution on a Bruker Vertex 70 FTIR spectrometer equipped with an MCT detector. The experiments were performed at room temperature. Cyt *c* was equilibrated by continuous diffusion of medium (phosphate buffer with KCl) across the dialysis membrane. After the absorption spectrum of the sample became stable, a 500 scan single beam spectrum (background spectrum) was recorded. Then 4 μl of potassium ferricyanide (200 mM) were added to the reservoir after which an acquisition of repeated spectra in the absorption mode, 150 scans each, was initiated. Under these conditions, oxidation of cyt *c* was first detected after 20 seconds and monitored until it was complete after 5 minutes. The system was brought back to the initial state by exchanging three to four times the sample medium in the reservoir with fresh one in 5–10 minute intervals. Cyt *c* was reduced by adding 2 μl sodium dithionite (200 mM) to the reservoir. The reaction was also first detected 20 seconds later and a completion was reached 5 minutes later. Typically, one oxidation-reduction cycle was carried out for 30–40 min.

Ca^{2+} -ATPase was measured in a medium of 100 mM TRIS pH 7 with 10 μM MgCl_2 , 100 μM CaCl_2 and 100 mM KCl. A stock solution of Ca^{2+} -ATPase sarcoplasmic reticulum vesicle suspension, prepared as given in [19] (80 μl), was dialyzed for 1 hour in 10 times diluted medium, then concentrated to a final concentration of around 150 mg/ml by adding aliquots of 20 μl on the ATR crystal and drying with a flow of N_2 . The last 8 μl were used for closing the dialysis setup. The FTIR spectra of Ca^{2+} -ATPase were recorded at 4 cm^{-1} resolution on a Bruker IFS 66/S spectrometer equipped with an MCT detector. The temperature for these measurements was 5°C. Single beam background spectra were taken with 1000 scans. Then the Ca^{2+} -ATPase substrate adenosine-5'-triphosphate (ATP), disodium salt, was added as 2 μl of 60 mM solution to the reservoir and several spectra recorded with 300 scans each.

3. The dialysis accessory

3.1. Description

The sample is placed between the total reflection surface of the ATR reflection element and the dialysis membrane (Fig. 1). The membrane is fixed by an O-ring, which snaps into a groove on the bottom conical part of the ligand reservoir. The reservoir is made of delrin – a polyacetal resin polyoxymethylene. The reservoir is let slide down in a cylindrical opening of a thermostating block, which can be assembled and secured tightly to the ATR bench. It sits on the horizontal plane of the metal block that covers the ATR unit. The height of the dialysis membrane above the internal reflection element is determined by the height of the bottom conical part of the reservoir. The ligand reservoir is pressed down by a screw cap which screws onto a thread on the thermostating block. The O-ring makes a tight contact with the walls of the conical dip in the metal block of the ATR unit. Thus a tight closure of the sample compartment is achieved while no pressure is exerted on the total reflection surface of the ATR reflection element. The latter point is crucial since the diamond ATR crystal, although inert and therefore not demanding in terms of the nature of the liquid samples measured, is on the other hand very sensitive to pressure since it is a thin diamond plate supported only on the periphery and not across the entire surface. The setup reported by Gourion-Arsiquaud et al. [17] uses pressure on the periphery which might impose the risk of breaking the crystal.

3.2. Operation of the dialysis accessory

The dialysis membrane is first soaked for 1–2 min in double distilled water and transferred without drying to the end of the conical opening of the reservoir. The membrane is attached to the reservoir by snapping a wet O-ring into the groove on the reservoir. The reservoir is then filled with the sample medium. A drop of 4 μl from our protein sample solution is placed on the total reflection surface of the ATR crystal. Another 4 μl of the sample are deposited as a hanging drop on the dialysis membrane at the bottom of the reservoir. The reservoir slides down the opening in the thermostating block and the setup is closed with the screw cap on top. The solution in the reservoir is stirred constantly with a small mechanical stirrer attached at the top. Initially we were closing with a total of 8 μl sample volume and the controls we did and show in the paper are with 8 μl but later we found out that the setup can work with as little as 3 μl .

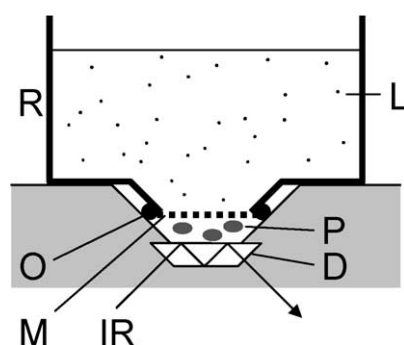


Fig. 1. Dialysis accessory for the diamond 9 reflections SensIR ATR unit. R: reservoir, O: O-ring, M: dialysis membrane, IR: infrared beam, D: diamond plate, P: protein (as an example for a macromolecule), L: ligand (as an example for the low molecular weight compound).

3.3. Equilibrating the system before the beginning of the experiments

Two to three hours after assembling the unit experiments can be started. The reason for the waiting time is that the absorption of the sample changes due to processes within the protein sample. The smaller the concentration of the sample is, the shorter it takes to obtain a stable absorption. Even if dialyzed protein is transferred to the ATR crystal, and the reservoir contains the dialysis buffer, it takes time before the absorption is stable. In our experiments, the ligands were added as solutions with the same concentrations of buffer and salts as the sample medium in the reservoir. A second possibility is to exchange the medium in the reservoir with a fresh one that has the same composition as before and in addition contains the ligand of interest (results not shown).

4. Results and discussion

A first test of our dialysis accessory was whether low molecular weight compounds added to the reservoir would arrive in the sample compartment. Multiple additions of for example ATP to the reservoir revealed that signals of added compounds can be observed within 10 s after the addition if the ligand is at high concentrations (10^{-2} M range final concentration). At lower concentrations (10^{-4} – 10^{-5} M range) the times lengthens 10-fold to 100 seconds. In these measurements the arrival of the low molecular weight compound in the sample compartment was detected directly via the infrared absorption of the compound. This is generally no longer possible if the concentration is in the μ M range. Recent measurements on a soluble protein and its inhibitor showed that at these concentrations (10^{-6} M range), arrival of the ligand in the sample compartment can be detected indirectly from difference signals arising from changes in the protein bands upon protein-ligand interaction and they take longer times to be observed (10–40 minutes, results not shown).

The difference spectra corresponding to reduction and reoxidation of cyt *c* are presented in Fig. 2. The two spectra are almost exact mirror images of each other. Both spectra are found to be fully reproducible in a large number of cycles of a single sample and display all the spectral features found in previous infrared studies of redox induced changes in the infrared absorption of cyt *c* [17,20–22]. In the earlier work, reduction and oxidation of cyt *c* was induced by electrochemical means. These reports also contain detailed analyses of the spectra with the current state of the band assignments. The agreement with previous results shows that our dialysis accessory can be used to obtain high quality spectra of a protein reaction. We note that the observed absorbance changes are smaller than 0.1% of the typical absorbance of an aqueous protein sample in transmission experiments.

Difference spectra of the Ca^{2+} -ATPase revealing the changes in protein absorption after the addition of ATP are presented in Fig. 3. Spectrum A was recorded 80 s after the addition and represents changes in the absorption that are not related to ATP binding to the ATPase. The two largest bands in this spectrum at 1531 and 1067 cm^{-1} coincide with bands of the buffer tris. These changes persist throughout the measurements and can be seen together with the changes in the protein observed at later times (Fig. 3B, 120 seconds after the addition). Figure 3C presents the spectrum in Fig. 3B corrected for the buffer absorbance change seen in Fig. 3A. The observed signals agree with spectra taken in the transmission mode, considered indicative of nucleotide binding to the Ca^{2+} -ATPase [23,24]. They were obtained using caged compounds, which photolytically release the compound of interest from an biologically inactive photosensitive precursor. While this approach is powerful, it requires the synthesis of an appropriate caged compound which is time-consuming and might be difficult to achieve. The work presented here shows that dialysis coupled ATR spectroscopy can be used as an alternative to monitor ligand binding to proteins.

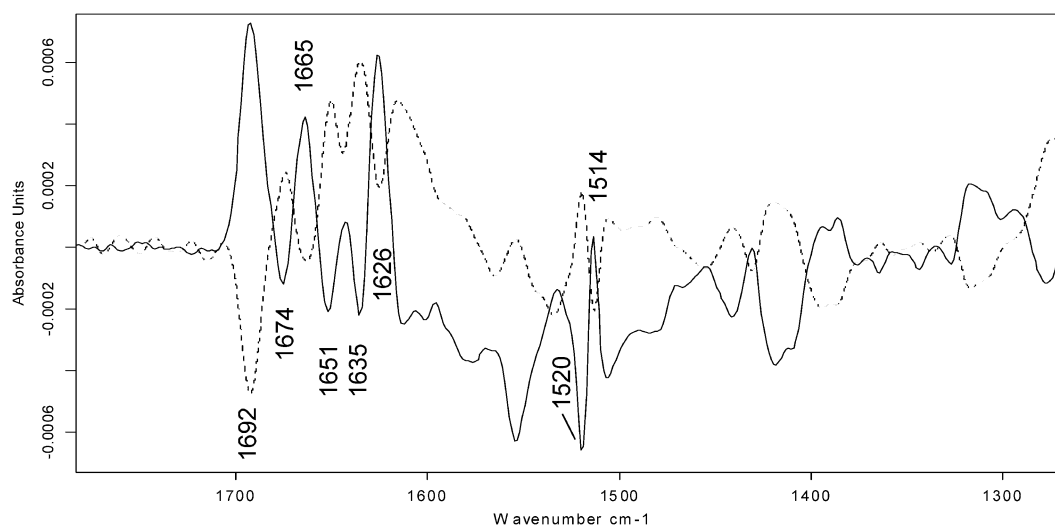


Fig. 2. Infrared difference spectra of reduced minus oxidized cyt *c* (solid line) and of oxidized minus reduced cyt *c* (dotted line). Reduced minus oxidized cyt *c* was obtained upon addition of reducing agent sodium dithionite ($2\ \mu\text{l}$, $200\ \text{mM}$) to the reservoir of the ATR accessory (final concentration $1 \times 10^{-4}\ \text{M}$). Concentrations in the sample compartment were $8\ \text{mM}$ cyt *c*, $100\ \text{mM}$ phosphate buffer, pH 6.8, $100\ \text{mM}$ KCl. Oxidized minus reduced cyt *c* was obtained upon addition of oxidizing agent potassium ferricyanide ($4\ \mu\text{l}$, $200\ \text{mM}$, final concentration $2 \times 10^{-4}\ \text{M}$).

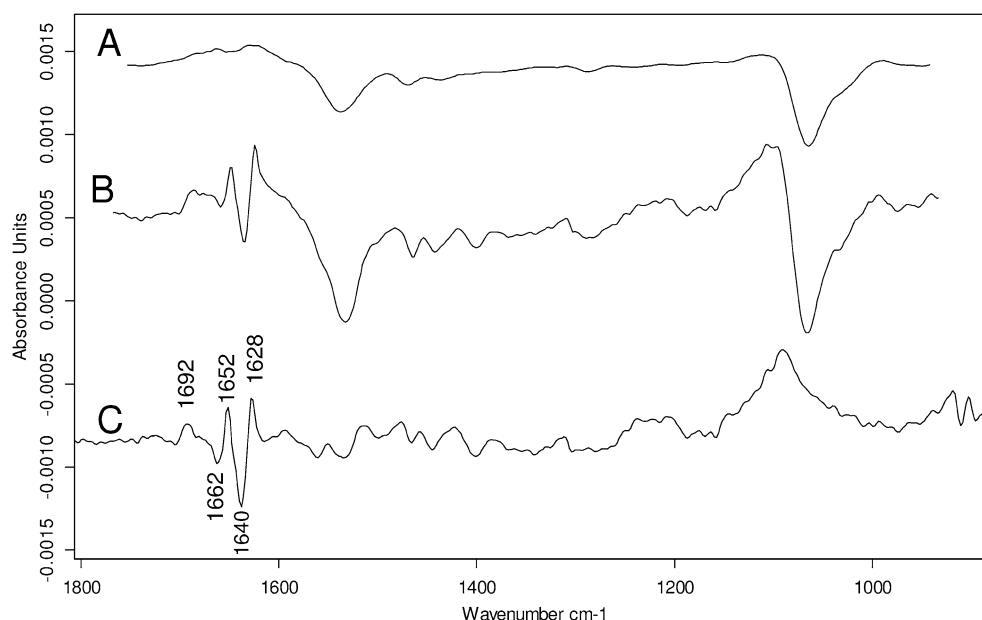


Fig. 3. Infrared difference spectra of Ca^{2+} -ATPase representing changes upon addition of ATP ($2\ \mu\text{l}$, $60\ \text{mM}$, final concentration $3 \times 10^{-5}\ \text{M}$) via perfusion through the dialysis membrane of the dialysis accessory. A: observed spectral changes $80\ \text{s}$ after the addition; B: $120\ \text{s}$ after the addition; C: Ca^{2+} -ATPase changes $120\ \text{s}$ after the addition (spectrum B) corrected for the baseline changes seen in spectrum A.

5. Conclusions

While reaction-induced infrared difference spectroscopy is a highly sensitive and highly informative method, the difficulty of inducing reactions or perturbations has been a major bottleneck for its general usability. The use of dialysis accessories to ATR units is becoming to overcome this bottleneck since it provides a general method to study perturbations of macromolecules with infrared spectroscopy. This work describes our dialysis accessory for the 9 reflections SensIR ATR unit and we showed that high quality spectra can be obtained with it using two examples – chemical oxidation and reduction of cytochrome *c* and substrate binding to the Ca^{2+} -ATPase. As dialysis coupled ATR infrared spectroscopy makes infrared spectroscopy a more universal method, in particular for studying the binding of small molecules to macromolecules, we expect infrared spectroscopy to expand to new fields, for example to that of drug development.

Acknowledgements

The authors are grateful to W. Hasselbach (Max-Planck-Institut, Heidelberg) for the gift of Ca^{2+} -ATPase. This work was supported by Vetenskapsrådet projektbidrag 621-2002-5884, and Knut och Alice Wallenbergs Stiftelse bidrag 2002.0115. MK acknowledges a post-doc grant from Wenner-Grenska Samfundet.

References

- [1] C. Zscherp and A. Barth, *Biochemistry* **40** (2001), 1875–1882.
- [2] S. Kim and B.A. Barry, *J. Phys. Chem.* **105** (2001), 4072–4083.
- [3] K. Gerwert, *Biol. Chem.* **380** (1999), 931–935.
- [4] C. Jung, *J. Molec. Recognit.* **13** (2000), 325–351.
- [5] W. Mänteles, *Trends in Biochemical Sciences* **18** (1993), 197–202.
- [6] C.W. Warton, *Nat. Prod. Rep.* **17** (2000), 447–453.
- [7] R. Vogel and F. Siebert, *Curr. Opin. Chem. Biol.* **4** (2000), 518–523.
- [8] N.J. Harrick, in: *Internal Reflection Spectroscopy*, Harrick Scientific Corp., Ossining, NY, 1979.
- [9] U.P. Fringeli, in: *Internal Reflection Spectroscopy. Theory and applications*, Quantum Chemical Corp., Morris, IL, 1992.
- [10] E. Goormaghtigh, V. Raussens and J.-M. Ruysschaert, *Biochim. Biophys. Acta* **1422** (1999), 105–185.
- [11] J.E. Baenzinger and J.P. Chew, *Biochemistry* **36** (1997), 3617–3624.
- [12] U.P. Fringeli, H.-J. Apell, M. Fringeli and P. Läger, *Biochim. Biophys. Acta* **984** (1989), 301–312.
- [13] F. Scheirlinckx, V. Raussens, J.-M. Ruysschaert and E. Goormaghtigh, *Biochem. J.* **382** (2004), 121–129.
- [14] R.M. Nyquist, D. Heitbrink, C. Bolwien, T.A. Wells, R.B. Gennis and J. Heberle, *FEBS Lett.* **505** (2001), 63–67.
- [15] K. Fahmi, *Biophys. J.* **75** (1998), 1306–1318.
- [16] M. Schwarzott, H. Engelhardt, T. Kluehspies, D. Baurecht, D. Naumann and U.P. Fringeli, *Langmuir* **19** (2003), 7451–7459.
- [17] S. Gourion-Arsiquaud, S. Chevance, P. Bouyer, L. Garnier, J.-L. Montillet, A. Bondon and C. Berthomieu, *Biochemistry* **44** (2005), 8652–8663.
- [18] E. Agic, O. Klein and W. Mänteles, in: *Book of Abstracts, 10th European Conference on the Spectroscopy of Biological Molecules*, Aug. 30–Sept. 4 (2003), Szeged, Hungary.
- [19] L. De Meis and W. Hasselbach, *J. Biol. Chem.* **246** (1971), 4759–4763.
- [20] D. Moss, E. Nabadryk, J. Breton and W. Mänteles, *Eur. J. Biochem.* **187** (1990), 565–572.
- [21] D.D. Schlereth and W. Mänteles, *Biochemistry* **32** (1993), 1118–1126.
- [22] K. Ataka and J. Heberle, *JACS* **126** (2004), 9445–9457.
- [23] A. Barth, F. von Germar, W. Kreutz and W. Mänteles, *J. Biol. Chem.* **271** (1996), 30637–30646.
- [24] F. von Germar, A. Barth and W. Mänteles, *Biophys. J.* **78** (2000), 1531–1540.

Paper II

Infrared Spectrum of Phosphoenol Pyruvate: Computational and Experimental Studies

Maria E. Rudbeck,^{*,†} Saroj Kumar,[†] Maria-Andrea Mroginski,[‡] Sten O. Nilsson Lill,[§] Margareta R. A. Blomberg,[§] and Andreas Barth^{*,†}

Department of Biochemistry and Biophysics, The Arrhenius Laboratories for Natural Sciences, Stockholm University, SE-106 91 Stockholm, Sweden, Institut für Chemie, Max-Volmer-Laboratorium, TU Berlin, PC 14, Straße des 17. Juni 135, D-10623 Berlin, Germany, and Department of Physics, Albanova, and Department of Biochemistry and Biophysics, The Arrhenius Laboratories for Natural Sciences, Stockholm University, SE-106 91 Stockholm, Sweden

Received: October 31, 2008; Revised Manuscript Received: January 16, 2009

The infrared spectrum of phosphoenol pyruvate (PEP) in aqueous solution was studied experimentally and theoretically in its fully ionized, singly protonated and doubly protonated form. The density functional theory with the B3LYP functional and with the 6-31G(d,p), 6-31++G(d,p), and 6-311++G(d,p) basis sets were used in the theoretical study. The calculations with the two latter basis sets and the CPCM continuum model for water showed good agreement with the experiments except for vibrations assigned to hydroxyl groups. These needed to be modeled with explicit water molecules. The effects of deuteration and of $^{13}\text{C}_{2,3}$ labeling of PEP were reproduced by the calculations.

Introduction

Glycolysis is a sequence of reactions which converts glucose to pyruvate and which produces small amounts of ATP. The final step is catalyzed by the enzyme pyruvate kinase (PK) and is a substrate-level phosphorylation step, forming pyruvate from phosphoenol pyruvate (PEP); see Figure 1. Transfer reactions of phosphate groups from phosphate esters, such as PEP, play a fundamental role in biological processes including metabolism, cell signaling and regulation.^{1–3}

Infrared spectroscopy is a powerful method to obtain information about the structure and function of molecules. It is used to provide information on several different properties such as bond lengths, bond strengths, protonation states, hydrogen bonding, and conformational changes. Assigning experimentally observed absorption bands to vibrational modes is not always straightforward, and usually several strategies are needed, for example, a combination of computational and experimental studies. Using quantum mechanical methods to calculate frequencies and intensities in order to assign the experimentally observed absorption bands to particular vibrations is today a widespread method. The calculated results can be further analyzed, regarding the composition of each normal mode, for example by animated atomic motion or by calculating the potential energy distribution (PED) of each normal mode.

Previously, computational and experimental studies have been performed on both the product pyruvate^{4–7} and on other monoester phosphates, especially dimethyl phosphate.^{8–13} Regarding PEP, the influence of hydrogen bonding between its phosphate group and water has been investigated;¹⁴ however, that study focused on the phosphate group and did for example not include vibrational data for the carboxyl group. The chemical

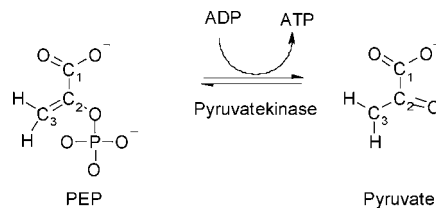


Figure 1. Reaction of PEP to pyruvate catalyzed by PK.

reactivity of the C3 atom of PEP has computationally been studied in terms of the hard–soft acid–base principle in enzymatic catalysis.¹⁵ The study indicates that enzymes can control the reactivity by conformational changes of PEP.

Despite the biological importance of PEP, no comprehensive theoretical study of the infrared spectrum seems to have been published. As a consequence, assignments of experimental spectra have to be based on common knowledge of group frequencies, a strategy which does not take into account the possible vibrational coupling between the carboxyl group, the phosphate group, and the carbon–carbon double bond, which are all in close proximity in PEP.

While experimental vibrational frequencies can be determined with wavenumber accuracy, quantum mechanical methods generally overestimate the frequencies. One source of error is the neglect of anharmonicity. Another problem in calculations is how to model the solvent effects. Today a common method is to use implicit solvent models, i.e., to represent the solvent as a bulk medium. Here, the self-consistent reaction field (SCRF) method is used which describes the solvent as a polarizable medium with a dielectric constant, ϵ . However, such models do not include localized hydrogen bonds between the solvent and the solute and may thereby neglect these important short-range interactions. These effects can be modeled by including explicit solvent molecules in the first solvation shell, a strategy which involves new problems such as the determination of the number and the orientation of the solvent molecules and also the treatment of many more local energy minima.¹⁶ Furthermore, calculations including a larger number of explicit solvent molecules will become prohibitively costly.¹⁶

* To whom correspondence should be addressed. E-mail: maria.rudbeck@dbb.su.se (M.E.R.); andreas.barth@dbb.su.se (A.B.).

[†] Department of Biochemistry and Biophysics, The Arrhenius Laboratories for Natural Sciences, Stockholm University.

[‡] Institut für Chemie, Max-Volmer-Laboratorium.

[§] Department of Physics, Albanova, and Department of Biochemistry and Biophysics, The Arrhenius Laboratories for Natural Sciences, Stockholm University.

In this study the IR spectrum of PEP was studied both experimentally and computationally for three different ionization states: fully ionized, singly protonated, and doubly protonated. The article will discuss the choice of basis set and solvent effects. Furthermore, the assignments of the different experimental bands of PEP will be discussed in detail.

Materials and Methods

Experimental Details. The monopotassium salt of unlabeled PEP was purchased from Sigma, labeled PEP from Cambridge Isotopes Laboratories, and deuterium oxide (99.9 atom % D) from Sigma-Aldrich.

FTIR spectra were recorded at 4 cm^{-1} resolution on a Bruker Vertex 70 FTIR spectrometer equipped with a MCT detector. 50 mM labeled and unlabeled PEP in $^1\text{H}_2\text{O}$ and in $^2\text{H}_2\text{O}$ were measured at different pH values. The PEP sample was placed on a diamond ATR reflection element and the sample spectrum (200 scans) was ratioed against a 500 scan background spectrum.

Computational Details. All calculations were performed with the GAUSSIAN 03 program.¹⁷ Both gas-phase and solvent geometries were optimized using density functional theory (DFT) with the B3LYP functional^{18,19} and with three different basis sets: 6-31G(d,p), 6-31++G(d,p), and 6-311++G(d,p). 6-31G(d,p) and 6-31++G(d,p) are double- ζ basis sets with polarization functions for all atoms, the double + indicates that there are diffuse functions for all atoms. 6-311++G(d,p) is a triple- ζ basis set with both polarization and diffuse functions for all atoms. To find the most favorable conformations, the geometry optimization was performed on several different starting structures in the gas phase. They were generated by rotating three different dihedral angles ($\text{O}-\text{C}_1-\text{C}_2-\text{O}$, $\text{C}_1-\text{C}_2-\text{O}-\text{P}$, and $\text{C}_2-\text{O}-\text{P}-\text{O}$) with 30° interval in the range from 0 to 180° . In addition, for the fully ionized PEP the $\text{O}-\text{C}_1-\text{C}_2-\text{O}$ angles were fixed at 0 , 30 , 50 , 70 , and 90° since no energy minima were found for these conformations. The purpose was to analyze whether an enzymatic control of PEP's conformation, as previously proposed,¹⁵ can be detected by infrared spectroscopy.

The solvent effects were taken into account using a self-consistent polarized model (PCM), more specifically the conductorlike screening model (CPCM),^{20,21} with the default values for water (dielectric constant, $\epsilon = 78.39$). For some of the structures, the solvent effect was described both implicitly and explicitly by using both the CPCM model and four explicit water molecules. Three water molecules were put to surround the phosphate and one water molecule was hydrogen bonded to the carboxyl group. No investigation was performed to find the global minima, i.e., the optimizations represent local minima and the energies can therefore not be compared.

Because of SCF convergence problems for some of the systems including the solvent model, parameters different from standard values were employed. First, the SCF=NOVARACC keyword was used in order to obtain a more strict SCF convergence. Second, the opt=GDII option was chosen, which is the recommended algorithm for the geometry optimization of large systems and when molecules with flat potential energy surfaces are studied.¹⁷

The vibrational frequencies and the infrared absorbance were calculated for the optimized geometries; no scaling factors were applied. The calculations were performed using the same method and basis set as the optimization. All frequencies were analyzed using the ChemCraft program²² and a PED program.²³

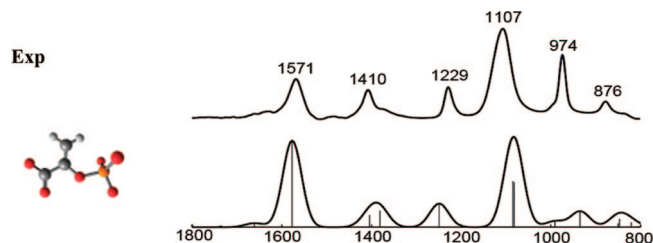


Figure 2. The infrared spectrum of fully ionized (FI) PEP. The top panel shows the experimental spectrum at pH 9, and the lower panel shows the computed spectrum using B3LYP/6-31++G(d,p). The computation included the CPCM to simulate the solvent effects.

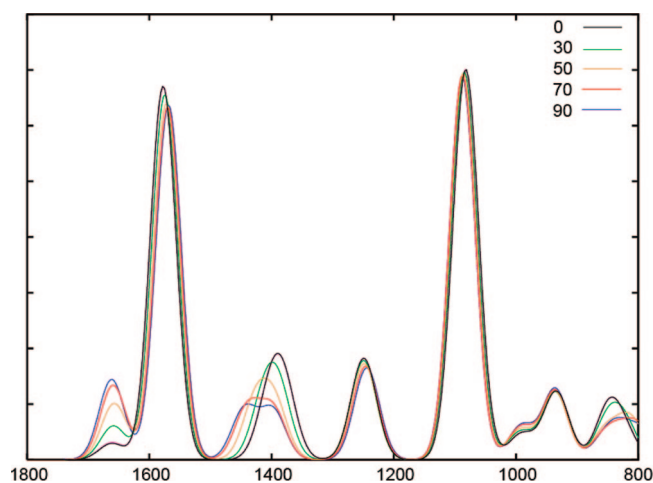


Figure 3. The computed infrared spectrum of FI-PEP during rotation of the dihedral angle $\text{O}-\text{C}_1-\text{C}_2-\text{O}$. The angle is frozen for all the calculations except for when the angle is 0° .

Results

We studied PEP in the gas phase by computation and in aqueous solution by computation and experiment. To model experiments in $^2\text{H}_2\text{O}$, hydroxyl-deuterated PEP was also examined theoretically. In addition, $^{13}\text{C}_{2,3}$ -labeled PEP was studied to clarify some of the band assignments. The experimental and computational results in water are reported in the main text, while a complete compilation of the experimental spectra (Figures S1–S3 of Supporting Information), a comparison of the calculations with the different basis sets for gas-phase calculations (Figures S4–S6 of Supporting Information) and for all CPCM-continuum calculations (Figures S7–S9 of Supporting Information), and the isotope effects on both the experimental and calculated spectra in water (Figures S10 and S11 of Supporting Information) can be found in the Supporting Information.

Comparison of Basis Sets. We studied several structures of PEP in three different ionization states. The infrared spectra for all conformations were computed using three different basis sets: 6-31G(d,p), 6-31++G(d,p), and 6-311++G(d,p). Figures 2, 4–6 show the calculations with the 6-31++G(d,p) basis set and the CPCM-continuum. Figures S7–S9 of Supporting Information show the remaining results of these calculations using the CPCM continuum and the corresponding experimental spectra. For all protonation states the infrared spectra computed with the two basis sets including the diffuse functions are almost identical and close to experimental values, while the frequencies computed using the 6-31G(d,p) basis set are often overestimated compared to the experiment and higher than for the larger basis sets. In other words, for the three basis sets studied, the vibrational frequencies shift to lower values with larger basis

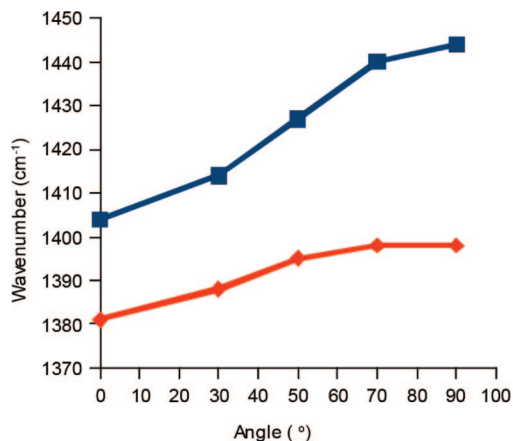


Figure 4. The relation between the two modes of FI-PEP which represent the 1410 cm^{-1} band. As the $\text{O}-\text{C}_1-\text{C}_2-\text{O}$ dihedral angle increases, the band gap increases.

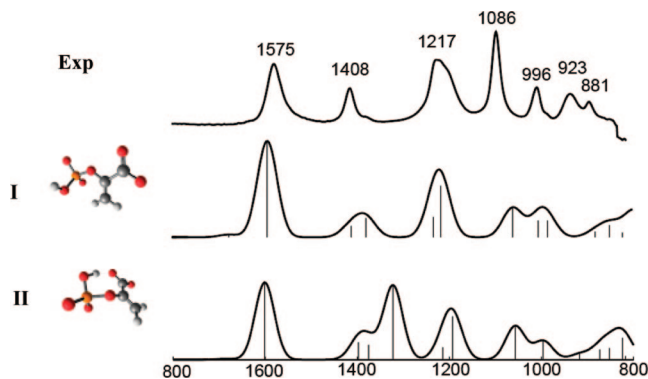


Figure 5. The infrared spectra of singly protonated phosphoenol pyruvate (SP-PEP). The top panel shows the experimental spectrum at pH 4. The middle panels show the computed spectrum of structure I and the lower panel that of structure II. All computations are performed using B3LYP/6-31++G(d,p) and included the CPCM to simulate the solvent effects.

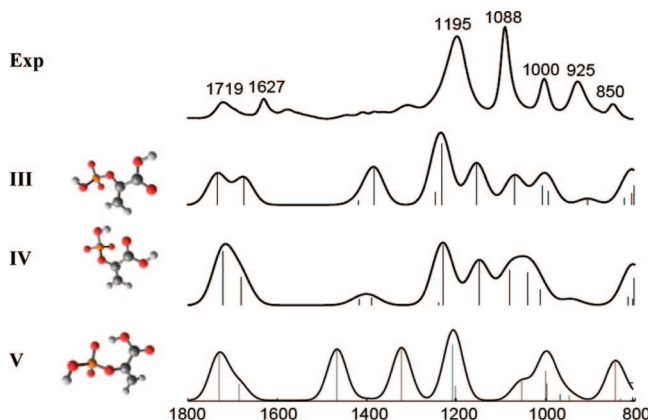


Figure 6. The infrared spectra of doubly protonated phosphoenol pyruvate (DP-PEP). The top panel shows the experimental spectrum at pH 2.1. All structures are computed using B3LYP/6-31++G(d,p) with the CPCM to simulate the solvent effects.

sets. For the fully ionized PEP, the root-mean-square deviation between calculation with CPCM-continuum and experiment in aqueous solution is 41 cm^{-1} for the 6-31G(d,p) basis set and 25 and 27 cm^{-1} for the 6-31++G(d,p) and 6-311++G(d,p) basis sets, respectively. Therefore, the results described below are those obtained with the 6-31++G(d,p) basis set.

Solvent Effects. The effects of the CPCM continuum were quantified for fully ionized PEP. The spectrum was computed

TABLE 1: Assignments and PEDs for FI-PEP Calculated with B3LYP/6-31++G(d,p) and CPCM Continuum^a

experimental $\tilde{\nu}/\text{cm}^{-1}$		calculated normal modes of PEP ($^1\text{H}_2\text{O}$)			
PEP ($^1\text{H}_2\text{O}$)	[$^{13}\text{C}_{2,3}$]PEP ($^1\text{H}_2\text{O}$)	$\tilde{\nu}/\text{cm}^{-1}$	RA	assignment	PED (%) ^b
		1661	62	C2=C3 STRE	68
1571	1589/1557 ^c	1577	1340	COO ⁻ STRE	90
1410	1401	1404	185	CH ₂ SCIS	60
1410	1401	1381	257	COO ⁻ STRE	45
				CH ₂ SCIS	23
1229	1206	1249	365	C—O(P) STRE	31
				CH ₂ ROCK	26
1107	1106	1085	712	P—O STRE	99
1107	1106	1081	694	P—O STRE	98
~980 sh		991	92	C—O(P) STRE	36
				CH ₂ ROCK	42
974	972	935	245	P—O STRE	93
		850	60	CH ₂ WAG	74
876	875	847	128	C1—C2 STRE	30
876	875			COO ⁻ SCIS	34
		820	77	COO ⁻ WAG	61

^a The wavenumber, $\tilde{\nu}$, is given for the experimental data (PEP and [¹³C_{2,3}]PEP in ¹H₂O) at pH 10 and for the computational data. Values in ²H₂O are not included because none of the protons of FI-PEP will exchange for deuterium and the observed experimental band positions were very similar. RA, relative absorbance; STRE, stretching; SCIS, scissoring; ROCK, rocking; WAG, wagging; sh, shoulder. ^b Internal coordinates with a PED contribution of 15% or more are listed. ^c Band splits into two bands upon isotopic labeling.

using B3LYP/6-31++G(d,p) for both the gas phase and with the CPCM-continuum; the results are given in Table 1 for the CPCM-continuum. Both results can be found in Table S3 of Supporting Information. The root-mean-square deviation between the calculation with the 6-31++G(d,p) basis set, and the experiment is 38 cm^{-1} for the calculation in gas phase and 25 cm^{-1} with the CPCM-continuum. Thus the continuum model has a significant effect on the spectra and improves the agreement with experimental results. The results described below are therefore calculated using B3LYP/6-31++G(d,p) with the CPCM-continuum.

FI-PEP. The chemical structure and the experimental and theoretical spectra for FI-PEP (pH = 9) are shown in Figure 2. Structural details of the energy minimized conformation are compiled in Table S2 of Supporting Information. The spectrum includes 6 distinct bands, the assignments of which are compiled in Table 1. At 1571 and 1410 cm^{-1} , the antisymmetric and the symmetric stretching vibrations of COO⁻ are observed, respectively. The calculations reveal that the symmetric stretching vibration is coupled to the scissoring (in plane bending) vibration of CH₂. The absorption at 1410 cm^{-1} includes an additional normal mode to which CH₂ scissoring contributes strongly.

Figure 3 shows the theoretical spectra of FI-PEP during the rotation of the dihedral angle O-C1-C2-O. The spectra show that the two modes that contribute to the 1410 cm^{-1} band are the only bands that significantly shift in frequency during the rotation. The changes in molecular energy and the vibrational frequencies are listed in Table 2. Figure 4 shows that the frequencies of both modes are higher when the angle increases from 0 to 90° and that the band gap between the two vibrations increases at larger angles. Another characteristic which appears during the rotation is the stronger absorption of the C=C stretching vibration at ~1600 cm^{-1} .

The band at 1229 cm^{-1} is caused by a normal mode that has contributions from several internal coordinates, mainly from the C-O stretching vibration of the C-O-P group, here abbrevi-

TABLE 2: Conformational Dependency of Selected Vibrational Frequencies of FI-PEP with Energies and Frequencies Calculated with B3LYP/6-31++G(d,p) and the CPCM Continuum

angles ^a	relative energy (kJ/mol)	vibration 1 ^b (cm ⁻¹)	vibration 2 ^b (cm ⁻¹)
nonfrozen 0°	0	1404	1381
30°	1.35	1414	1388
50°	4.01	1427	1395
70°	7.08	1440	1398
90°	8.09	1444	1398

^a The angle between C=C and COO⁻. ^b The computed frequencies of the modes that constitute the experimental band at 1410 cm⁻¹.

ated C–O(P), and the rocking vibration of CH₂. The asymmetric and symmetric PO₃²⁻ stretching vibrations absorb at 1107 and 974 cm⁻¹, respectively. The small shoulder at the high wavenumber side of the 974 cm⁻¹ band is likely caused by a normal mode involving the C–O(P) stretching vibration and the CH₂ rocking vibration. The band at 876 cm⁻¹ is a superposition of two bands that are caused by the wagging vibration of the methylene and the C1–C2 stretching vibration coupled to the scissoring of the carboxylate group. Of the two bands, only the former is shifted in the calculation with isotopic-labeled [¹³C_{2,3}]PEP. This explains why there is only a small shift in the experimental [¹³C_{2,3}]PEP spectrum; see Table 1 (and Figure S3 of Supporting Information).

Singly Protonated (SP) PEP. The pK_a values of carboxylate and phosphate groups at pH 4.6 indicate that for the SP-PEP, the hydrogen atom is positioned on the phosphate group. This is also inferred from the experimental infrared spectra, see Figure 5, where the carboxylate bands (1575 and 1408 cm⁻¹) are still observed at pH 4.6, while the bands of the ionized phosphate group (1107 and 974 cm⁻¹) are no longer present. SP-PEP can adopt many conformations with local minima but two conformations are energetically more favorable. Their spectra are shown in Figure 5, their energies are given in Table S1 of Supporting Information and their structural details in Table S2 of Supporting Information. Conformation I has an extended form because of the repulsion from the negatively charged carboxylate and phosphate groups. Conformation II exhibits an internal hydrogen bond between the phosphate hydroxyl group and one of the oxygens of the carboxyl group. Conformer II was energetically favorable by 11 kJ/mol, when the solvent effects were modeled implicitly with the CPCM model. In aqueous solution, conformer I is expected to be better stabilized, compared to conformer II, by the hydrogen bonds from water molecules and by the minimized electrostatic repulsion in the extended conformation. The relative energies of the models with four explicit water molecules (and the CPCM model) are listed in Table S1 in the Supporting Information; however, it should be mentioned that these energies should not be directly compared since global minima were not obtained.

The calculated spectra for the two conformations are similar (see Figure 5). The assignments are listed in Table 3. An exception is that conformer II with the internal hydrogen bond has an extra vibration at 1322 cm⁻¹, with a strong absorption coefficient. This normal mode is caused by the POH in-plane-bending vibration and is upshifted by 317 cm⁻¹ compared to the structure without the internal hydrogen bond. It is also the only case where the two basis sets with diffuse functions give very different frequencies - the difference is 32 cm⁻¹ for conformer II.

As indicated by this large difference between the two conformers, the vibrational frequency of the POH in-plane-bending vibration is very sensitive to hydrogen bonding. Therefore, we studied whether this vibration in the extended structure I is affected by explicit water molecules in the calculation. The molecule was reoptimized with four explicit water molecules (also including the CPCM model). Indeed, placing hydrogen bonded water molecules close to the hydroxyl hydrogen and to the two unprotonated terminal oxygens of the phosphate group, shifted the POH bending vibration from 1005 up to 1164 cm⁻¹. Because of the sensitivity of this vibration to hydrogen bonding, it will cause a broadband in the experimental spectrum that we expect to contribute to the band at ~1200 cm⁻¹, which is in agreement with Chapman et al.'s²⁴ experimental infrared study of orthophosphates. In line with this assignment, the low wavenumber shoulder of the 1217 cm⁻¹ band in ¹H₂O is missing in ²H₂O (see Figure S10 of Supporting Information). The calculated POH bending frequency shifts to the 900 cm⁻¹ region upon deuteration which is consistent with reference.²⁴ A similar upshift of the POH-bending vibration, as for conformer I after including the explicit water molecules, can also be seen for conformer II. The POH-bending vibration is calculated at 1322 cm⁻¹ without the explicit water molecules for the SP-PEP but appears at ~1360 cm⁻¹ when the water molecules are included. This upshift excludes that the POH-bending vibration contributes to the experimental absorption at ~1200 cm⁻¹. The vibration can neither contribute to the experimental absorption at 1410 cm⁻¹ since the experimental spectrum of SP-PEP (Figure 5) is very similar to that of FI-PEP (Figure 2) in this region. In SP-PEP there is no POH-bending vibration because the phosphate group is unprotonated. Therefore, the POH-bending vibration of conformer II does not seem to be observed in the experimental spectrum and we conclude that conformation II is little populated in aqueous solution.

Apart from the POH bending vibration, two additional normal modes contribute to the absorption at ~1200 cm⁻¹, one consists of the C–O(P) stretching and CH₂ rocking vibrations and the other is attributed to the antisymmetric PO₂⁻ stretching vibration. The bands at 1577 and 1408 cm⁻¹ are assigned to the antisymmetric and symmetric stretching vibration of COO⁻, respectively, and the computations show that the second band includes a further mode dominated by the CH₂ scissoring vibration as also found for FI-PEP. The band at 1086 cm⁻¹ is assigned to the symmetric PO₂⁻ stretching vibration while the band at 996 cm⁻¹ arises from the coupling between C–O(P) stretching and CH₂ rocking vibrations. The small shoulder on the low wavenumber side of the 996 cm⁻¹ band is the residual 974 cm⁻¹ band for FI-PEP (see Figure 2), indicating that a small proportion of PEP remains unprotonated at pH 4.6. The small bands at 923 and 881 cm⁻¹ are not easily assigned from the computations when the solvent effects are only considered by a continuum model. To aid their assignment, SP-PEP with four explicit water molecules (and the CPCM model) was also analyzed. Almost all frequencies were in agreement with the model without the explicit water molecules except for the P–O(H) stretching vibration where both a large upshift from 794 to 851 cm⁻¹ and a higher intensity was calculated. This vibration is therefore expected to contribute to the 923 cm⁻¹ band. A second mode, CH₂ wagging, contributes additionally. The absorption at 880 cm⁻¹ is linked to the C1–C2 stretching vibration as is the 876 cm⁻¹ band of FI-PEP. This interpretation explains why the absorption of the 923 cm⁻¹ band is relatively strong and why the band does not exist for FI-PEP. It also

TABLE 3: Assignments and PEDs for Singly Protonated (SP) PEP Calculated with B3LYP/6-31++G(d,p) and CPCM Continuum

experimental $\tilde{\nu}$ /cm ⁻¹		structure I of PEP (¹ H ₂ O) ^a				structure II of PEP (¹ H ₂ O) ^a			
PEP (¹ H ₂ O)	PEP (² H ₂ O)	$\tilde{\nu}$ /cm ⁻¹	RA	assignment ^c	PED (%) ^b	$\tilde{\nu}$ /cm ⁻¹	RA	assignment ^c	PED (%) ^b
		1677	37	C2=C3 STRE	70	1686	12	C2=C3 STRE	73
1575	1584	1593	1287	COO ⁻ STRE	91	1601	1033	COO ⁻ STRE	87
1408	1408	1411	154	CH ₂ SCIS	66	1398	234	CH ₂ SCIS	56
								COO ⁻ STRE	24
1408	1408	1379	260	COO ⁻ STRE	54	1375	200	COO ⁻ STRE	41
				CH ₂ SCIS	19			CH ₂ SCIS	29
						1322	990	POH BEND ^c	87
1217	1219	1232	272	C—O(P) STRE	29	1214	166	C—O(P) STRE	31
				CH ₂ ROCK	29			CH ₂ ROCK	29
1217	1219	1216	689	P—O STRE	91	1193	580	P—O STRE	96
1086	1088	1060	394	P—O STRE	90	1057	450	P—O STRE	97
1217	1219	1005	224	POH BEND ^c	84				
996	996	985	225	C—O(P) STRE	41	996	253	C—O(P) STRE	40
				CH ₂ ROCK	37			CH ₂ ROCK	38
923	919	881	77	CH ₂ WAG	94	917	76	CH ₂ WAG	96
						874	138	TORS O—P—O—H	91
881	879	850	162	C1—C2 STRE	33	853	156	C1—C2 STRE	25
				COO ⁻ SCIS	23			COO ⁻ SCIS	36
		822	66	COO ⁻ WAG	70	818	51	COO ⁻ WAG	69
923 ^d	919 ^d	794	333	P—O(H) STRE	90	824	293	P—O(H) STRE	86

^a See Figure 5 for more information about the structures. ^b Internal coordinates with a PED contribution of 15% or more are listed. ^c See text for assignment of this vibration to a band in experimental spectrum. ^d This vibration is sensitive to hydrogen bonding (see text). The band assignment was based on a calculation with explicit water molecules. ^e RA, relative absorbance; STRE, stretching; SCIS, scissoring; ROCK, rocking; WAG, wagging; sh: shoulder.

explains why there is only a small shift for both bands in ²H₂O (see Figure S2 of Supporting Information).

Doubly Protonated (DP) PEP. The experimental spectrum for DP-PEP at pH 2.1, see Figure 6, indicates that both the carboxyl and the phosphate groups are protonated since the bands of the carboxylate group (1577 and 1409 cm⁻¹) are no longer observed. For DP-PEP, three conformations were studied in both the gas phase and when the continuum model was included. One has an extended conformation (III), see Figure 6, and the hydrogen atom can be positioned on the different phosphate oxygens without considerable change in energy. The second and third conformations (IV and V) exhibit an internal hydrogen bond between the carboxyl and the phosphate group. The energies of all these conformations are very close to each other (within 7 kJ/mol) when solvent effects are included. The energies and bond lengths of the conformations are listed in Tables S1 and S2 of Supporting Information.

The calculated infrared spectra of the different conformations for DP-PEP are represented in Figure 6. The assignments for conformations III, IV, and V are given in Table 4. The band at 1719 cm⁻¹ is assigned to the C=O stretching vibration and the 1627 cm⁻¹ band to the C2=C3 stretching vibration. The small band near 1577 cm⁻¹ is the residual absorption of the carboxylate group, indicating that this group is ionized in a small fraction of the molecules. Between 1600 and 1250 cm⁻¹, the experimental spectrum is featureless. In contrast, for structure III one and for structure V two strong absorption bands are calculated in this region and assigned to delocalized modes involving the COH group. For structure IV, only weakly absorbing bands are calculated. Because of the discrepancy between computation and experiment in this spectral region, we explored whether the COH modes are affected by hydrogen bonding to explicit water molecules. Figure 7 shows the spectra of DP-PEP modeled with both explicit water molecules and the CPCM continuum model. The explicit water molecules do not affect the mode of structure IV; the mode might therefore contribute to the small bands between 1500 and 1300 cm⁻¹ in the experimental

spectrum. However, the explicit waters slightly upshift the two bands of structure V. Since details of hydrogen bonding seem to have little effect on the bands of structure V, we expect two distinct strong bands around 1400 cm⁻¹ for structure V. This is not observed, and we conclude that structure V is little populated in aqueous solution.

For structure III, the explicit water molecules cause a frequency downshift and intensity increase of the mode involving the COH group from 1382 to 1315 cm⁻¹. This strong shift indicates a high sensitivity toward hydrogen bonding and we expect therefore the experimental band to be broad. Since even the inclusion of explicit water molecules models the hydration effect incompletely (as found for SP-PEP) we expect the experimental absorption of structure III considerably lower than 1315 cm⁻¹ and suggest that the COH mode contributes to the band near 1200 cm⁻¹.

Thus, the broadband at ~1200 cm⁻¹ is an overlap of several normal modes. The mode compositions with the two different solvation models (with and without the explicit water molecules) are different; however they include the vibrations of the same internal coordinates: C—O(H) stretching, COH bending and C1—C2 stretching, C—O(P) stretching, CH₂ rocking and COH bending, the antisymmetric PO₂⁻ stretching, and POH bending (for structures III and V where this vibration is upshifted from around 1000 cm⁻¹ when including the explicit water molecules) vibrations. That the broadband includes the POH and COH bending vibrations is supported by the fact that the experimental absorption at ~1200 cm⁻¹ is reduced in ²H₂O (see Figure S11 of Supporting Information). The COH contribution increases the intensity of this band and changes its shape in comparison with the corresponding band of SP-PEP. The band at 1088 cm⁻¹ corresponds to the PO₂⁻ symmetric stretching vibration and the 1000 cm⁻¹ band is attributed to a mode that couples C—O(P) stretching and CH₂ rocking vibrations.

As for SP-PEP, DP-PEP needs to be modeled with explicit water molecules in order to assign the bands at 925 and 850 cm⁻¹. For structure III, the 925 cm⁻¹ band is again assigned to

TABLE 4: Assignments and PEDs for DP-PEP Calculated with B3LYP/6-31++G(d,p) and CPCM Continuum

experimental $\tilde{\nu}/\text{cm}^{-1}$			structure III ^a				structure IV ^a				structure V ^a			
PEP (¹ H ₂ O)	PEP (² H ₂ O)	[¹³ C _{2,3}]PEP (¹ H ₂ O)	$\tilde{\nu}/\text{cm}^{-1}$	RA	assignment	PED (%) ^b	$\tilde{\nu}/\text{cm}^{-1}$	RA	assignment	PED (%) ^b	$\tilde{\nu}/\text{cm}^{-1}$	RA	assignment	PED (%) ^b
1719	1707	1719	1732	372	C=O STRE	79	1721	641	C–O STRE	72	1731	525	C–O STRE	73
1627	1635	1578	1673	325	C2=C3 STRE	68	1681	334	C2=C3 STRE	66	1687	188	C2=C3 STRE	70
											1466	580	COH BEND	85
			1417	56	CH ₂ SCIS	83	1417	70	CH ₂ SCIS	71	1401	20	CH ₂ SCIS	83
1195 (III) ^c			1382	438	C–O(H) STRE	25	1389	87	C–O(H) STRE	24	1321	597	C–O(H) STRE	43
					C1–C2 STRE	19			C1–C2 STRE	16			C1–C2 STRE	22
					COH BEND	19								
1195	1208	1186	1245	153	C–O(P) STRE	22	1239	33	C–O(P) STRE	23				
					CH ₂ ROCK	21			CH ₂ ROCK	17				
					COH BEND	21			COH BEND	29				
1195	1208	1186	1231	730	P–O STRE	87	1229	711	P–O STRE	88	1206	635	P–O STRE	52
1195	1208	1186	1153	499	C–O(H) STRE	49	1148	531	C–O(H) STRE	49	1200	167	C–O(H) STRE	21
					COH BEND	43			COH BEND	36			P–O STRE	43
1088	1091	1088	1068	353	P–O STRE	90	1080	418	P–O STRE	53	1051	218	P–O STRE	66
													POH BEND	18
1195	1208	1186	1006	232	POH BEND	82	1040	390	P–O STRE	45	997	334	POH BEND	73
													P–O STRE	18
1000	996	995	993	164	C–O(P) STRE	37	1012	185	C–O(P) STRE	35	994	192	C–O(P) STRE	40
					CH ₂ ROCK	39			CH ₂ ROCK	45			CH ₂ ROCK	38
											964	71	COO(H) WAG	86
925	925	925	905	76	CH ₂ WAG	98	943	73	CH ₂ WAG	98	943	58	CH ₂ WAG	97
850	820	843	822	83	C1–C2 STRE	40	815	99	C1–C2 STRE	36	828	16	C1–C2 STRE	33
				15	C–O(H) STRE	15							CO ₂ SCIS	15
850	820	843	806	140	COO(H) WAG	59	805	75	COO(H) WAG	57	800	39	COO(H) WAG	77
925 ^d	927 ^d	925 ^d	801	228	P–O(H) STRE	80	802	322	P–O(H) STRE	83	840	430	P–O(H) STRE	88

^a See Figure 6 for more information about the structures. ^b Internal coordinates with a PED contribution of 15% or more are listed. ^c See text. ^d This vibration is sensitive to hydrogen bonding (see text). The band assignment was based on the calculation with explicit water molecules.

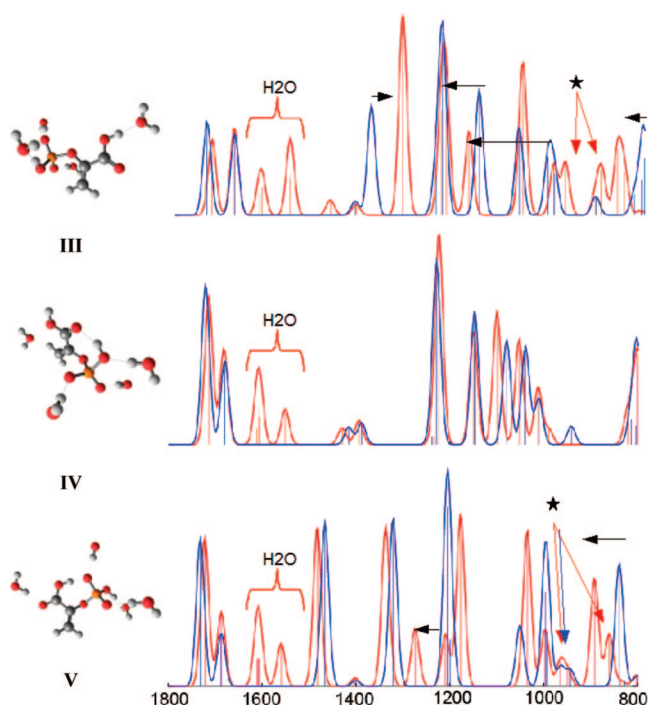


Figure 7. The calculated infrared spectra of DP-PEP. All structures are computed using B3LYP/6-31++G(d,p); the solvent effects are modeled with the CPCM and with explicit water molecules. Black arrows, from blue to red bands, indicate band shifts due to explicit water molecules. The stars indicate out-of-plane vibrations which are not observed in solution in the experimental spectrum.

the P–O(H) stretching vibration - after including the four explicit water molecules, see Figure 7, the vibration shifts up from 801 to 858 cm⁻¹ (840 to 892 cm⁻¹ for structure V). A second normal mode dominated by the CH₂ wagging vibration

contributes to a small extent. The predominant contribution of the P–O(H) stretching vibration explains why the band is not affected by isotopic substitution in [¹³C_{2,3}]PEP and hardly by deuteration (see Table 4 and Figure S3 of Supporting Information). For structure IV, a shift of the P–O(H) stretching vibration is not observed after including the explicit water molecules. It is calculated at 802 cm⁻¹ and may give rise to an absorption below 800 cm⁻¹, which is outside the experimentally accessible spectral region. Therefore structure IV does not seem to contribute to the 925 cm⁻¹ band. Since we have excluded structure V as a major species above, we conclude that the 925 cm⁻¹ band is due to conformation III, which is therefore significantly populated in aqueous solution. The band at 850 cm⁻¹ is assigned to the C1–C2 stretching vibration coupled to the C–O(H) stretching vibration and is downshifted compared to FI-PEP and SP-PEP in both experiment and calculation due to the protonation of the carboxyl group. This assignment also explains why the 850 cm⁻¹ band shifts for both ²H₂O and [¹³C_{2,3}]PEP; see Table 4.

For all computations of SP-PEP and DP-PEP with explicit water molecules there are additional normal modes in the spectral range from 1800 to 800 cm⁻¹. They were not discussed above because they were not present in the spectra calculated with only the continuum model. For structure III, these additional modes are the POH and COH out-of-plane bending vibrations calculated at 892 and 969 cm⁻¹, respectively. They are expected to have considerably lower frequency after deuteration. Such band shifts are however not observed in the experimental spectra (compare Figures S1 and S2 in Supporting Information). This is in accordance with the literature, which describes the out-of-plane bending bands as very broad, due to many different relative orientations of interacting water molecules, and only visible in gas phase.^{25–27}

Discussion

We calculated the infrared spectrum of PEP in three different protonation states using B3LYP with the three different basis sets 6-31G(d,p), 6-31++G(d,p), and 6-311++G(d,p) and together with the CPCM continuum model. Some structural models also included explicit water molecules in addition to the continuum model. The two larger basis sets show significant improvement of the calculated frequencies. For all protonation states the two spectra computed with basis sets including the diffuse functions are almost identical, and one can therefore conclude that the 6-31++G(d,p) basis set is sufficient for these molecular systems. Larger basis sets than 6-31G(d,p) are generally needed to describe the electronic structure of anions.^{28,29}

One source of error in the quantum chemical calculations of vibrational frequencies is the neglect of anharmonicity effects. The calculated frequencies are therefore typically larger than those experimentally observed, however larger basis sets tend to yield better results.^{30,31} According to Figures S7–S9 of Supporting Information, the B3LYP/6-31G(d,p) method generally overestimates the vibrational frequencies. For the larger basis sets, frequencies higher than 1200 cm⁻¹ are often overestimated, while the frequencies below 1200 cm⁻¹ are generally underestimated. Most vibrational frequencies are just slightly over- or underestimated (<3%); some are strongly affected by hydrogen bonding, as discussed below, and deviate up to 15% from experimental values.

A common technique to improve the agreement between the calculated frequencies and measured spectra is to use different scaling methods. Scaling the frequencies uniformly would not be fully satisfactory since some vibrations are underestimated while others are overestimated in our unscaled computations. Another approach is to scale the force constants depending on the type of atom and type of vibration, the so-called scaled quantum mechanical (SQM) method.^{11,12} Both Florián et al.¹¹ and Katsyuba et al.¹² have scaled the force factors for molecules including phosphorus after optimization with B3LYP/6-31G(d) and obtained frequencies that compare well with experiments for most vibrations. However, to the best of our knowledge, not all scaling factors are available in the literature for the protonated PEP structures, for example, for the P–O(H) stretching vibration, and since most vibrational frequencies are in agreement with the experimental results, we decided not to introduce scaling.

Another source of error is the difficulties in modeling the solvent. Previous studies show that the hydrogen bonding may effect both the vibrational frequencies and the infrared intensities.^{32,33} In this study, a discrepancy between calculated and measured frequencies was observed for vibrations involving protonated groups, i.e., PO(H) and CO(H) stretching and bending vibrations. These frequencies turned out to be very sensitive to hydrogen bonding. Therefore, the structures were reoptimized after including explicit water molecules that were hydrogen bonded to the phosphate and to the carboxyl groups. The results (see Figure 7) reveal several interesting details. First the P–O(H) stretching vibration is upshifted by 50 cm⁻¹ for structure III while the remaining terminal P–O stretching modes do not shift. Second, the POH in-plane bending mode upshifts more than 100 cm⁻¹. Third, the intensities for all vibrations become more consistent with the experimental results, for example, the intensity for the P–O(H) stretching vibration increases when the explicit water molecules are included.

The close proximity of a carboxyl, a phosphate group, and a C2=C3 double bond in PEP raises the question as to the extent of vibrational coupling between these groups. This is an

important aspect for the interpretation of experimental spectra of this biomolecule, since these groups give rise to relatively strong absorption and are therefore experimentally observable in studies of the catalytic mechanism of enzymes that have PEP as a substrate. According to Tables 1, 3, and 4 many of the normal modes are due to the vibration of predominantly one internal coordinate, whereas others comprise several internal coordinates which are strongly coupled. Significant coupling occurs with vibrations of the CH₂ group. The CH₂ scissoring vibration couples to the symmetric COO⁻ stretching vibration and the CH₂ rocking vibration to the C–O(P) stretching vibration. However, there is little coupling between the carboxyl group, the phosphate group and the C2=C3 double bond, and the vibrations of these groups in PEP have similar frequencies as in other molecules. Information on these groups from other molecules can therefore also be applied to PEP.

Conclusions

This work reports a combined experimental and theoretical analysis of the vibrational modes of the important biomolecule PEP in water for three ionization states. An extended conformation is suggested to exist in aqueous solution for the singly and the doubly protonated ionization states. For these conformations, the computational frequencies are very close to the experimental ones which allowed a complete band assignment in the studied spectral range from 1800 to 800 cm⁻¹. Therefore, using the B3LYP method in combination with a double- ζ basis set with diffuse functions and CPCM continuum model provides a satisfactory description of most vibrations in aqueous solution. However, vibrations involving the hydroxyl group are very sensitive to hydrogen bonding and should be modeled with a few explicit water molecules present.

The O–C1–C2–O dihedral angle correlates with the chemical reactivity of PEP.¹⁵ We have shown here that for the FI-PEP the two modes that contribute to the experimental band at 1410 cm⁻¹ experience frequency shifts when the angle is rotated. Because of the shifts, the conformation of PEP bound to an enzyme can be assessed by infrared spectroscopy. This will give important insight into the enzymatic mechanism.

Acknowledgment. We are grateful to the Knut och Alice Wallenbergs Stiftelse for funding the infrared spectrometer, to Ventenskapsrådet for providing the running costs and to the Center of Biomembrane Research for a stipend to Maria Rudbeck in the initial phase of the project. We would also like to thank one of the reviewers for pointing us to reference 15.

Supporting Information Available: The relative energies and structural details of the minimized conformations, the experimental infrared spectra of PEP in ¹H₂O and ²H₂O and of [¹³C_{2,3}]PEP in ¹H₂O for the three protonation states of PEP. Furthermore, it includes the computational infrared spectra and the PED for FI-PEP, SP-PEP, and DP-PEP in gas phase, for hydroxyl-deuterated PEP, and for DP-PEP with four explicit water molecules. This material is available free of charge via the Internet at <http://pubs.acs.org>.

References and Notes

- (1) Florián, J.; Warshel, A. *J. Am. Chem. Soc.* **1997**, *119*, 5473.
- (2) Westheimer, F. *Science* **1987**, *235*, 1173.
- (3) Knowles, J. *Ann. Rev. Biochem.* **1980**, *49*, 877.
- (4) Duczmal, K.; Darowska, M.; Raczynska, E. *Vib. Spectrosc.* **2005**, *37*, 77.
- (5) Kakkar, R.; Pathak, M.; Radhika, N. *Org. Biomol. Chem.* **2006**, *4*, 886.

- (6) Reva, I.; Stepanian, S.; Adamowicz, L.; Fausto, R. *J. Phys. Chem. A* **2001**, *105*, 4773.
- (7) Raczyńska, E.; Duczmal, K.; Darowska, M. *Vib. Spectrosc.* **2005**, *39*, 37.
- (8) Petrov, A. S.; Funseth-Smotzer, J.; Pack, G. R. *Int. J. Quantum Chem.* **2005**, *102*, 645.
- (9) Shimanouchi, T.; Tsuboi, M.; Kyogoku, Y. *Advances in Chemical Physics: Structure & Properties of Biomolecules*; Wiley Interscience: New York, 1964.
- (10) Liang, C.; Ewig, C. S.; Stouch, T. R.; Hagler, A. T. *J. Am. Chem. Soc.* **1993**, *115*, 1537.
- (11) Florian, J.; Baumruk, V.; Strajbl, M.; Bednarova, L.; Stepanek, J. *J. Phys. Chem.* **1996**, *100*, 1559.
- (12) Katsyuba, S.; Vandyukova, E. *Chem. Phys. Lett.* **2003**, *377*, 658.
- (13) Kang, N. S.; Jung, D. H.; No, K. T.; Jhon, M. S. *Chem. Phys. Lett.* **2002**, *364*, 580.
- (14) Brandán, S. A.; Díaz, S. B.; López, J. J.; Disalvo, E. A.; Ben Altabef, A. *Spectrochim. Acta A* **2007**, *66*, 884.
- (15) Li, Y.; Evans, J. *Proc. Natl. Acad. Sci. U.S.A.* **1996**, *93*, 4612.
- (16) Cramer, C. J.; Truhlar, D. G. *Chem. Rev.* **1999**, *99*, 2161.
- (17) Frisch, M. J.; Trucks, G. W.; Schlegel, H. B.; Scuseria, G. E.; Robb, M. A.; Cheeseman, J. R.; Montgomery, J. A., Jr.; Vreven, T.; Kudin, K. N.; Burant, J. C.; Millam, J. M.; Iyengar, S. S.; Tomasi, J.; Barone, V.; Mennucci, B.; Cossi, M.; Scalmani, G.; Rega, N.; Petersson, G. A.; Nakatsuji, H.; Hada, M.; Ehara, M.; Toyota, K.; Fukuda, R.; Hasegawa, J.; Ishida, M.; Nakajima, T.; Honda, Y.; Kitao, O.; Nakai, H.; Klene, M.; Li, X.; Knox, J. E.; Hratchian, H. P.; Cross, J. B.; Bakken, V.; Adamo, C.; Jaramillo, J.; Gomperts, R.; Stratmann, R. E.; Yazyev, O.; Austin, A. J.; Cammi, R.; Pomelli, C.; Ochterski, J. W.; Ayala, P. Y.; Morokuma, K.; Voth, G. A.; Salvador, P.; Dannenberg, J. J.; Zakrzewski, V. G.; Dapprich, S.; Daniels, A. D.; Strain, M. C.; Farkas, O.; Malick, D. K.; Rabuck, A. D.; Raghavachari, K.; Foresman, J. B.; Ortiz, J. V.; Cui, Q.; Baboul, A. G.; Clifford, S.; Cioslowski, J.; Stefanov, B. B.; Liu, G.; Liashenko, A.; Piskorz, P.; Komaromi, I.; Martin, R. L.; Fox, D. J.; Keith, T.; Al-Laham, M. A.; Peng, C. Y.; Nanayakkara, A.; Challacombe, M.; Gill, P. M. W.; Johnson, B.; Chen, W.; Wong, M. W.; Gonzalez, C.; Pople, J. A. *Gaussian 03*; Gaussian, Inc.: Wallingford, CT, 2004.
- (18) Becke, A. D. *J. Chem. Phys.* **1993**, *98*, 5648.
- (19) Lee, C.; Yang, W.; Parr, R. G. *Phys. Rev. B* **1988**, *37*, 785.
- (20) Barone, V.; Cossi, M. *J. Phys. Chem. A* **1995**, *102* (1998), .
- (21) Cossi, M.; Rega, N.; Scalmani, G.; Barone, V. *J. Comput. Chem.* **2003**, *24*, 669.
- (22) <http://www.chemcraftprog.com>.
- (23) Spies, M.; Smit, K.; Mrogiński, M. A.; Mark, F. *GVA Program*, revision 2007; University of Duisburg and Max Planck Institut für Strahlenchemie.
- (24) Chapman, A. C.; Thirlwell, L. E. *Spectrochim. Acta* **1964**, *20*, 937.
- (25) Coates, J. *Interpretation of Infrared Spectra, A Practical Approach*; Meyers, R. A., Ed.; John Wiley & Sons Ltd: Chichester, 2000..
- (26) Ostrowska, J.; Narebska, A. *Colloid Polym. Sci.* **1979**, *257*, 128.
- (27) Colthup, N. B.; Daly, L. H.; Wimerley, S. E. *Introduction to Infrared and Raman Spectroscopy*; Academic Press: Boston, 1990.
- (28) Rienstra-Kiracofe, J. C.; Tschumper, G. S.; Schaefer, H. F., III; Nandi, S.; Ellison, G. B. *Chem. Rev.* **2002**, *102*, 231.
- (29) Millet, A.; Gimbert, Y.; Greene, A. E. *J. Comput. Chem.* **2006**, *27*, 157.
- (30) Meier, R. J. *Vib. Spectrosc.* **2007**, *43*, 26.
- (31) Merrick, J. P.; Moran, D.; Radom, L. *J. Phys. Chem. A* **2007**, *111*, 11683.
- (32) Smets, J.; McCarthy, W.; Maes, G.; Adamowicz, L. *J. Mol. Struct.* **1999**, *476*, 27.
- (33) Dimitrova, Y.; Daskalova, L. I. *THEOCHEM* **2007**, *823*, 65.

JP809638U

Paper III

Phosphoenolpyruvate and Mg^{2+} binding to pyruvate kinase monitored by infrared spectroscopy

Saroj Kumar and Andreas Barth

Department of Biochemistry and Biophysics, Stockholm University, Stockholm, Sweden

Correspondence to: A. Barth, Department of Biochemistry and Biophysics, The Arrhenius Laboratories for Natural Sciences, Stockholm University, S-106 91 Stockholm, Sweden, Tel: +46 8 162452; Fax: +46 8 155597; E-mail: Andreas.Barth@dbb.su.se

Keywords: Vibrational spectroscopy, ATR, FTIR, ligand binding, PK, PEP

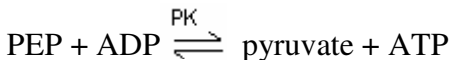
Abbreviations: ATR, attenuated total reflection; FTIR, Fourier transformed infrared; IR, infrared; PEP, phosphoenolpyruvate; PK, pyruvate kinase

Abstract

Structural changes in rabbit muscle pyruvate kinase (PK) induced by phosphoenolpyruvate (PEP) and Mg^{2+} binding were studied by attenuated total reflection Fourier transform infrared (ATR-FTIR) spectroscopy in combination with a dialysis accessory. The experiments indicated a largely preserved secondary structure upon PEP and Mg^{2+} binding but revealed also small backbone conformational changes of PK involving all types of secondary structure. In order to assess the effect of the protein environment on the bound PEP we assigned and evaluated the infrared absorption bands of bound PEP. These were identified using 2,3- $^{13}\text{C}_2$ labeled PEP. We obtained the following assignments: 1589 cm^{-1} (antisymmetric carboxylate stretching vibration), 1415 cm^{-1} (symmetric carboxylate stretching vibration), 1214 cm^{-1} (C-O stretching vibration) 1124 and 1110 cm^{-1} (asymmetric PO_3^{2-} stretching vibration) and 967 cm^{-1} (symmetric PO_3^{2-} stretching vibration). The corresponding band positions in solution are 1567 , 1407 , 1229 , 1107 , and 974 cm^{-1} . The differences for bound and free PEP indicate specific interactions between ligand and protein. Quantification of the interactions with the phosphate group indicated that the enzyme environment has little influence on the P-O bond strengths, and that the bridging P-O bond, which is broken in the catalytic reaction, is weakened by less than 3 %. Thus there is only little distortion towards a dissociative transition state of the phosphate transfer reaction when PEP binds to PK. Therefore our results are in line with an associative transition state. Carboxylate absorption bands indicated a maximal shortening of the length of the shorter C-O bond by 1.3 pm. PEP bound to PK in the presence of the monovalent ion Na^+ exhibited the same band positions as in the presence of K^+ indicating very similar interaction strengths between ligand and protein in both cases.

Introduction

Pyruvate kinase (PK) is a key enzyme of the glycolytic pathway that catalyzes the transfer of phosphate from phosphoenolpyruvate (PEP) (Fig. 1a) to adenosine diphosphate (ADP).



The physiological reaction of pyruvate kinase proceeds in two chemical steps. The first step is phosphoryl transfer from PEP to ADP which produces ATP and the enolate of pyruvate [1]. The second step is the addition of a proton to the enolate of pyruvate to produce pyruvate [2].

Rabbit muscle pyruvate kinase (EC 2.7.1.40, sequence code AAB61963) consists of four subunits of 530 residues each. Each subunit folds into four domains: A, B, C and N. Domain N (residues 1-42) is a short helix-turn-helix motif, domain A (residues 43-115 and residues 224-387) is a parallel (β/α)₈ barrel, domain B (residues 116-223) is a nine stranded β -barrel and domain C (residues 388-530) is composed of five α -helices and a five stranded β -sheet. The active site lies in the pocket between domains A and B of the same subunit. Structures of the active site with bound ligands indicate that the side chains of Arg⁷² and Lys²⁶⁹ bind the phosphate group of PEP or the γ -phosphate of ATP [3, 4].

Pyruvate kinase has four metal binding sites; it requires divalent cations [5-7] and monovalent cations [8-10] for activity. In the presence of divalent cations, pyruvate kinase is active in a medium containing the univalent cations K⁺, Rb⁺ or NH₄⁺, but only weakly active in the presence of Na⁺ [11, 12]. By use of NMR, Mildvan and Cohn [13] have observed that K⁺ enhances the relaxation rate of water protons in the ternary complex pyruvate kinase-manganese-phosphoenolpyruvate. This indicates that K⁺ affects the conformation of the enzyme in the presence of PEP and Mn²⁺. The crystal structure of rabbit muscle pyruvate kinase [14] provides insight into the roles of various groups in binding of divalent and monovalent cations. Mn²⁺ [14] or Mg²⁺ [4] coordinates to the protein through the carboxylate side chains of Glu²⁷¹ and Asp²⁹⁵ and K⁺ coordinates to four protein ligands: Thr¹¹³, Ser⁷⁶, Asn⁷⁴ and Asp¹¹². Crystal structures have been obtained with several ligands [3, 4, 14] but not with PEP due to the slow hydratase activity of pyruvate kinase. As a close analogue, L-phospholactate has been used [4]. Interestingly, the active sites of different subunits adopt different conformations that result in different degrees of closure of the cleft that forms the active site [4]. One of eight sites is closed and Mg²⁺ coordinates to L-phospholactate and protein. The other sites are open and coordination between Mg²⁺ and L-phospholactate is lost. Open and closed conformations have also been observed in NMR relaxation measurements, indicating an open conformation in the complex with Mn²⁺ but closed conformations in the ternary complexes with PEP and L-phospholactate [15]

In this study we used *reaction-induced infrared difference spectroscopy* to study structural changes of PK induced by PEP binding. The method is more sensitive than a comparison of infrared absorption spectra of samples with and without PEP and yields valuable information on ligand induced structural changes [16-20]. We used a variant of the attenuated total reflectance (ATR) technique in which a sample compartment in contact to the ATR crystal is separated by a dialysis membrane from a reservoir [21, 22]. The absorption of the solution in the sample compartment is probed by the infrared beam.

The protein is confined to the sample compartment. The ligands on the other hand can exchange freely between the sample compartment and the reservoir via the dialysis membrane. Therefore the sample composition can be altered by adding a substance to the reservoir. Our results demonstrate a conformational change of pyruvate kinase upon binding of PEP and small changes in the bond strengths of PEP when it binds.

Experimental procedures

Materials

Pyruvate kinase (PK) from rabbit muscle, monopotassium salt of PEP, pyruvate, ADP and MOPS (3-[N-morpholino] propanesulphonic acid) and deuterium oxide (99.9 atom % D) were purchased from Sigma. Labeled PEP (2,3-¹³C₂) was purchased from Cambridge Isotopes Laboratories, Inc. The labeled carbon atoms are indicated by asterisks in Fig. 1a. Tris-HCl was obtained from Angus. KCl, NaCl and MgSO₄ were obtained from Scharlau. Cellulose dialysis membranes CelluSep F3 of MWCO 12000-14000 were purchased from Orange Scientific, Belgium.

Methods

PK sample preparation

For difference spectroscopy 0.8 mM rabbit muscle PK were prepared in buffer (Tris-HCl + MOPS, pH, 7.5) containing 200 mM KCl or NaCl and 4 mM of MgSO₄. Deuterated samples of PK were prepared in a similar way and the pD adjusted to 7.6. The pH meter reading was corrected by -0.4 to obtain pD [24]. For recording of absorption spectra, labeled and unlabeled PEP and pyruvate (Fig. 1b) were dissolved in H₂O and the absorption spectrum measured at pH 7.5.

FTIR studies

Our ATR-dialysis setup has been described previously [22]. The PK sample was placed between the ATR reflection element and the dialysis membrane in the following way: A 2 µl drop of PK sample was placed on the ATR crystal and another 4 µl were deposited as hanging drop on the dialysis membrane at the bottom of the reservoir. Then the sample compartment was closed by approaching the reservoir towards the ATR crystal. The solution in the reservoir was stirred with a small mechanical stirrer for fast equilibration. FTIR spectra were recorded at 4 cm⁻¹ resolution on a Bruker Vertex 70 FTIR spectrometer equipped with an HgCdTe detector. The experiments were performed at room temperature. PK was equilibrated by continuous diffusion of buffer and salts across the dialysis membrane. The absorbance spectrum was recorded in regular intervals. Within 2-3 h, the protein absorption increased because the protein settled on the ATR crystal. After the absorption spectrum of the sample became time-independent, a 500 scan single beam spectrum (background spectrum) was recorded. Then 2 µl of PEP (50 mM, pH 7.5), were added to the 4 ml solution in the reservoir after which 20 spectra in the absorption mode (150 scans each) were recorded for 4 minutes. Addition of PEP and spectra recording was repeated up to 3 times. For activity measurements, 50 µM of ADP was added to the reservoir before recording of the background spectra and PEP addition.

Evaluation of bond strengths and bond lengths

Bond parameters for the phosphate group were derived following our work on the Ca^{2+} -ATPase [25] which was based on a study by Deng et al. [26]. From the band positions of the symmetric and asymmetric stretching vibrations of the terminal P-O bonds, a fundamental frequency or wavenumber ν can be calculated according to $\nu = [(\nu_s^2 + 2\nu_{as}^2) / 3]^{1/2}$ [26]. The fundamental wavenumber can be used to calculate the bond valence of P-O bonds using the formula [26]

$$(1) s = [0.175 \times \ln (224500 \text{ cm}^{-1} / \nu)]^{-4.29}$$

where s is bond valence in valence units (vu) of the terminal phosphate bonds and ν the fundamental wavenumber. Interactions between terminal phosphate oxygens and their environment were quantified according to the bond valence model [27], which states that the sum of all bond valences around oxygen atoms is two. This sum includes covalent bonds and external bonds, i.e. interactions with the environment. Thus, the bond valence due to the interactions to each of the terminal oxygens is 2 minus the bond valence of the terminal bond. Parameters for the bridging P-O bond can similarly be obtained by subtracting the summed bond valences of the terminal P-O bonds from the atomic valence of phosphorous, which is five.

Since bond valences are defined by experimentally determined bond lengths, bond lengths can be determined from bond valences. We used equation 2 [27] with the parameters used to derive the frequency versus bond valence correlation (equation 1) [26].

$$(2) L_s^N = L_1^N / s$$

where L_s the bond length of a bond with bond valence s measured in vu, and L_1 the bond length of a bond with a bond valence of 1 vu. L_1 and N are constants for a given type of bond [28, 29]. For P-O bonds they are $N = 4.29$ and $L_1 = 1.622 \text{ \AA}$ [29].

Two approaches were used to estimate the reduction of bond dissociation energy of the bridging P-O bond due to binding of PEP to PK. (i) Bond dissociation energy can be regarded as linear to bond valence [30]. (ii) Bond length L and bond dissociation energy E are correlated: for several oxides, the inverse relationship $E \sim (L - L_0)^{-1}$ has been found [31], where $L_0 = 1.171 \text{ \AA}$ for P-O bonds [32].

Results

Infrared absorption spectra of PEP, pyruvate

In our study of PEP binding to PK we first measured the infrared absorption of the substrate PEP and the product pyruvate. Absorption spectra of ADP and ATP have been published before by us [33] and by others, see for example reference 34. The absorption spectrum of unlabeled PEP at pH 7.5 is presented in Fig.2A. The absorption band at 1569 cm^{-1} is attributed to the COO^- antisymmetric stretching vibration and the band of the symmetric stretching vibration was observed at 1407 cm^{-1} [35]. The band at 1229 cm^{-1} is attributed to the C-O(P) stretching vibration according to density functional theory calculations [36] and in analogy to the phenyl C-O-P linkage [35]. In the phosphate absorption region, the ($-\text{PO}_3^{2-}$) stretching vibration bands were observed at 1103 and 974 cm^{-1} and a mode composed of C-C stretching and COO^- scissoring vibrations at 879 cm^{-1} [36]. The band positions in D_2O were the same as in H_2O except for the COO^- stretching vibrations and for the symmetric $-\text{PO}_3^{2-}$ stretching vibration, which were observed at 1574 cm^{-1} ($+5\text{ cm}^{-1}$), 1411 cm^{-1} ($+3\text{ cm}^{-1}$) and 972 cm^{-1} (-2 cm^{-1}) respectively. The spectrum of (2,3- $^{13}\text{C}_2$) labeled PEP at pH 7.5 is presented in Fig.2b. The antisymmetric COO^- stretching vibration splits into two bands at 1589 and 1558 cm^{-1} with the main band shifting downwards by 11 cm^{-1} . The symmetric stretching vibration shifts only by 5 cm^{-1} to lower wavenumbers, whereas a strong 24 cm^{-1} downshift is observed for the C-O stretching vibration. All other band positions are only slightly affected by labeling shifting down 1, 2, and 4 cm^{-1} for the asymmetric and the symmetric $-\text{PO}_3^{2-}$ stretching vibrations and the C-C stretching/ COO^- scissoring vibration, respectively.

The absorption spectrum of pyruvate at pH 7.5 is presented in Fig.2c. The keto carbonyl stretch is observed at 1708 cm^{-1} , while the COO^- antisymmetric stretching vibration absorbs at 1600 cm^{-1} [37]. The COO^- symmetric stretching vibration contributes to two bands at 1421 cm^{-1} and 1399 cm^{-1} [37] and the band of the CH_3 deformation vibration is observed at 1358 cm^{-1} . The band at 1175 cm^{-1} is due to the C- CH_3 stretching vibration [38]. The COO^- antisymmetric stretching vibration was observed at 1616 cm^{-1} in D_2O , while other band positions were the same as in H_2O .

Infrared difference spectra of PEP binding to PK: general features and data evaluation

In the following we will discuss absorbance changes upon PEP binding to PK. The spectra shown are *difference* spectra, revealing the absorbance change due to binding. Positive bands in the difference spectra are due to bound and free PEP as well as to protein absorption of the quaternary complex $\text{PK}\cdot\text{PEP}\cdot\text{Mg}^{2+}\cdot\text{K}^+$, whereas negative bands are due to protein absorption of $\text{PK}\cdot\text{Mg}^{2+}\cdot\text{K}^+$. The effect of three PEP additions to PK samples in H_2O and in the presence of K^+ is shown in Fig.3 (difference spectra a-e). The difference spectra were recorded at pH 7.5 at room temperature within 4 minutes after PEP addition. Difference spectra a-c show absorbance changes due to PEP binding to PK upon the first addition of PEP at different times after the addition (84, 180 and 240s). Protein conformational changes are indicated particularly by bands in the amide I region ($1700\text{--}1610\text{ cm}^{-1}$). Subsequent additions of PEP (difference spectra d and e for the second and third additions, respectively) cause absorbance changes due to an increase of the concentration of free PEP (bands at 1567, 1407, 1229, 1107 and 974 cm^{-1}). These band positions are slightly different from those found in the absorption spectra because of different buffer and salt concentrations. No distinct features are observed in the amide I

region in the second and third addition demonstrating the absence of conformational changes and that the amount of PEP added in the first addition was sufficient to saturate the binding sites.

The initial difference spectrum at 84s after the first addition is mainly due to formation of the PK-PEP complex, whereas the difference spectrum 240s after the first addition contains also a contribution of the absorption of free PEP. This is concluded from the shift of the symmetric PO_3^{2-} band near 970 cm^{-1} , which is evident in difference spectra a-c of Fig.3. The shift is shown more clearly in Fig.4. Panel a of Fig.4 depicts the evolution of this band upon the first addition of PEP. The $-\text{PO}_3^{2-}$ stretching vibration band shifts gradually from 966.6 cm^{-1} to 970.5 cm^{-1} , as the PEP concentration increases. This is because initially all PEP is bound to PK whereas later the proportion of free PEP increases. Panel b of Fig.4 shows the kinetics of the band shift. In addition 2 (Fig.4b) and addition 3, the band position is 974.5 cm^{-1} which coincides with the position of PEP in aqueous solution (Fig.2a). The final band position after the first addition is still 4 cm^{-1} below that of the 2nd addition indicating ~50% free PEP at the end of the first addition.

In order to determine the best time interval for the observation of the PEP-PK complex with only little contribution by free PEP, we evaluated also the kinetics of secondary structure changes of PK upon PEP binding, using the band at 1696 cm^{-1} . The result is shown in Fig.4c. At 150s this signal of protein structural change saturates, indicating that binding is essentially complete. The rate-limiting step in our experiments is the diffusion of the ligand into the sample compartment. In order to minimize the contribution of free PEP and to maximize the signal of the PEP-PK complex, we evaluated the time interval 84-144s and normalised the spectrum to the amplitude of the amide I signals in the 240s spectrum. The resulting difference spectrum is shown in Fig.5a and is called *PEP binding spectrum*. It has the symmetric PO_3^{2-} stretching band at 968.1 cm^{-1} indicating less than 20% of free PEP.

Infrared difference spectra of PEP binding to PK: band assignment

Fig.5 compares PEP binding spectra for different conditions. They were obtained as described in the previous section. In PEP binding spectrum a, difference bands are observed in the amide I spectral region which is predominantly a C=O vibration of the protein backbone and absorbs between 1700 and 1610 cm^{-1} . The amide I absorption is sensitive to protein backbone structure and has been used for secondary structure analysis. According to the literature [39,40,41,42,43,44,45,46] we tentatively assign the $1696(+)$ and $1678(-)\text{ cm}^{-1}$ bands to turns or β -sheets, the signal at $1663(+)\text{ cm}^{-1}$ to α -helical structures and the bands in the spectral region 1647 - 1621 cm^{-1} to β -sheets. The assignment of the 1696 , 1678 , 1663 and 1647 cm^{-1} bands to amide I modes is supported by the respective PEP binding spectrum recorded in D_2O (spectrum b in Fig.5) where these bands are found at slightly lower wavenumbers. These results indicate that PK undergoes conformational changes when the substrate PEP binds, which involve all types of secondary structures.

The positive bands at 1590 and 1551 cm^{-1} (difference spectra a-c in Fig.3) are assigned to the antisymmetric stretching mode of COO^- groups, which is supported by their upshifts in spectra recorded in D_2O (Fig.5b). The positive band at 1415 cm^{-1} (Fig.5a) is assigned to the symmetric stretching mode of COO^- groups.

The band at 1485 cm^{-1} is in the spectral range of the absorption of the asymmetric CH_3 bending vibration. The band shifts in D_2O to 1467 cm^{-1} which is indicative of Thr CH_3 absorption [48]. Since the side chain of Thr³²⁷ lies in the active site and interacts with the carboxylate of L-phospholactate [4], we tentatively assign the band at 1485 cm^{-1} to the asymmetric CH_3 bending vibration of Thr³²⁷. Bands at 1214 cm^{-1} and below will be assigned in the following paragraph with help of a PEP binding spectrum obtained with labeled PEP.

Infrared difference spectra of PEP binding to PK: bands of bound PEP

Bands of bound PEP were assigned with help of 2,3- $^{13}\text{C}_2$ labeling of PEP (see Fig.1). The PEP binding spectrum obtained for the isotopomer is shown in Fig.5c and is compared in the following to the respective spectrum for unlabeled PEP in panel a. The coincidence of all signals in the amide I region ($1700\text{-}1610\text{ cm}^{-1}$) illustrates the excellent reproducibility of our spectra. Isotopic labeling perturbs the bands at 1590 , 1415 , 1214 and 968 cm^{-1} . The latter three shift down by a few cm^{-1} as expected for isotopic labeling of PEP according to Fig.2 and are therefore assigned to the symmetric carboxylate stretching vibration, the C-O stretching vibration and the symmetric PO_3^{2-} stretching vibration, respectively, of bound PEP. The respective band positions of PEP in solution are 1407 , 1229 and 974 cm^{-1} which indicates that binding changes geometry and bond strengths of the carboxylate and phosphate groups. Regarding the 1111 cm^{-1} band, the second derivative of the two PEP binding spectra (data not shown) reveals two components at 1124 and 1110 cm^{-1} . The former can clearly be seen as shoulder in the PEP binding spectrum and the latter corresponds to the main band. We assign both components to the phosphate group of bound PEP because the band area of the asymmetric stretching vibration is considerably larger than that of the symmetric stretching vibration according to Fig.2. The expected isotope shift of 1 cm^{-1} will be difficult to detect in the difference spectrum, partly due to the presence of a small fraction of free PEP molecules which alters the position of the main band. Both component bands of the asymmetric PO_3^{2-} stretching vibration of bound PEP are upshifted with respect to the respective band of PEP in aqueous solution which is found at 1107 cm^{-1} under the conditions of our experiment (Fig.3e).

The situation is more complicated for the 1590 cm^{-1} band. It clearly loses intensity and splits into two bands at 1596 and 1576 cm^{-1} . The downshift is 15 cm^{-1} according to the component band positions in the second derivative spectra (not shown). This number is close to the 11 cm^{-1} shift observed in aqueous solution. Therefore we assign the 1590 cm^{-1} band to the antisymmetric carboxylate stretching vibration of bound PEP. The upshift for the high frequency component at 1596 cm^{-1} is 6 cm^{-1} which is smaller than the expected 21 cm^{-1} . We note that the upshifted component band is expected to have a very low intensity according to Fig.2 and might be masked by overlapping protein bands or bands from minor binding modes of PEP.

In conclusion, the isotope effect on the 1590 cm^{-1} band clearly indicates that the antisymmetric carboxylate stretching vibration of bound PEP absorbs near 1590 cm^{-1} . The band position is 21 cm^{-1} upshifted compared to the band position in aqueous solution revealing a distinct interaction with the protein which will be further discussed below. The adjacent carboxylate band at 1551 cm^{-1} is not perturbed by isotopic labeling of PEP.

It is therefore assigned to carboxylate groups of Asp or Glu residues, tentatively to those of Glu²⁷¹ and Asp²⁹⁵ which coordinate Mg²⁺ or to Asp¹¹² which binds K⁺ [4].

PEP binding spectrum in the presence of the activating monovalent ion Na⁺

The effect of the activating monovalent cation on PEP binding was also studied. Fig.5d shows the PEP binding spectrum in the presence of Na⁺, whereas those previously discussed were in the presence of K⁺ (Fig.5a). The shape of the PEP binding spectrum is similar with both cations above 1650 cm⁻¹. Thus α -helical and turn secondary structure elements are perturbed in a similar way by PEP binding with both cations. Differences are observed in the β -sheet region where a band at 1647 in the presence of K⁺ shifts to 1641 cm⁻¹ in the presence of Na⁺ and the negative band at 1632 cm⁻¹ (K⁺) is not observed with Na⁺. Bands of bound PEP are found at the same positions for Na⁺ and K⁺, with the exception of the band of the symmetric carboxylate vibration of PEP which shifts from 1415 cm⁻¹ with K⁺ to 1417 with Na⁺. Overall, the spectra indicate very similar interactions between protein and substrate with both cations, with a slight modification of the interactions of the carboxylate group.

Infrared difference spectra of Mg²⁺ binding to PK

The following section discusses absorbance changes upon Mg²⁺ binding to PK. The difference spectra obtained are named Mg²⁺ binding spectra. Positive bands in the Mg²⁺ binding spectra are due to PK·Mg²⁺·K⁺, whereas negative bands are due to PK·K⁺. The Mg²⁺ binding spectrum in the presence of K⁺ in H₂O is shown in Fig.5e. Spectrum e was obtained upon the first addition of Mg²⁺. Second and third additions gave featureless spectra (data not shown). In the Mg²⁺ binding spectrum, difference bands are observed in the spectral region 1750-900 cm⁻¹. Upon comparison with the respective spectrum in D₂O (spectrum f in Fig.5), some of the bands can be assigned. The band at 1694 cm⁻¹ shifts down to 1675 cm⁻¹ which is indicative of the C=O stretching vibration of Asn or Gln. The bands at 1485 cm⁻¹ in H₂O and 1467 cm⁻¹ in D₂O induced by PEP binding (Fig.5a) are also found upon Mg²⁺ binding and are again tentatively assigned to the asymmetric CH₃ bending mode of Thr³²⁷. The positive band at 1417 cm⁻¹ is due to the symmetric stretching mode of COO⁻ groups, which is supported by its upshift in spectra recorded in D₂O (Fig.5f). All other bands are in convoluted regions of the spectrum and there is no unique way to interpret the shifts observed in D₂O. Possible assignments [47,49,50] and deuteration induced shifts are: 1664 cm⁻¹ (H₂O) → 1647 cm⁻¹ (D₂O, Asn, Gln), 1664 cm⁻¹ → 1606 cm⁻¹ (Arg), 1645 → 1647 cm⁻¹ (β -sheet, band shift probably only apparent because of overlap by other bands), 1645/1630 cm⁻¹ → 1606/1587 cm⁻¹ (Arg), 1616, 1596 cm⁻¹ (H₂O, not observed in D₂O, Asn, Gln), 1569/1545 cm⁻¹ → 1587/1569 cm⁻¹ (Asp, Glu, shift is larger than usual probably because of overlap by other bands), 1545 cm⁻¹ (H₂O, not observed in D₂O, amide II).

Infrared difference spectrum of the catalytic reaction

The spectrum shown in Fig.6 shows absorbance changes due to the catalytic reaction of PK. The initial state of the sample was a mixture of PK and ADP, then PEP was added and the difference spectra reveal the absorbance changes upon PEP addition. The spectrum shown in Fig.6 is the average of spectra recorded during 4 minutes after PEP addition. Because of coincidence of the band positions in the difference spectrum (Fig.6)

with those of reactants and products (Figs.2a and 2c, references [33,34]), we attribute the positive bands at 1600, 1358 and 1176 cm^{-1} to the formation of pyruvate (Fig.2c), absorption at 1248 - 1232, 989 and 914 cm^{-1} to ATP production [35,36], the negative band at 940 cm^{-1} to ADP consumption [33,34] and the negative bands at 975 cm^{-1} and 1103 cm^{-1} to PEP consumption (Fig.2a). This indicates that PK is active in our IR samples.

The spectra are difficult to interpret in the amide I region because some bands are caused by protein backbone changes and others by the formation of pyruvate and ATP. For example the bands at 1702 and 1619 cm^{-1} could be due to bound pyruvate. Compared to the PEP binding spectrum (Fig.5a), new bands are observed at 1680(+) and 1638(-) cm^{-1} and the positive band at 1644 cm^{-1} is missing in the spectrum of steady state turnover. This indicates that the conformation at steady state is different from that induced by PEP binding.

Discussion

The structural change of PK upon PEP binding

Spectroscopic studies can provide a detailed understanding of the conformational changes that occur when a ligand binds to a protein. In the case of pyruvate kinase, X-ray [3,4,51,52,53], NMR [13,15], small angle neutron scattering [54] and IR [23] studies are available. PEP binding by PK leads to a more compact conformation of the protein [4,54] due to closure of the cleft between A and B domains. The previous IR study showed that PEP binding does not induce significant interconversion between secondary structures in PK, but does affect the microenvironment of the backbone [23]. Our results agree with this finding. However, using reaction induced IR difference spectroscopy we were able to detect the small infrared absorbance changes associated with PEP and Mg^{2+} binding. Only the changes at 1661 and 1639 cm^{-1} (Fig.5b) have been identified in the previous IR study [23].

Our spectra give evidence for an involvement of β sheets, turns and α helical segments in the structural change upon PEP binding. The spectra can be interpreted in terms of secondary structure changes but are also sensitive to more subtle changes of backbone structure and hydrogen bonding within persisting secondary structure elements. In order to quantify the structural changes of the polypeptide backbone upon PEP binding to PK, we used the *change of backbone structure and interaction* (COBSI) index [45,55]. It relates the integrated intensity in the amide I region, which is redistributed upon the reaction, to the integrated total protein absorbance in that region. The COBSI index for PEP binding to PK is 0.0014, which is more than 2 orders of magnitude smaller ($< 1\%$) than COBSI indices for 100% secondary structure changes [55]. This indicates that around 1% of the peptide groups contribute to a *net* change in backbone structure. The COBSI index gives realistic estimates of the net change of secondary structure [45,56]. However, the total number of residues that experience a secondary structure change may be larger, these are not revealed in the IR spectra when opposing changes in different regions of the protein largely compensate [56]. We conclude that the net change of backbone structure of PK upon PEP binding is small but clearly detectable with FTIR spectroscopy.

Infrared absorption of bound PEP

From our experiments with labeled PEP, we identified all major absorption bands of PEP bound to PK. We obtained the following assignments: 1590 cm^{-1} (antisymmetric carboxylate stretching vibration), 1415 cm^{-1} (symmetric carboxylate stretching vibration), 1214 cm^{-1} (C-O stretching vibration) 1124 and 1110 cm^{-1} (asymmetric PO_3^{2-} stretching vibration) and 968 cm^{-1} (symmetric PO_3^{2-} stretching vibration). The corresponding band positions in solution are 1567, 1407, 1229 1107, and 974 cm^{-1} under the conditions of our experiment (Fig.3d,e). The spectral positions of bound PEP are shifted from their positions in aqueous solution which indicates different interactions in water and when bound to the protein. In the following we will quantify the changes in bond parameters between bound and free form.

Bond parameters of the phosphate group of bound PEP

Bond parameters for the phosphate group were derived following our previous work on the Ca^{2+} -ATPase [25] as described in Experimental Procedures. They are collected in Table 1. The absolute error in bond lengths determined in this way has been estimated to 0.004 Å from a comparison between measured bond lengths and lengths determined from vibrational frequencies [26]. This corresponds to an error in bond valence of 0.011 vu for the bridging P-O bond and of 0.015 vu for the terminal P-O bonds using the relationship between bond length and bond valence (equation2). This error holds when the correlation is applied to a set of different molecules. As pointed out previously [57], a large contribution to this error is due to the coupling of the P-O vibrations with other vibrations, which is different for different molecules. However, the coupling will be very similar and the error largely abolished when the same molecule in slightly different environments is compared. Therefore, the error in the present case is mainly determined by the accuracy of determining the band position. For free PEP we assumed an accuracy of the band position of $\pm 0.5 \text{ cm}^{-1}$ which is an upper limit of the actual error. A deviation of $\pm 0.5 \text{ cm}^{-1}$ in the band positions changes bond valences by less than 0.002 vu and bond lengths by less than 0.001 Å. For the symmetric P-O stretching vibration we used its initial band position at 967 cm^{-1} in the evaluation and assumed the same accuracy of 0.5 cm^{-1} . The main error for the asymmetric P-O stretching vibration stems from the difficulty to observe a clear isotope shift. The values calculated are based on the assignment given above where the 1124 and the 1110 cm^{-1} components were assigned to the two asymmetric stretching vibrations of the phosphate of bound PEP. Two limiting cases were used to estimate the error of the bond parameters: one where both asymmetric vibrations absorb at 1110 cm^{-1} and one where both absorb at 1124 cm^{-1} . In all cases, the upshift of the asymmetric phosphate stretching vibration indicates a shortening of the terminal P-O bonds. They are ≤ 0.3 pm shorter for bound PEP, illustrating the extraordinary sensitivity of infrared spectroscopy to bond length changes. Their bond valence is 1.330 vu for bound PEP and 1.325 vu for free PEP, i.e. <1% higher for bound PEP. These effects are due to weaker interactions of the terminal oxygens of bound PEP with their environment which amount to 0.670 vu ($2 - 1.330$) for bound PEP and 0.675 vu for free PEP, i.e. 1% weaker for bound PEP. These values can be compared to that for hydrogen bonds between water molecules (0.17 vu) [27] which indicates that the strength of interaction with the terminal phosphate oxygens amounts to nearly 4 typical hydrogen bonds per oxygen for bound and free PEP. In conclusion, there is little change in the bond

parameters of the terminal P-O bonds due to binding of PEP and the strength of interaction between phosphate group and environment is similar for bound and free PEP. This indicates that there is little contribution of the phosphate group to the binding enthalpy of PEP.

The bond length of the bridging P-O bond is ≤ 3 pm longer for bound PEP. Its bond valence was determined to 1.01 vu ($5 - 3 \times 1.330$) for bound PEP and to 1.025 vu for free PEP, i.e. 1.4% weaker for bound PEP. Thus, the enzyme environment weakens the bond that is cleaved in the enzymatic reaction already in the ground state of the complex between PK and PEP. This weakening is however very small. Regarding bond dissociation energy as linear to bond valence [30] and assuming that the bridging P-O bond of free PEP has a typical P-O single bond energy of 420 kJ/mol, the bond energy is reduced by 6 kJ/mol (1.4%) upon binding of PEP. A second estimation, using a bond energy versus bond length correlation, gives a similar reduction. The maximum reduction in bond energy, obtained in one of the limiting cases is 3%. This is in sharp contrast to our study on the E2P phosphoenzyme of the Ca^{2+} -ATPase [25] where the P-O bond to be cleaved is weakened considerably by the enzyme environment. In conclusion, the bond dissociation energy of the bridging P-O bond is weakened by only a few percent upon binding of PEP to PK. Thus there is no indication that binding considerably distorts the substrate PEP towards a dissociative transition state in the phosphate transfer reaction. This is in line with the suggestion of an associative transition state [58].

Bond parameters of the carboxylate group of bound PEP

For the interactions of the carboxylate group, we evaluated quantum chemical calculations on the Hartree-Fock level published by Nara et al. [59]. This study calculated vibrational frequencies and bond parameters for acetate in 15 different environments, with and without interaction with explicit water and several ions in different coordination modes. We found that the shorter bond length L_{short} correlates with the band position of the antisymmetric stretching vibration of the carboxylate group (ν_{as}). From the correlation (data not shown) a shortening of the shorter bond on the order of 0.5 pm is inferred when PEP binds to PK. However, this length change is similar to the deviation of individual data points from the trend line (0.7 pm). Therefore, a shortening of the shorter bond cannot safely be concluded. However, the maximum length change of the shorter bond can be estimated to ~ 1.3 pm ($0.5 + 0.7$ pm). As for the phosphate group it is concluded that the bond length of the shorter carboxylate C-O bond is only little perturbed upon binding of PEP to PK.

Monitoring enzyme activity with infrared spectroscopy

Fig.8 illustrates the benefits of using IR spectroscopy for enzyme activity measurements [60] where often UV-VIS spectroscopy is used in indirect enzyme activity assays. In contrast, infrared spectroscopy is a method by which one can directly follow enzymatic reactions and also identify their reactants and products. Here, we were able to observe the consumption of ADP and PEP as well as the production of ATP and pyruvate due to the enzymatic activity of PK.

Conclusions

This work presents the first reaction-induced infrared difference spectra of PK. Infrared absorbance changes upon binding of PEP were recorded with high sensitivity and high reproducibility. They indicate small secondary structure changes affecting all types of secondary structure. The absorption bands of bound PEP were identified with help of isotopic labeling of PEP. They indicate only little perturbation of the covalent bonds of PEP upon binding: a weakening of the bridging P-O bond by less than 3% and a bond length change of the stronger carboxylate C-O bond by maximal 1.3 pm. Replacement of the activating monovalent ion K^+ by Na^+ does not change the binding mode of PEP. It is concluded that the protein environment distorts the structure of PEP very little towards that of a dissociative transition state in the phosphate transfer reaction. The smallness of the effect is in line with an associative transition state.

Acknowledgements

We are grateful to Sven och Lilly Lawskis fond för naturvetenskaplig forskning for a PhD stipend to S.K. and thank Knut och Alice Wallenberg Stiftelse for funding the spectrometer. The running costs were provided by Vetenskapsrådet.

References

1. Seeholzer, S. H., A. Jaworowski, and I. A. Rose. 1991. Enolpyruvate: chemical determination as a pyruvate kinase intermediate. *Biochemistry* 30:727-732.
2. Rose, I. A. 1970. Stereochemistry of pyruvate kinase, pyruvate carboxylase, and malate enzyme reactions. *J. Biol. Chem.* 245:6052-6056.
3. Larsen, T. M., M. M. Benning, I. Rayment, and G. H. Reed. 1998. Structure of the bis (Mg^{2+})-ATP-oxalate complex of the rabbit muscle pyruvate kinase at 2.1 Å resolution: ATP binding over a barrel. *Biochemistry* 37:6247-6255.
4. Larsen, T. M., M. M. Benning, G. E. Wesenberg, I. Rayment, and G. H. Reed. 1997. Ligand-induced domain movement in pyruvate kinase: structure of the enzyme from rabbit muscle with Mg^{2+} , K^+ and L-phospholactate at 2.7 Å resolution. *Arch. Biochem. Biophys.* 345:199-206.
5. Gupta, R. K., R. M. Osterling, and A. S. Mildvan. 1976. Dual divalent cation requirement for activation of pyruvate kinase: essential roles of both enzyme and nucleotide bound metal ions. *Biochemistry* 15:2881-2887.
6. Gupta, R. K. and A. S. Mildvan. 1977. Structures of enzyme-bound metal nucleotide complexes in the phosphoryl transfer reaction of muscle pyruvate kinase. *J. Biol. Chem.* 252:5967-5976.
7. Baek, Y. H., and T. Nowak. 1982. Kinetic evidence for a dual cation role for muscle pyruvate kinase. *Arch. Biochem. Biophys.* 217:491-497.
8. Boyer, P. D., H. A. Lardy, and P. H. Phillips. (1942). The role of potassium in muscle phosphorylations. *J. Biol. Chem.* 146:673-682.
9. Kayne, F. J. 1973. Pyruvate kinase. *Enzymes* (Boyer, P. D., ed.), pp 353-382, Academic, New York.
10. Nowak, T., and C. H. Suelter. 1981. Pyruvate kinase: activation by and catalytic role of the monovalent and divalent cations. *Mol. Cell. Biochem.* 35:65-75.
11. Suelter, C. H., R. Jr. Singleton, F. J. Kayne, S. Arrington, J. Glass, and A. S. Mildvan. 1966. Studies on the interaction of substrate and monovalent and divalent Cations with

pyruvate kinase. *Biochemistry*, 5(1):131-139.

12. Wilson, H. R., J. H. Evans, and R. R. Becker. 1967. The effect of univalent cation salts on the stability and on certain physical properties of pyruvate kinase. *J. Biol. Chem.* 242:3825-3832.

13. Mildvan, A. S., and M. Cohn. 1966. Kinetics and magnetic resonance studies of pyruvate kinase reaction. II. complexes of enzyme, metal and substrates. *J. Biol. Chem.* 241:1178-1193.

14. Larsen, T. M., T. Laughlin, H. M. Holden, I. Rayment, and G. H. Reed. 1994. Structure of rabbit muscle pyruvate kinase complexed with Mn^{2+} , K^+ and pyruvate. *Biochemistry*, 33:6301-6309.

15. Nowak, T. 1978. Structural changes at the active site of pyruvate kinase during activation and catalysis. *J. Biol. Chem.* 253:1998-2004.

16. Gourion-Arsiquaud, S., S. Chevance, P. Bouyer, L. Garnier, J.-L. Montillet, A. Bondon, and C. Berthomieu. 2005. Identification of a Cd^{2+} and Zn^{2+} binding site in cytochrome *c* using FTIR coupled to an ATR microdialysis setup and NMR spectroscopy. *Biochemistry*, 44:8652-8663.

17. Barth, A., and C. Zscherp. 2000. Substrate binding and enzyme function investigated by infrared spectroscopy. *FEBS Letters*, 477:151-156.

18. Zscherp, C., and A. Barth. 2001. Reaction induced infrared difference spectroscopy for the study of protein reaction mechanisms. *Biochemistry*, 40:1875-1882.

19. Kim, S., and B. A. Barry. 2001. Reaction induced FTIR spectroscopic studies of biological energy conversion in oxygenic photosynthesis and transport. *J. Phys. Chem.* 105:4072-4083.

20. Jung, C. 2000. Insight into protein structure and protein ligand recognition by Fourier transform infrared spectroscopy. *J. Molec. Recognit.* 13:325-351.

21. Fahmy, K. 1998. Binding of transducin and transducin-derived peptides to rhodopsin studied by attenuated total reflection Fourier transform infrared difference spectroscopy. *Biophys. J.* 75:1306-1318.

22. Krasteva, M., S. Kumar, and A. Barth. 2006. A dialysis accessory for attenuated total reflection infrared spectroscopy. *Spectroscopy* 20:89-94.

23. Y. Shaoning, L. L.-Y. Lee, and J. C. Lee. 2003. Effects of metabolites on the structural dynamics of rabbit muscle pyruvate kinase. *Biophysical Chemistry* 103:1-11.

24. Glasoe, P. K., and F. A. Long. 1960. Use of glass electrodes to measure acidities in deuterium oxide. *J. phys. Chem.* 64:188-190.

25. Barth, A., and Bezlyepkina, N. 2004. P-O bond destabilization accelerates phosphoenzyme hydrolysis of sarcoplasmic reticulum Ca^{2+} -ATPase. *J. Biol. Chem.* 279:51888-51896.

26. Deng, H., Wang, J., Callender, R., and Ray, W. J. 1998. Relationship between bond stretching frequencies and internal bonding for $[^{16}O_4]^-$ and $[^{18}O_4]$ phosphates in aqueous solution. *J. Phys. Chem. B.* 102:3617-3623.

27. Brown, I. D. 2002. The chemical bond in inorganic chemistry. The bond valence model, Oxford University Press, Oxford.

28. Brown, I. D., and Shannon, R. D. 1973. Empirical bond-strength-bond-length curves for oxides. *Acta Cryst. A.* 29:266-282.

29. Brown, I. D., and Wu, K. K. 1976. Empirical parameters for calculating cation-oxygen bond valences. *Acta Cryst. B.* 32:1957-1959.

30. Ziolkowski, J. 1983. Advanced bond-strength model of active sites on oxide catalysis. *J. Catal.* 84:317-332.
31. Ziolkowski, J., and Dziembaj, L. 1985. Empirical relationship between individual cation-oxygen bond length and bond energy in crystals and in molecules. *J. Solid State Chem.* 57:291-299.
32. Ziolkowski, J. 1985. New relation between ionic radii, bond length, and bond strength. *J. Solid State Chem.* 57:269-290.
33. Barth, A., and W. Mäntele. 1998. ATP-induced phosphorylation of the sarcoplasmic reticulum Ca^{2+} ATPase: molecular interpretation of infrared difference spectra. *Biophys. J.* 75:538-544.
34. Takeuchi, H., H. Murata, and I. Harada. 1988. Interaction of adenosine 5' triphosphate with Mg^{2+} : vibrational study of coordination sites by use of O^{18} labeled triphosphates. *J. Am. Chem. Soc.* 110:392-397.
35. Colthup, N. B., L. H. Daly, and S. E. Wiberley. 1975. *Introduction to Infrared and Raman Spectroscopy*, 2nd ed.; Academic Press: New York.
36. Rudbeck, M. E., Kumar, S., Mroginski, M-A., Lill, SO. N., Blomberg, M. R. A. and Barth, A. 2009. Infrared spectrum of phosphoenolpyruvate: computational and experimental studies. *J. Phys. Chem. A.* 113 (12):2935-2942.
37. Wright, W. W., and J. Vanderkooi. 1997. Use of IR absorption of the carboxyl group of amino acids and their metabolites to determine pKs, to study proteins and to monitor enzymatic activity. *Biospectroscopy* 3:457-467.
38. Kakihana, M., and M. Okamoto. 1984. Vibrational analysis of pyruvate ion molecules and estimation of equilibrium constants for their hydrogen isotopic exchange reactions. *J. Phys. Chem.* 88: 1797-1804.
39. Goormaghtigh, E., V. Raussens and J. M. Ruyschaert. 1999. Attenuated total reflection infrared spectroscopy of proteins and lipids in biological membranes. *Biochim. Biophys. Acta.* 1422:105-185.
40. Susi, H., and D. M. Byler. 1987. Fourier transform infrared study of proteins with parallel beta chains. *Arch. Biochem. Biophys.* 258:465-469.
41. Arrondo, J. L. R., N. M. Young, and H. H. Mantsch. 1988. The solution structure of concanavalin a probed by FTIR spectroscopy. *Biochem. Biophys. Acta* 952:261-268.
42. Krimm, S., and J. Bandekar. 1986. Vibrational spectroscopy and conformation of peptides, polypeptides and proteins. *Adv. Prot. Chem.* 38:181-367.
43. Arrondo, J. L. R., A. Muga, J. Castresana, and F. M. Goni. 1993. Quantative studies of the structure of proteins in solution by Fourier transform infrared spectroscopy. *Prog. Biophys. Mol. Biol.* 59:23-56.
44. Jackson, M., and H. H. Mantsch. 1995. The use and misuse of FTIR spectroscopy in the determination of protein structure. *Crit. Rev. Biochem. Mol. Biol.* 30:95-120.
45. Barth, A., and C. Zscherp. 2002. What vibrations tell us about proteins. *Quart. Rev. Biophys.* 35:369-430.
46. Barth, A. 2007. Infrared spectroscopy of proteins. *Biochim. Biophys. Acta–Bioenergetics* 1767:1073-1101.
47. Barth, A. 2000. The infrared absorption of amino acid side chains. *Prog. Biophys. Mol. Biol.* 74:141-173.
48. Pawluko, A., Leciejewicz, J., Tomkinson, J. and Parker, S. F. 2001. Neutron Scattering, infrared, Raman spectroscopy and ab initio study of L- threonine.

Spectrochimica. Acta A. 57:2513-2523

49. Chiragadze, Y. N., O. V. Fedorov, and N. P. Trushina. 1975. Estimation of amino acid residue side-chain absorption in the infrared spectra of protein solutions in heavy water. *Biopolymers* 14:679-94.

50. Venyaminov, S. Y., N. N. Kalnin. 1990. Quantitative IR spectrometry of peptide compounds in water (H₂O) solutions 1. Spectral parameters of amino-acid residue absorption bands. *Biopolymers* 30:1243-57.

51. Mattevi, A., G. Valentini, M. Rizzi, M. L. Speranza, M. Bolognesi, and A. Coda. 1995. Crystal structure of Escherichia coli pyruvate kinase I: molecular basis of the allosteric transition. *Structure* 3:729-741.

52. Muirhead, H., Clayden, D. A., Barford, D., Lorimer, C. G., Fothergill-Gilmore, L. A., Schiltz, E. and Schmitt, W. 1986. The structure of cat muscle pyruvate kinase. *EMBO. J.* 5:475-481.

53. Friesen, R. H. E., Castellani, R. J., Lee, J. C. and Braun, W. 1998. Allostery in rabbit pyruvate kinase: development of a strategy to elucidate the mechanism. *Biochemistry* 37:15266-15276.

54. Consler, G. T., C. E. Uberbacher, J. G. Bunick, N. M. Liebman, and J. C. Lee. 1988. Domain interaction in rabbit muscle pyruvate kinase. *J. Biol. Chem.* 25:2794-2801.

55. Barth, A., F. Von Germar, W. Kreutz, and W. Mäntele. 1996. Time resolved infrared spectroscopy of the Ca²⁺ ATPase: the enzyme at work. *J. Biol. Chem.* 271:30637-30646.

56. Liu, M., and A. Barth. 2004. Phosphorylation of the sarcoplasmic Ca²⁺ ATPase from ATP and ATP analogs studied by infrared spectroscopy. *J. Biol. Chem.* 279:49902-49909.

57. Cheng, H., S Sukal, H Deng, TS Leyh, and R Callender. 2001. Vibrational structure of GDP and GTP bound to RAS: an isotope-edited FTIR. *Biochemistry* 40:4035-4043.

58. Hassett, A., W. Blattler, and J. R. Knowles. 1982. Pyruvate kinase: is the mechanism of phospho transfer associative or dissociative? *Biochemistry* 21:6335-6340.

59. Nara, M., Torii, H., and Tasumi, M. 1996. Correlation between the vibrational frequencies of the carboxylate group and the types of its coordination to a metal ion: an ab initio molecular orbital study. *J. Phys. Chem.* 100:19812-19817

60. Thoenges, D., and A. Barth. 2002. Direct measurement of enzyme activity with infrared spectroscopy. *J. Biomol. Screen.* 7:353-357.

Table 1. Properties of the phosphate group of bound and free PEP. The error of the bond parameters for bound PEP was determined as described in the text.

	Phosphate group of bound PEP		Phosphate group of free PEP	
	terminal oxygen	bridging P-O	terminal P-O	bridging P-O
Wavenumbers of P-O stretching vibrations / cm^{-1}	1124, 1110, 967		1107, 974	
P-O fundamental frequency or wavenumber / cm^{-1}	1069		1065	
P-O bond valence / vu	1.330 ± 0.005	1.010 ± 0.015	1.3251 ± 0.0005	1.0246 ± 0.0015
Bond valence of external bonding / vu	0.670 ± 0.005		0.675 ± 0.0005	
P-O bond length / Å	1.5177 ± 0.0014	1.618 ± 0.006	1.5190 ± 0.0002	1.6128 ± 0.0006
Reduction of bond dissociation energy of bound PEP relative to free PEP		1.4 % (range 0 - 3%) 6 kJ/mol (range 0 - 12 kJ/mol)		

Figure legends

Figure 1. Chemical structures of PEP (a) and pyruvate (b). Asterisks indicate the ^{13}C labeled carbon atoms in panel a.

Figure 2. Infrared spectra of 100 mM unlabeled PEP (a) and 50 mM labeled PEP (b) and 100 mM pyruvate (c) dissolved in H_2O at pH 7.5.

Figure 3. Infrared absorbance changes of PK upon PEP binding in the presence of K^+ and Mg^{2+} in H_2O . Traces a, b and c reflect 96, 180 and 240 sec spectra after addition of 25 μM PEP. Trace d and e show spectra of the subsequent additions of 25 μM PEP measured 240s after each addition. The spectra have been shifted vertically for a clearer presentation.

Figure 4. Evolution of the 970 cm^{-1} band after addition of PEP to PK. (a) Series of overlaid spectra showing the band of the symmetric PO_3^{2-} stretching vibration after the first PEP addition. The spectra were recorded in H_2O within 240s after the addition of PEP and were smoothed over 25 cm^{-1} . The band amplitude increased with time and the band position shifted. (b) Time course of the band position after the first (I) and the second addition (II) of PEP. Spectra were smoothed over 25 data points before evaluation of the band position. Kinetics of the infrared absorbance change of PK, monitored by integrated band intensities at 1695 cm^{-1} , upon PEP binding in H_2O (c).

Figure 5. Binding induced absorbance changes of PK and ligand. All spectra were recorded 84–144s after the addition of ligand and normalised to the amplitude of the amide I signals in the 240 s spectrum. (a, b) Binding of unlabeled PEP in the presence of K^+ and Mg^{2+} in H_2O (a) and D_2O (b). (c) Binding of [2,3- ^{13}C] PEP in H_2O . (d) Binding of PEP in the presence of Na^+ and Mg^{2+} in H_2O . (e, f) Mg^{2+} binding to PK in the presence of K^+ in H_2O (e) and D_2O (f). Band positions are labeled in panels b to d if they differ from the respective positions in panel a. In panel f, only those bands are labeled that have a different position in panel e. The spectra have been shifted vertically for a clearer presentation.

Figure 6. Enzymatic reaction of PK. Changes of infrared absorbance induced by addition of PEP to PK and ADP. The initial state of the sample was a mixture of $\text{PK}\cdot\text{Mg}^{2+}\cdot\text{K}^+$ and ADP, then PEP was added. The spectrum shown is averaged over the first 4 minutes after PEP addition.

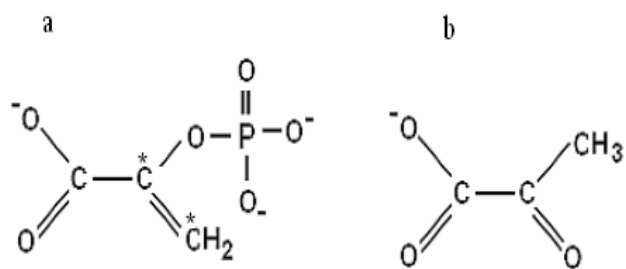


Figure 1.

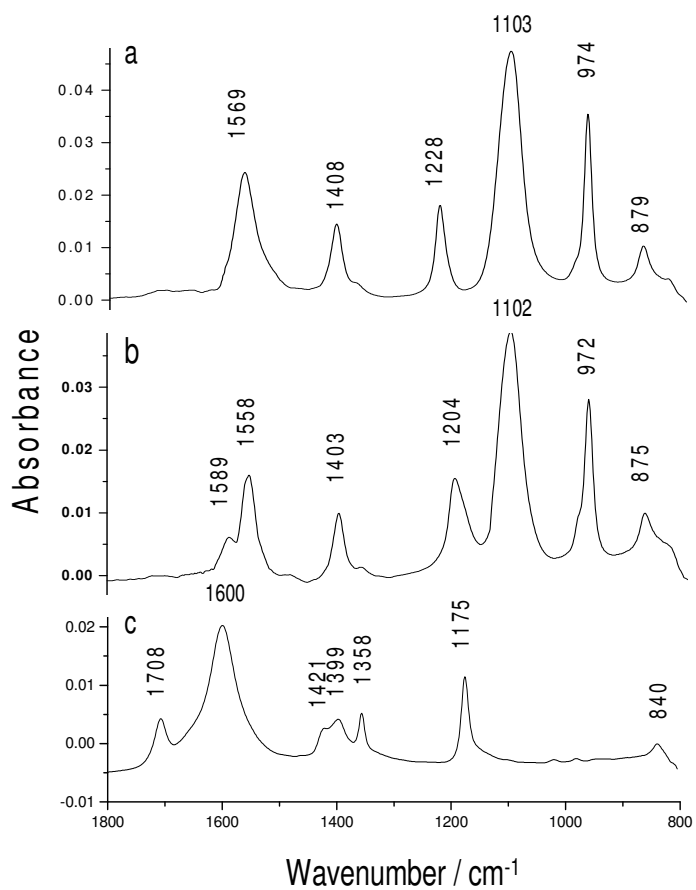


Figure 2.

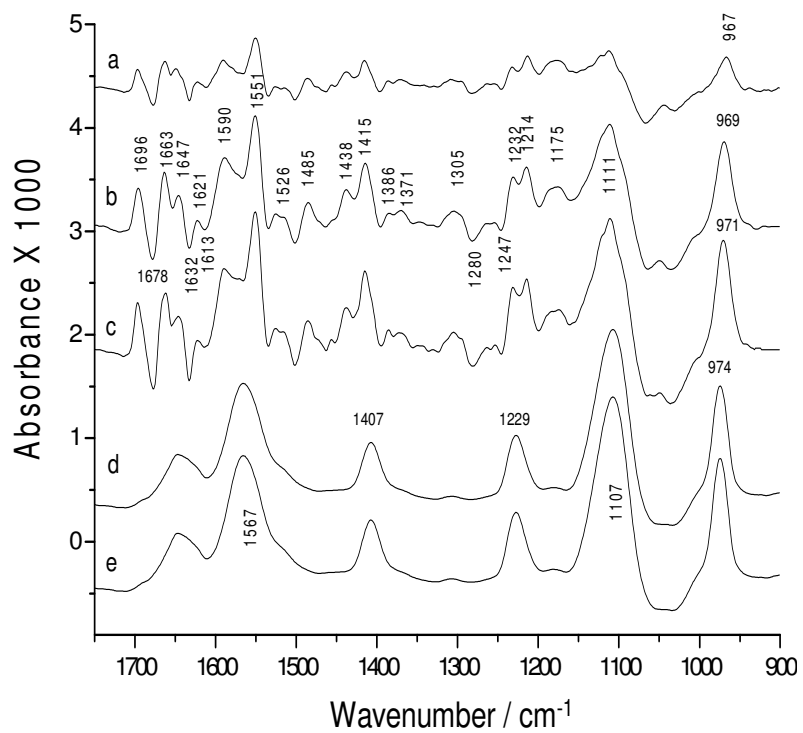


Figure 3.

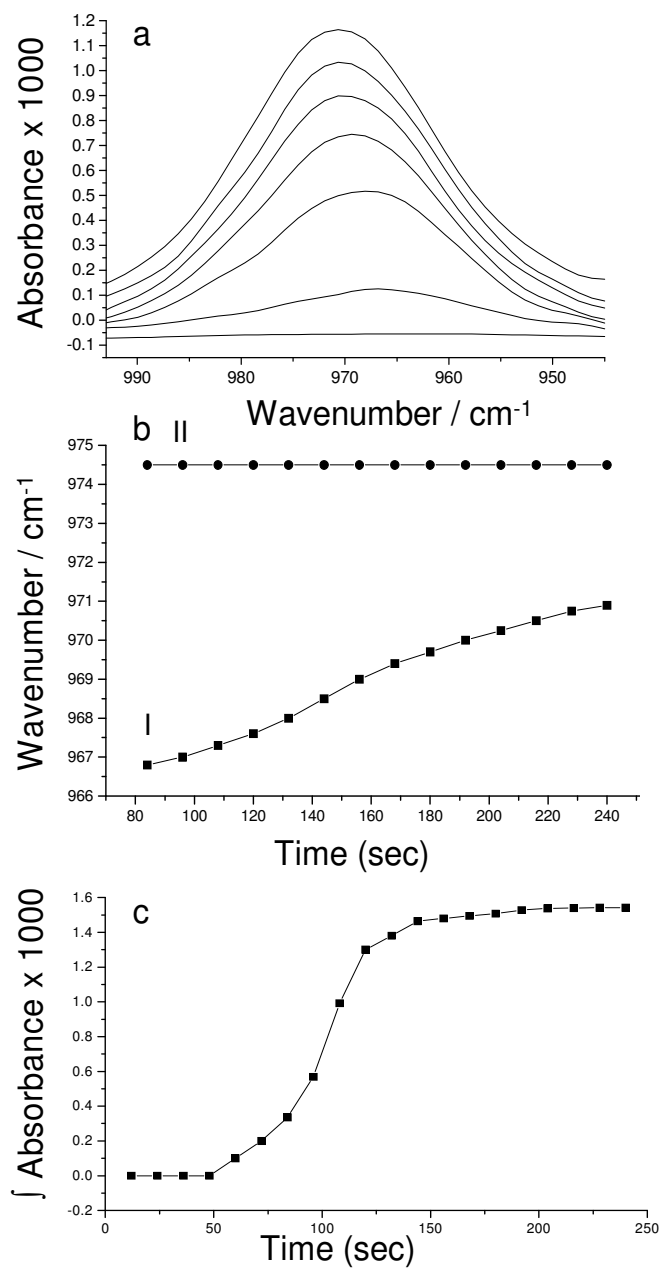


Figure 4.

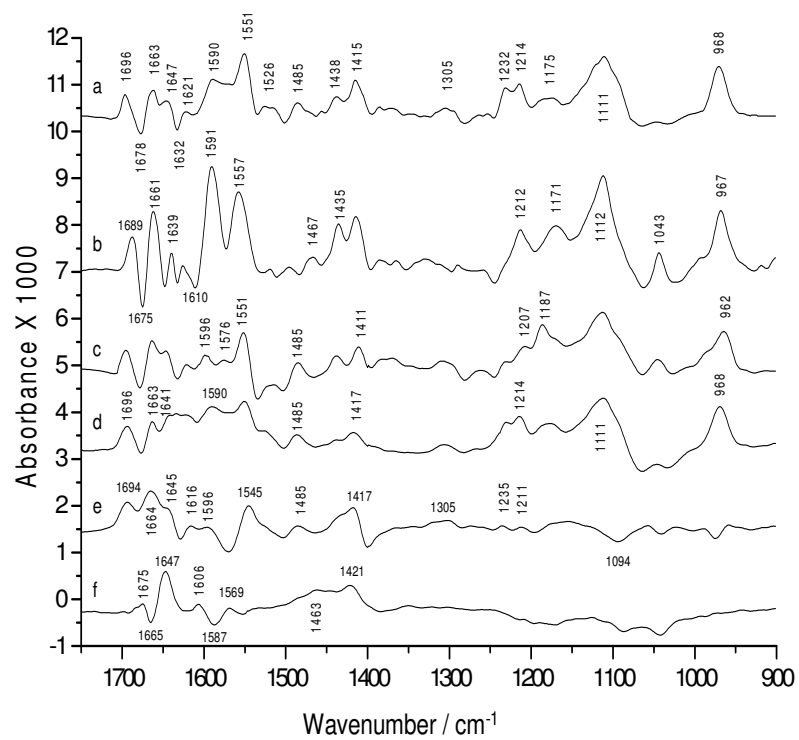


Figure 5.

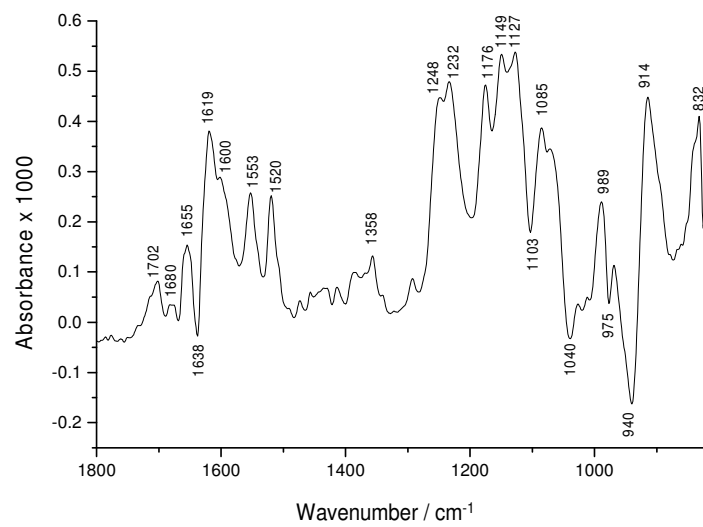


Figure 6.